R·I·T

Rochester Institute of Technology

RIT/PSY/TR–15/1
Final Technical Report

Improving Operator Situational Awareness with Wide Area Geographic Data View Displays of the Electric Power Grid

By

Esa M. Rantanen and Limor Hochberg
Rochester Institute of Technology, Rochester, NY

Diego Klabjan and Mingyang Di
Northwestern University, Evanston, IL

For

EPTD Smart Grid Program Clean Energy RDD
New York State Energy Research and Development Authority (NYSERDA)
17 Columbia Circle, Albany, NY 12203

September 24, 2015

Department of Psychology
College of Liberal Arts
18 Lomb Memorial Drive
Rochester, New York 14623-2953

Technical Report Documentation Page

1. Report Title **Improving Operator Situational Awareness with Wide Area Geographic Data View Displays of the Electric Power Grid**	2. Report No. RIT/PSY/TR-15/1 3. Report Date September 24, 2015
4. Authors Esa M. Rantanen, Limor Hochberg, Diego Klabjan, and Mingyang DI	5. Type of Report Final Technical Report
6. Performing Organization Name and Address Rochester Institute of Technology, Rochester NY and Northwestern University, Evanston, IL	7. Performing Agency Code NA
8. Sponsoring Organization Name and Address EPTD Smart Grid Program Clean Energy RDD, New York State Energy Research and Development Authority (NYSERDA).	9. Sponsoring Agency Code Contract No. 30732

10. Supplementary Notes

This research was undertaken with support of a grant from EPTD Smart Grid Program Clean Energy RDD, New York State Energy Research and Development Authority (NYSERDA). Mr. Michael Razanousky was the Project Manager.

11. Abstract

To reduce clutter on wide-area geographic data view displays of electric power systems, substations in geographically compact areas should be spread out and line overlaps and intersections minimized. Such pat- terns optimized with respect to given constraints can be modeled as a multicommodity flow problem. Due to the size of the developed model, we developed two clustering-based iterative algorithms to decompose the global network into smaller regions and then iteratively solve the subproblem in each region by readjusting some values. Three solutions were selected for experimental evaluation. The experimental results were somewhat inconclusive, due to naïve participants, simple task, and limitations of the eye tracker. Nevertheless, two of the decluttered maps appeared to have distinct advantage over the baseline map, where substations were simply connected by straight lines, in terms of performance time and workload.

Improving Operator Situational Awareness with Wide Area Geographic Data View Displays of the Electric Power Grid (Contract No. 30732)

by

Esa M. Rantanen and Limor Hochberg
Rochester Institute of Technology, Rochester, NY

Diego Klabjan and Mingyang Di
Northwestern University, Evanston, IL

Final Technical Report

Submitted to

Mr. Michael Razanousky, Project Manager
EPTD Smart Grid Program Clean Energy RDD
New York State Energy Research and Development Authority (NYSERDA)
17 Columbia Circle, Albany, NY 12203

September 24, 2015

Executive Summary

This report details the findings of a research project undertaken with support from the New York State Energy Research and Development Authority (NYSERDA). Mr. Michael Razanousky from NYSERDA served as the project manager. The research effort was split between Rochester Institute of Techhnology (RIT) in Rochester, NY (PI Rantanen), and Northwestern University in Evanston, IL (co-PI Klabjan). Prof. Klabjan and his team at Northwestern developed the algorithm and produces several decluttering solutions used to redraw electric transmission maps. Prof. Rantanen and his team at RIT experimentally evaluated a subset of the decluttering solutions.

We performed cognitive work analysis (CWA) to the extent possible given the limited access to operators at a local electric control center (ECC). This analysis revealed a wide variety of geographic data view (GDV) tools the operators used in different tasks but also much inconsistencies in the layouts and coding conventions. Such inconsistencies potentially increase the probability of human error, especially in emergency situations where the operators are under severe time stress. Therefore, a single GDV display that provides operators with all the information they may need at any time is very desirable. Such a display will also place heavy demands on effective visualization of different system elements and control of clutter.

To reduce clutter on wide-area GDV displays of electric power systems, substations in geographically compact areas (e.g., cities) should be spread out and transmission lines between them drawn, for example, in a rectilinear pattern, to minimize line overlaps and intersections. Such patterns optimized with respect to given constraints can be modeled as a multicommodity flow problem with side constraints and a complex objective function over an embedded display grid. Unfortunately, due to the size of the developed model, it cannot be solved to a satisfactory quality within a reasonable computational time by any commercial software. Therefore, finding effective solution methodologies was the main focus of our research.

Very large scale integration (VLSI) global routing, which is closely related to the topic of this research, has received considerable attention from both computer science and operations research communities. Various techniques and strategies have been proposed, including sequential routing, multicommodity flow techniques, and hierarchical methods. Our research found inspirations from all these methods, especially the hierarchical ones. In particular, we developed two clustering-based iterative algorithms—a Lagrangian relaxation-based algorithm and a progressive hedging (PH)-based algorithm—to decompose the global network into smaller regions and then iteratively solve the subproblem in each region by readjusting some values. Intuitively, the nature of such solution methodologies is quite coherent with the traditional hierarchical routing methods, but in this research we incorporated several novel aspects.

We generated a total of eight alternative NY state electric power system maps. Three of these solutions were selected for experimental evaluation. A total of 22 participants, recruited from the student population

at RIT, participated in the experiment. An abstract, simplified task to be performed on the experimental system maps was created. The dependent variables included a total time to perform the task as well as several measures of eye movements recorded by a remote eye tracking system. The experimental results were largely inconclusive, primarily due to the naïve participants (i.e., they had little or no experience in reading maps or wiring diagrams), the simple task, and the limitations of the eye tracker. Nevertheless, two of the decluttered maps appeared to have distinct advantage over the baseline map, where substations were simply connected by straight lines, in terms of performance time and workload.

To the best of our knowledge, this was the first-ever attempt to apply computational techniques to the problem of decluttering GDV displays for ECC use. The problem indeed proved to be solvable, and future research should further suggest a truly optimal decluttering solution for operational use. However, close collaboration between the researchers and experienced operators in all phases of the work is essential for a successful outcome.

Contents

1 Background **1**

1.1 Geographic Data View Displays 2

1.2 The Current State of Research and Development of the Technology 3

1.3 Display Design Challenges 4

2 Cognitive Work Analysis **5**

2.1 Observations and Interviews at RG&E Energy Control Center 6

2.1.1 The Energy Desk 6

2.1.2 Transmission Desk 7

2.1.3 Distribution Desks 8

2.2 Summary of Cognitive Work Analysis 9

3 Decluttering Solutions **11**

3.1 Human Factors Considerations 11

3.2 Basic Decluttering Algorithm 12

3.3 Map Coordinates 12

4 Algorithm Development **13**

4.1 Mathematical Formulation of the Problem 15

4.2 Algorithms 19

4.2.1 Sequential Routing Algorithm 19

4.2.2 Locating the Substations 20

4.2.3 Revised Dijkstra's Shortest Path Algorithm 20

4.2.4 The Sequential Routing Algorithm 22

4.3 Clustering-Based Optimization Algorithms . . . 23
4.3.1 The Clustering Algorithm . . . 23
4.3.2 Two Clustering-Based Algorithms . . . 25
4.4 Computational Results . . . 33
4.4.1 Implementation . . . 33
4.4.2 Results . . . 34
4.4.3 Discussions . . . 37
4.5 Redrawn Maps . . . 38

5 Empirical Testing of the Solutions 49

5.1 Method . . . 49
5.1.1 Participants . . . 49
5.1.2 Apparatus . . . 49
5.1.3 Experimental Materials . . . 49
5.1.4 Experimental Task . . . 50
5.1.5 Independent Variables . . . 54
5.1.6 Dependent Variables . . . 54
5.1.7 Experimental Design . . . 55
5.1.8 Procedure . . . 55
5.2 Results . . . 56
5.2.1 Data Reduction and Cleanup . . . 56
5.2.2 Data Analyses . . . 56
5.2.3 Orientation and Task Times . . . 57
5.2.4 Saccade Amplitude . . . 59

5.2.5 Saccade Peak Velocity 60
5.2.6 Fixation Durations 62
5.2.7 Pupil Diameter 63
5.2.8 Subjective Responses 65
5.3 Subsequent Operator Interviews 66
5.4 Discussion 66

6 General Discussion **67**
6.1 GDV Displays in Control Centers 68
6.2 Participatory Ergonomics in Systems Development 69
6.3 Recommendations for Future Research 69

7 Conclusion **70**

Appendices **77**

A Complete Model for Lagrangian Relaxation Algorithm **77**

B Complete Model for Progressive Hedging Algorithm **80**

C Proof of Lemma 1 **81**

List of Figures

1 A control room with video wall display 1

2 An example of a cluttered dynamic GDV display 3

3 An example of a decision tree analysis 10

4 A Graphical Illustration of Loops 16

5 A Path in the Network 19

6 Counter-example of Revised Dijkstra's Algorithm 22

7 A Graphic Illustration of Neighborhood 24

8 Graphic Illustration of the Iterative Algorithm 28

9 Comparison of Decluttering and Original Display 35

10 Running Time of Major Components in the Solution Process 37

11 Baseline map 40

12 Solution 1 41

13 Solution 2 42

14 Solution 3 43

15 Solution 4 44

16 Solution 5 45

17 Solution 6 46

18 Solution 7 47

19 Solution 8 48

20 Baseline experimental map 51

21 Experimental map based on solution 1 52

22 Experimental map based on solution 3 53

23 Experimental map based on solution 4 54

24 Plot of trial durations 58

25 Plot of saccade amplitudes 60

26 Plot of saccade peak velocities 61

27 Plot of fixation durations 63

28 Plot of pupil diameters 64

29 A Graphical Illustration of How to Construct p 83

List of Tables

1 Comparison of the Three Decluttering Algorithms 35

2 Performance Analysis of Lagrangian Algorithm 36

3 Performance Analysis of PH Algorithm 36

4 The Objectives and Associated Parameters for Alternative Decluttering Solutions 39

5 Descriptive Statistics of Task Performance Time 58

6 Descriptive Statistics of Saccade Amplitudes 59

7 Descriptive Statistics of Saccade Peak Velocities 61

8 Descriptive Statistics of Fixation Durations 62

9 Descriptive Statistics of Pupil Diameter 64

10 Summary Table of Experimental Results 67

1 Background

Reliability of electric power transmission is critical to all areas of a modern society. Correspondingly, the economic cost of disruptions to power delivery can be staggering. The 2003 blackout in the U.S. Northeast was estimated to have cost up to $10 billion. Ultimately, the reliability of the electric grid is in the hands of human operators who manage it on multiple levels. Operators in electric power system control centers serve a critical role in ensuring the integrity of the nation's electric grid and in preventing disruptions to the supply of electric power at any time, for any reason. This will remain the case even with the advent of the smart grid and the extensive automation associated with it. Therefore, the best way to ensure reliability of both the present and the future smart grid is to empower and equip human operators to effectively shoulder that responsibility. Well-designed visualizations of complex data allow humans to process vast amounts of information rapidly and reliably, making visual displays the primary tool for operators (see Figure 1).

Figure 1: A large video wall display at the NYISO control center

The basic operations of electric power systems can be divided into two categories. Switching operations take place at a local level and consist of scheduling, coordinating, managing, and supervising maintenance and repair work that takes place in the field. At a more complex and critical level are operations known as

reliability coordination. In Local and Regional Centers (LRCs) operators not only monitor the grid from moment to moment, but also plan for anticipated future changes in supply and demand and for potential disruptions. In essence, the operators try to stay one step ahead of contingencies to ensure uninterrupted reliability of the grid.

1.1 Geographic Data View Displays

Until only some 10 years ago, the operational quantities relevant to operators in power system control centers, such as power flows and voltages, were represented either as analog fields on substation one-line displays or as numeric fields on tabular displays. System-level overview information was typically displayed on static map boards; the only dynamic data shown using different colored lights. Recent advances in display technology have made the display of truly dynamic system data both possible and affordable [1]. Following the August 14, 2003 Northeast U.S. blackout there has also been increasing demand to broaden the views of power system control centers to also encompass neighboring control areas. The rationale behind wide-area displays is to allow operators earlier warnings of possibly cascading events that may originate outside their area of responsibility and disrupt the grid over large geographical areas [2].

These system visualizations are known as geographic data views (GDVs). With the GDV approach, power system visualizations can be dynamically created using power system information along with geographic information embedded in the system model. Since the year 2000 many power system control centers have adopted advanced visualization techniques for wide-area displays. Despite the many advantages of dynamic GDVs, they suffer from some disadvantages. For example, when the task switches from monitoring to corrective control or analysis, it can be difficult to design a priori a single display, or even a set of displays, that contain all the information needed to make effective, corrective control decisions. Displaying such information on an existing GDV designed for system monitoring could result in slow display performance and a cluttered appearance. Hence, there is a continual need to develop novel display solutions, afforded by new technologies and availability of data, to meet the operators' needs.

Two main problems that degrade the readability of displays and that are to be avoided in display design are visual "noise", which may result from careless use of animation and color, and clutter from displaying too much information in too small a display space (see Figure 2 for an example). These present-day challenges are further aggravated by the future need to display predicted values (to augment human working memory in extrapolating system states into the future) and visualizing dynamic information. In particular, rate of change information and displaying of uncertain (probabilistic) and old (unreliable) information will be paramount to support human operator performance.

A key advantage of GDVs is that they can be used to visualize a wide variety of different power system field

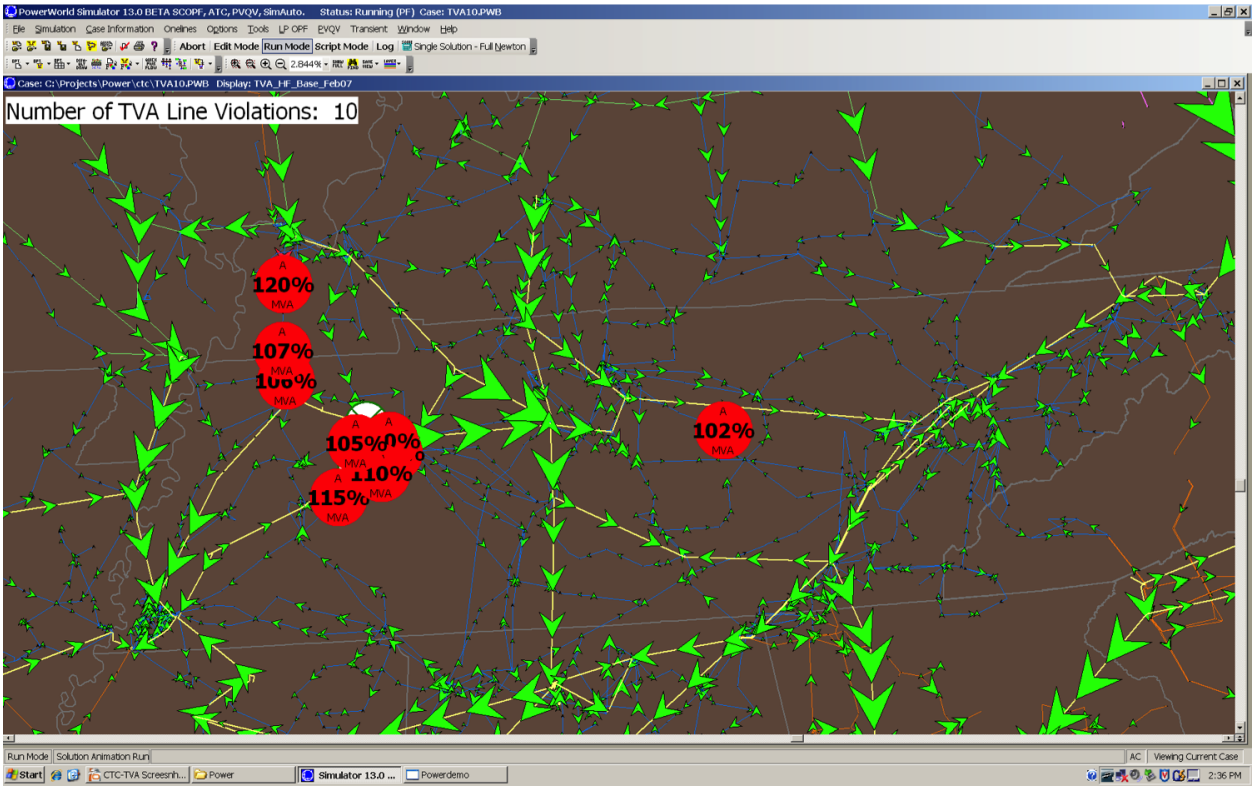

Figure 2: An example of a cluttered dynamic GDV display. In this simulator-screen capture the arrows move to indicate power flow and are proportionally sized to display the amount of current the line is carrying. The red pie charts show line overloads

values with the ability to use different display attributes to simultaneously show different fields. The GDV displays show power transmission lines and substations laid on a geographic map; consequently certain areas (e.g., in and around cities) become extremely cluttered. To reduce clutter, closely located substations could be spread (distorting the true geographic relationships in a carefully controlled manner) out and transmission lines between them drawn, for example, in rectilinear pattern minimizing line overlaps and crossings. Such patterns optimized with respect to given constraints can be created by a number of operations research (OR) techniques.

1.2 The Current State of Research and Development of the Technology

Visual displays allow for rapid integration of complex information and thus help human operators in development and maintenance of good situation awareness of systems under their control. Such advantages have also been recognized by the Electric Power Research Institute (EPRI) who argued that purely numeric representations for system data do not sufficiently convey information to operators [3]. Solutions to visualize relevant data were thus a necessary evolution. These developments received a renewed impetus from the August 14, 2003 northeast U.S. blackout. This event made very clear how important it is for operators to

have a view of the system outside their immediate area of responsibility and how visualization solutions can help in the formation and maintenance of accurate situation awareness during rapidly cascading dynamic events [4].

Recent visualization innovations include depiction of the flow of power in an electricity network by animated arrows along power line representations, where the size, orientation, and speed of the arrows indicate the direction of power flow on the line. Another visualization solution that has proven useful for quickly detecting overloads in a large network are dynamically sized pie charts, where the percentage fill in each pie chart indicates how close each transmission line is to its thermal limit [5, 6, 7, 8]. These solutions have the problem of cluttering displays to a degree that renders them useless: that is, at high densities such as during overload events these visual element obscure each other as well as other relevant information [9, 10]. One solution to the problem of displaying vast amounts of information (e.g., bus values in a large system) is to use algorithms that blend voltage magnitudes between buses to create continuous, color-graded, spatial contours on GDV displays [3]. Other variables that would also be very useful to power systems operators include current, voltage and phase angle estimates from phasor measurement units (PMUs) that have become increasingly widespread throughout power networks.

As far as we know, the problem of clutter on large-scale GDVs and visual presentation of additional variables that are becoming increasingly available have never been systematically addressed. Solving the decluttering problem mathematically may result in an optimal compromise between declutttering the display while maintaining reasonably accurate representations of geographic relations of the display elements.

1.3 Display Design Challenges

The primary challenge in the design of information displays for power transmission control room applications is the mapping of system variables to graphical variables, subject to the constraints of human perceptual and cognitive capabilities. This challenge arises from the asymmetry between the very large number of system variables operators must monitor and the very limited number of graphical elements than can be used on the displays. However, even if this challenge is met and proper graphical variables (i.e., perceptually and cognitively salient and unambiguous) are defined and the operationally most important system variables mapped to them, display clutter still remains a problem.

Minimizing clutter will create room for other information to be displayed in innovative ways without overwhelming the human operators using the display. Given the number of buses and other devices, substations, and transmission lines, the design of wide-area displays presents a daunting challenge. Another challenge is the large geographic areas covered by individual control centers. For example, the Midcontinent Independent System Operator (MISO) is responsible for an area covering 15 U.S. states and the province

of Manitoba in Canada [11]. This dual challenge makes design of wide-area displays layouts by hand nearly impossible. Therefore, we sought to solve the problem computationally.

We developed a linear integer programming model for the task. Due to the size of the problem, however, a commercial solver could not solve it to a satisfactory quality within a reasonable computational time. As a result, further research was required to develop effective and tailored solution methodologies for solving the model. Different Lagrangian relaxation techniques were a natural choice. Another option was to reformulate the model by using so-called path variables. Such a reformulation requires a branch-and-price algorithm due to an excessive number of variables.

To our knowledge, mathematical optimization of power systems GDV display layouts has never been done before. Optimization of display layouts can nevertheless be seen as fundamental to all other display innovations and operators' ability to effectively use the displayed information.

2 Cognitive Work Analysis

Design of displays should rely heavily on participation of those who will use the displays in the design process. In other words, it is the operators who know best what they need to perform their tasks. However, although experienced operators are experts in their domain, they are usually not trained in cognitive psychology or human factors and may not be able to access their expertise beyond skilled performance. That is, experts often cannot articulate *why* and *how* they perform their tasks or decompose their performance into sub- and sub-subtasks, which is necessary for design of new tools for them.

There are many methods to access covert expertise. Cognitive Work Analysis (CWA) is a comprehensive framework that systematically analyzes the work people do, the tasks they perform, the decisions they make, and the ways they seek and use information to perform their work for the ultimate purpose of establishing human-system integration requirements for a work domain [12]. The main goal of CWA is to support the development of systems that allow workers to adapt to novel situations and change throughout the entire system [13]. To identify areas of work that might hinder the adaptability of a system, CWA provides techniques and analyses that create representations of how work and information are dispersed throughout the system, which aids in the identification of limits to work, and restrictions to adaptability. Finally, CWA is seamlessly linked to a display development technique known as *ecological interface design* (EID) [14] [15].

A full CWA consists of 6 distinct stages. We did not have sufficient access to operators to perform a complete CWA, but we made use of the framework as far as it could be populated by the data were were able to collect by observing and interviewing the operators. In particular, stage 3, or the *Cognitive Transformations Analysis* that examines cognitive states established during task execution, and cognitive

processes used to effect the transitions between states [12] proved to be very useful. The product of this stage of analysis is a suite of *decision ladders*, originally developed by Rasmussen [16]. Decision ladders are an extremely powerful tool to investigate just *how* operators perform their tasks and what information they need to do so.

The entire process of CWA is integral to *ecological interface design* (EID) [14] [15]. EID thus seamlessly integrates analysis, design, and evaluation functions facilitating a truly user-centered design process. Operator participation in future efforts to further evaluate and refine the products of this study is therefore very important.

2.1 Observations and Interviews at RG&E Energy Control Center

We were given access to the Rochester Gas and Electric (RG&E) Energy Control Center (ECC). We visited the ECC on about 10 different occasions between November 2013 and January 2014 to observe and interview operators there. In addition, two operators visited RIT in May 2014 to discuss their use of transmission maps in greater depth. This section summarizes the results of observations and interviews within the CWA framework.

The control room at the RG&E ECC has four desks. These are the energy desk, the transmission desk, the Rochester distribution desk, and surrounding areas distribution desk. We observed operators in each desk and familiarized ourselves with their tasks. In particular, we noted their use of different visualizations and geographic information.

Our observations were on the current systems at RG&E ECC. In 2015 RG&E will get a new system from Siemens, called Spectrum, that will integrate various systems and maps. We were unable to make contact with Siemens to learn more about the new system, despite requests made by ECC operators on our behalf.

2.1.1 The Energy Desk

The energy operator is mostly concerned with hydro and gas power, the main supplies to the area of RG&E's responsibility. The main tasks include hourly (probably to help maintain vigilance) recording of values and temperature, monitoring values and load on a load map (top right on large project screen), watching for alarms, and taking calls from within RG&E as well as from customers after hours. The operator made frequent use of the voltage summary. The station maps update in real-time (multiple times/min), but since it is hard to notice an individual voltage change the voltage summary is monitored.

The voltage values at each station are important, but so are the relative values of groups of stations.

Knowledge of geography is also important. One operator pointed out that one station was several kV lower than others in its area, but this was due to its distance from the group and line loss.

The operator's main task is to make sure voltage values at each station are within a given range, or tolerance. There are alarms for exceedances. The operator can access critical values via a sub-menu from the voltage summary. If voltage values exceed their limits, the operator must take some action, usually add a capacitor. Factors considered in this decision include equipment wear (capacitors are heavy) and knowledge of overall trends (e.g., whether the peak time of energy use such as morning or dinner time is almost over). There are only a few capacitors available and their locations are well know to operators, so geographic factors do not play a major role in the common tasks at this desk.

Operators also refer to standard operating procedures (SOPs), including emergency SOPs, which are available to them via computer, but the operators have considerable leeway and they are expected to use their best judgment and common sense. Visual variables of interest in this position include connections between stations, the relative location of stations and the distance between them, and direction and value of flow. Operators use voltage summary for overall picture but need geographic information for specific scenarios. The operators also constantly monitor Ginna nuclear power station, which must have sufficient power available at all times.

The energy desk also uses supervisory control and data acquisition (SCADA) system made by Siemens. The black-background power systems map deals with 11 and 34 kV lines. The color coding on the Siemens map does not match the line color coding in other maps at the ECC, which the operators pointed out as a potential source of confusion. We observed the operators throughout the ECC using several other maps made by different entities that had very different color coding, symbology, and other graphic features. Clearly, a single map with all the necessary information available to all the operators would be a vast improvement over the present system.

2.1.2 Transmission Desk

The main task of the transmission operator is to monitor the system and plan for contingencies, or disruptions to the system. The operator we observed made use of a map and customer calls to make educated guesses where an outage is, but outages cannot always be pinpointed exactly. A map is used to highlight a path from a specific point to its substation or a tie, from where a line segment could be isolated and de-energized. Many alarms are seen as annoying disruptions, caused by door and electric fence alarms or crews working on a station, and are not a cause of any action.

The Western part of Rochester is vulnerable due to the single 345 kV East-West line going from Niagara down to NYC and insufficient back-up lines in the area. If this line is overloaded the only solution is to cut

off customers and to then send out a crew to fix the problem. RG&E will be adding a new station somewhere in W. Rochester to ameliorate this situation. Major sources of power to the area include Station 9, a gas turbine, and Allegany, a combined cycle (gas-turbine–steam) stations. Operators at the transmission desk will sometimes have to coordinate activity with neighboring National Grid (NG) operators. For example, when voltages are especially high, the transmission desk operator might ask the National Grid to adjust a capacitor at Mortimer, which is within NG's area of responsibility.

Clutter on the system maps was mentioned as a specific problem, and decluttering was high on the operators' wish list. Also some filtering functions were mentioned as a solution to the clutter problem. The Genesee Valley area map is spatially distorted as some lines are shown "backwards". However, with the very few high-voltage lines the transmission desk operator is responsible for and their familiarity with the geography of the area, the operators seldom need to refer to maps to solve emergent problems.

2.1.3 Distribution Desks

There are two distribution desks at the ECC, one for the city of Rochester and its suburbs, and another for the surrounding areas. Distribution operators work below the station level (4–12 kV lines), while transmission operators transfer power between stations. The primary task of distribution operators is switching operations in response to power outages and crews working on lines and other equipment. Distribution operators write switching orders for 3 years before they get to work at the distribution desks. They can then work their way up to the transmission and energy desks). A generic switching procedure is described in [17]:

1. Define the line segment to be worked on
2. Open circuit breakers at all points that can supply power to the line segment; check for zero voltage on potential transformer secondaries.
3. Open and lock open disconnect switches on the line side of circuit breakers that can supply power to the line segment
4. Close and lock closed the station ground switches.
5. Clear the line for work, e.g., "the ABC xxxx voltage line between open disconnects at stations PDQ and XYZ is cleared for work and you may report on the line using local grounds".

In a switching order, an operator takes into account the maximum load any phase can take, and when the operator wants to add load, she must make sure the load is less than than the phase's max capacity. Not all circuits have SCADA to log historical load information. For circuits without SCADA, operators must refer to paper wheels found in binders, which are analog logs of load for each day/time, created by

a Geiger counter. To determine max capacity, there are paper log-books used as reference. Generally, the highest-load phase is used to make the decision.

The primary tool for distribution operators is a map called SmartMap, which has a similar interface to Google maps. The SmartMap is homegrown and made by a company in Maine. It will be replaced by the Siemens Spectrum system in 2015. Two variables of interest on the SmartMap are direction of flow, which is shown by triangles, and color coding by the feed, allowing visual tracing of a line to the source. However, there were many colors, some of which were very close in terms of hue, saturation, and value (e.g., pink, tan, light orange) indicating lines in close proximity that were very difficult to differentiate visually. Resolution of the maps was also an issue; for example, if two power lines run along the same street, it is very hard to tell ground crews where to go.

We observed an operator with several switching orders on deck. One was about a "bad" underground cable in a subdivision and a number of houses were now supplied by a different circuit. Line crews opened and closed switches/tie points. When finished, line crews updated the operator, who in turn updated SmartMap. On SmartMap, a thick green highlight over a line means it's not in service; orange means current is flowing.

The SmartMaps has two modes, current and study mode. The study mode is labelled only by tiny print label in upper right hand corner. This may lead to what is known as mode confusion and lead to mode errors. Also the SCADA system uses color coding of lines that are not easily distinguishable (e.g., fuchsia and purple). SmartMap mixes real-time and future information. For example, a green-highlighted area might be highlighted due to a future switching order that puts it out of service. All text in system is also in all caps, which is less readable than upper- and lower case lettering. All text in system is also in all caps, which is less readable than upper- and lower case lettering. When SmartMaps does not provide operators with sufficient detail, they must retrieve secondary, hand-drawn, black and white, maps from microfiche. The operators we observed wished for more high-fidelity information on SmartMaps.

There were also other sources of potential confusion. Line crews use physical tags in the field (a tag-out system) to determine status and possible actions at each site (the technical term is "isolated work area"). The flags on the SmartMap operators use to indicate various notes and statuses do not correspond to the tags used by line crews in the field.

2.2 Summary of Cognitive Work Analysis

We are grateful to the operators at the RG&E ECC for granting us access to their workplace and for showing us their tools, procedures, and tasks they engage in every day. However, we also must acknowledge that the time we were able to spend at the ECC and speak with the operators was not sufficient for a complete, thorough, CWA. Nevertheless, our observations revealed the wide variety of maps operators at the ECC

used in their jobs, ranging from SCADA one-line diagrams to the SmartMaps and the hand-drawn maps on microfiche, all with different graphic conventions and codings.

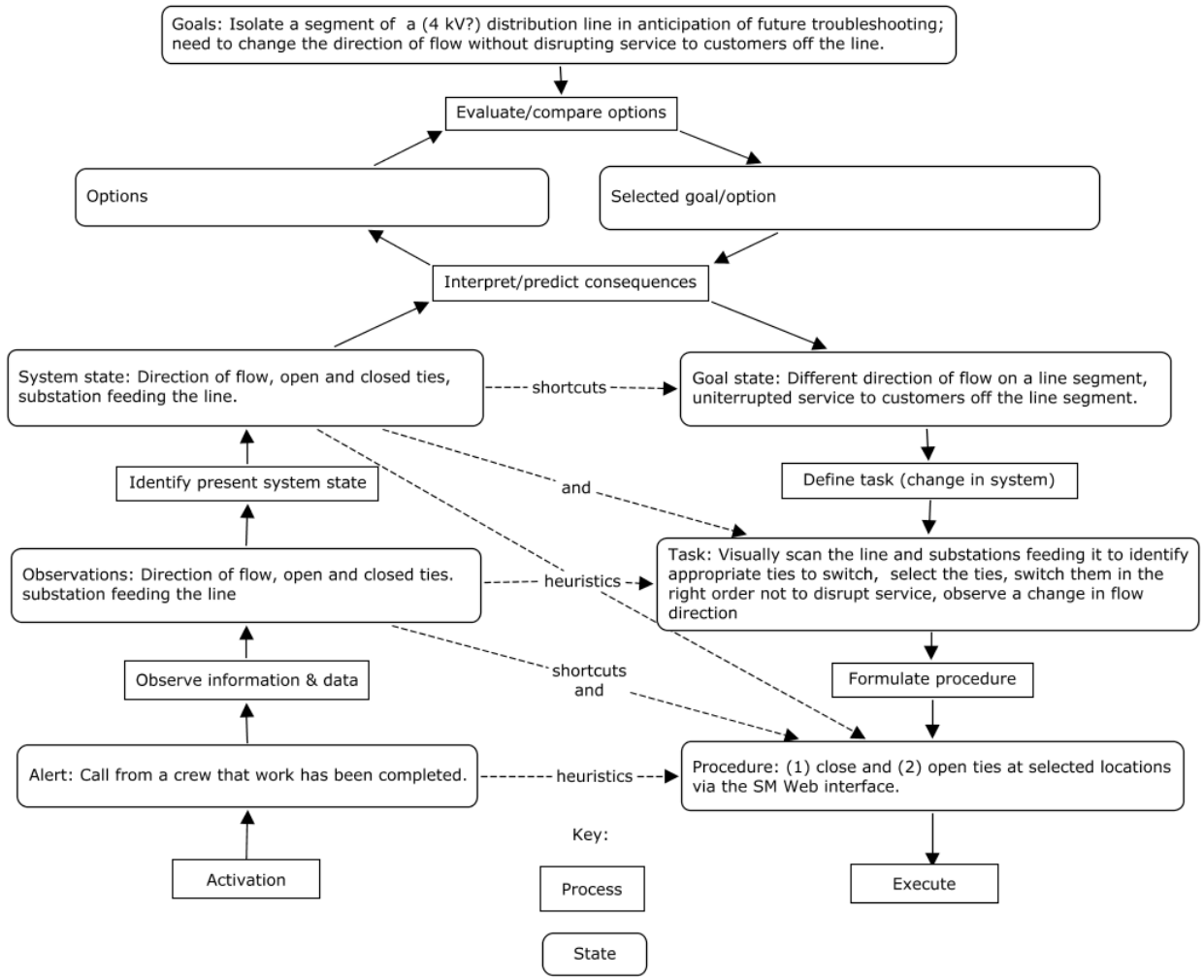

Figure 3: After installation of a new device the operator wanted to change the direction of flow on a line segment where the device was installed, presumably to facilitate future troubleshooting. This was to be done by dynamic switching, closing and opening ties at given points along the line so that the feed would come from a different direction. This decision tree illustrates the operators cognitive processes to arrive at the correct procedure. Note that in this case the decision was relatively straightforward and did not necessitate evaluation of multiple options

Figure 3 shows a decision tree analysis of a typical task at the distribution desk. In this case, the operator wanted to change the direction of flow on a line segment where a device was installed to facilitate future troubleshooting. This was to be done by dynamic switching, closing and opening ties at given points along the line so that the feed would come from a different direction. The procedure was sufficiently straightforward so that the operator did not need to evaluate multiple options, but identification of the relevant ties to be opened and closed required extensive searching on the system map, in this case using the SmartMaps application. Finding the appropriate ties to open and close on the SmartMap was a time-consuming process

and required much panning and zooming to bring up the necessary details.

3 Decluttering Solutions

3.1 Human Factors Considerations

Geographic relations are very important to power systems operators. Many critical system parameters depend of geographical distances between generators and substations, rerouting power around open lines obviously requires detailed knowledge of the locations of the neighboring substations and lines that may be used to circumvent the problem, and intervening in cascading failures necessitates mastery of systemwide geography. The question therefore is how to best display the geographic information to operators so that it is available to them at all times and for all possible situations.

Our search for relevant, existing research on optimal layouts for wide-area GDV displays resulted in very few published works. To the best of our knowledge, the problem has never been researched in operational electric power control context. The operators' task solving line problems is very much like maze-solving, and there are a few laboratory studies that have used maze-solving tasks. The results from these studies also converge to suggest design criteria for GDV displays.

To summarize: Fixation durations have been shown to increase as a linear function of the length and number of turns in the path segment between the current and the upcoming fixation points, suggesting that much mental processing relates to the length and turns in that segment [18]. Another study [19] found a positive linear correlation between number of turns in a maze-solving task and response time. In yet another experiment [20] the length of a curved line segment rather that the Euclidean distance between two targets determined the response time of comparing two targets along the line.

These results suggest that power lines depicted on GDV displays should not have turns in them, for turns make their visual tracing more difficult and time-consuming. Other potential sources of confusion while visually tracing lines is the number of lines crossing each other. Self-evidently no lines or substation symbols should overlap, which would make it impossible to differentiate between them on a visual display.

Because the primary objective of the decluttering solution was to "spread" substations clustered in densely populated areas (cities) to make the GDV maps more readable and because moving substations away from their true geographic locations would necessarily also change the orientation of the straight lines between them, we concluded that preservation of the spatial *relationships* between substations was paramount, even if the distances between them would necessarily be distorted to declutter displays around densely populated areas.

3.2 Basic Decluttering Algorithm

A map of electric transmission lines was generated and the lat./long. coordinates of substations (transmission lines are straight lines between these) transformed so that the following criteria were met:

1. The lines should be either vertical or horizontal so that (a) intersections between lines and (b) turns in them are minimized. The conditions may be mutually exclusive, in which case they may need to be defined hierarchically. Thus, lines will be drawn between points in such manner that they can be easily visually traced on a display, that is, with minimum number of line crossings and turns in them where the eye might get confused).

2. Different substation symbols and lines must not overlap. In other words, all display elements must be visible to the operators at all times regardless of the display scale (zoom).

3. The relative positions between substations must be preserved; if there is a substation A and another substation B North and East of it, this relation should be preserved, that is, after the algorithm is done moving the substations around, B should still be North and East (or, above and to the right) of A.

4. The magnitude of positional change for the substations from natural geographical to the schematic coordinates per the above constraints must be minimized. This problem may be solved iteratively by a computer.

3.3 Map Coordinates

Exact coordinates of the NY state electric system elements were not available to us due to Federal Energy Regulatory Commission (FERC) Critical Energy Infrastructure Information (CEII) regulations (Michael Swider, NYISO, personal communication, April 16, 2013). We were, however, given a PDF copy of the system map. This map was created for the NYISO by a cartographer who derived the system element coordinates from Google Maps satellite images (Michael Swider, NYISO, personal communication, May 29, 2014). The system element coordinates were thus not accurate to begin with, and the errors in this map were carried over to the redrawn maps.

The NYISO State Electrical System Map represents the network of existing and proposed stations and transmission lines connecting them. Most stations are transmission stations; the others are generating stations, including hydro, pumped storage, thermal, nuclear, combustion turbine, combined cycle, and wind stations. Transmission lines are above 115 kV. The PDF copy of the system map was converted to TIFF format via a software package. It was then uploaded into another software application, GetData Graph

Digitizer. Based on axes and units set by the user, the program extracts coordinates for user-selected points on the image. Using this program, coordinates were logged for each existing transmission and generating station. Stations not connected to other stations, as well as proposed stations, were excluded. In addition, where relevant, additional nodes were added to specify locations in which a transmission line forked or branched, in order to provide a more accurate representation of the network.

These coordinates were entered into a spreadsheet, which also noted the station name and type (e.g. transmission, hydro, thermal, etc.). Next, another spreadsheet listed pairs of connected stations, as well as the type of line connecting them, characterized in terms of voltage (e.g. 230 kV) and location (overhead or underground). We used Google maps to obtain the true latitudes and longitudes of the Ginna Nuclear station and the Pannell transmission stations, which were readily identifiable in the Google satellite images. A simple linear function was calculated describing the transformation of the coordinates from the GetData Graph Digitizer program into latitude and longitude coordinates. This function was then applied to the rest of the coordinates extracted from the system map.

4 Algorithm Development

To reduce clutter, geographically compact substations should be spread out and transmission lines between them drawn, for example in rectilinear pattern to minimize line overlaps and intersections. Such patterns optimized with respect to given constraints can be modeled as a multicommodity flow problem over an embedded display grid. Unfortunately, due to the size of the developed model, it cannot be solved to a satisfactory quality within a reasonable computational time by any commercial software. Hence, developing effective solution methodologies is the focus of this paper.

A stream of research that is closely related to ours is VLSI (very large scale integration) global routing. As one of the most challenging discrete optimization problems in computational practice, VLSI global routing has received considerable attention from both computer science and operations research communities. Various techniques and strategies have been proposed, including sequential routing [21, 22], multicommodity flow techniques [23, 24, 25, 26], and hierarchical methods [27, 28, 29, 30, 31, 32, 33]. This paper finds inspirations from all of the above techniques, especially from hierarchical methods. In particular, we develop two clustering-based iterative algorithms - Lagrangian relaxation based algorithm and progressive hedging (PH) based algorithm - to decompose the global network into smaller regions and then iteratively solve the subproblem in each region by readjusting some parameters. Intuitively speaking, the nature of such solution methodologies is quite coherent with the traditional hierarchical routing methods except that we apply systematic clustering techniques such as k-means to capture geographic compactness and connectivity between substations rather than randomly decompose the network into several equal-sized blocks. To our

best knowledge, this is the first time for clustering techniques being incorporated into a routing problem.

Furthermore, unlike the traditional VLSI global routing or multicommodity flow problem, the visualization decluttering problem addressed in this paper also considers setting apart closely located terminals (i.e., substations) so that the transmission lines among these relocated terminals could be routed to avoid extremely cluttered area. This part can be modeled as a facility location problem, and thus forms a hybrid with the multicommodity flow nature of the routing problem. Although divide-and-conquer approach has been widely used in both categories to facilitate the solution process, using it to tackle the two problems simultaneously remains open.

The two iterative algorithms proposed to address this open question are novel versions of classic Lagrangain and PH algorithms. Unlike the traditional Lagrangian relaxation approach in which the hardest constraints are relaxed, or its most recent application in VLSI global routing to relax crosstalk constraints [34], the Lagrangian algorithm presented in this paper first decomposes the entire network into smaller clusters so that the subproblem in each cluster can be easily solved, and then relax all the *connections* between the clusters. This points out a promising direction to extend the application of Lagrangian relaxation method in solving large-scale routing and multicommodity flow problems with the help of clustering techniques. On the other hand, PH was originally developed to solve multi-stage stochastic programming problem with only continuous variables [35]. However in this paper, we show that it works successfully for a single-stage scenario-based (thanks to the integration of clustering techniques again) problem with integer variables and thus demonstrate its applicability of solving similar large-scale network optimization problem with equilibrium constraints.

Finally, we also develop a sequential routing approach based on a revised shortest path algorithm, and conduct intensive numerical experiments to evaluate and compare the three proposed solution methodologies. Our findings show that the two iterative algorithms deliver similar high quality solutions within 5 to 10 hours, while the sequential routing algorithm could give a preliminary result in a much shorter time. We also find out through extensive evaluations that the output from the iterative algorithms could be implemented right away, but the solution generated by the sequential approach possesses serious defects and needs further processing before implementation. Thus, the comparison between the iterative and sequential approaches is indeed a trade-off between computational resources (i.e., time and memory) and the quality of the solution.

The contribution of this paper goes beyond the three methodologies to solve a novel display visualization problem. Most importantly, we develope a graph-decomposition based divide-and-conquer approach for solving large-scale network optimization problems, and demonstrate its practicability by performing a case study on a real-world power grid in the U.S. We also upgrade the traditional shortest path algorithm to incorporate several unique features (e.g., turns, line crossings and overlaps), which have a wide spectrum of applications in transportation network design, information display technology and VLSI global routing.

The rest of the algorithm development section is organized as follows. Section 4.1 presents the model for the decluttering algorithm. In Section 4.2, we formalize the clustering technique used in this paper, and then develop the three solution methodologies. Section 4.3 gives the findings from numerical experiments and discusses what will happen if the grid discretization becomes finer. Finally, we conclude in Section 4.4.

4.1 Mathematical Formulation of the Problem

The primary goal of the decluttering algorithm is to re-design the layout of the visual elements to minimize the clutter on the electric power control display. A map of electric transmission lines will be drawn in which the latitude and longitude coordinates of the substations are redefined and the transmission lines are rerouted so that the following criteria are met:

1. The transmission lines should be either vertical or horizontal so that the total number of turns in the lines and (b) the total number of intersections between them are minimized. The transmission lines are rectilinear straight lines between substations regardless of their true paths across the terrain.
2. The overlaps between different substation symbols and transmission lines must be minimized. In other words, all display elements must be as visible as possible to the operators regardless of the display scale.
3. The magnitude of substations' potential deviations from natural geographic to the schematic coordinates per the above constraints must be minimized.
4. The relative position between each pair of substations should be preserved as much as possible. To be more specific, if there is a substation 1 and another substation 2 south west of it, the algorithm should try to relocate them to coordinates A and B so that B is still south west of A.
5. The total number of loops should be minimized. A loop is defined as a transmission line whose length is over three times longer than the taxicab distance between its terminals (an example of loop is provided in Figure 1, in which the transmission line from s to t is called a loop but the line from m to n is not).

Notice that these criteria may be mutually exclusive and thus can be defined hierarchically, e.g., *first* minimize turns and *then* minimize intersections. After all, display is an art of compromise.

The entire concept relies on the notion of an embedded display network. We assume that the display is discretized into an orthogonal grid in which the edges consist of only vertical and horizontal lines. The intersections of edges are referred as nodes, and they correspond to possible locations of substations. Although

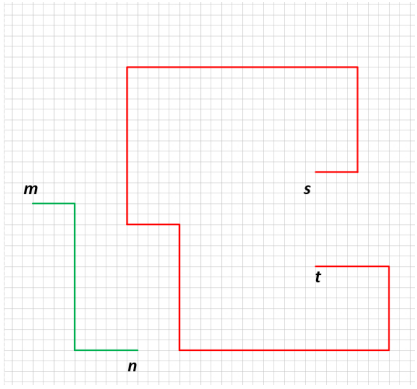

Figure 4: A Graphical Illustration of Loops

it suffices to have undirected edges for the sake of display grid, modeling the layout requires directed edges (see Figure 2).

Let us introduce the following notations:

- Let G=(N, A) be the underlying network, in which N is the set of all nodes (all possible locations of substations) and A is the set of all possible edges connecting the nodes.
- Let S be the set of all substations
- Let $M \subset (S,\ S)$ be the multi-set of all transmission lines. This is a multi-set because a pair of substations can have multiple lines. Pairs in M are treated as ordered.
- Let $I_1(k), O_1(k)$ be the set of all incoming, outgoing horizontal edges of node k.
- Let $I_2(k), O_2(k)$ be the set of all incoming, outgoing vertical edges of node k.

In order to display locations of substations and draw the actual transmission lines, the following binary variables are introduced:

$$x_{s,k} = \begin{cases} 1 & \text{if substation } s \text{ is placed at node } k \\ 0 & \text{if otherwise} \end{cases} \qquad y_{m,a} = \begin{cases} 1 & \text{if edge } a \text{ is used to display transmission line } m \\ 0 & \text{if otherwise} \end{cases}$$

Furthermore, to capture the objective of minimizing the total number of turns, intersections and overlaps, three additional families of variables are required:

$$u_{m,k} = \begin{cases} 1 & \text{if line } m \text{ has a turn at node } k \\ 0 & \text{if otherwise} \end{cases} \qquad v_{k,\tilde{m},\bar{m}} = \begin{cases} 1 & \text{if line } \tilde{m} \text{ and line } \bar{m} \text{ has an intersection at node } k \\ 0 & \text{if otherwise} \end{cases}$$

$$o_a = \begin{cases} 1 & \text{if edge } a \text{ is repeatedly used} \\ 0 & \text{if otherwise} \end{cases}$$

In line with the above criteria 1 – 5, the objective function reads:

$$\begin{aligned}\min \quad & a\sum_{m\in M}\sum_{k\in N}u_{m,k}+b\sum_{k\in N}\sum_{\tilde{m}\in M}\sum_{\bar{m}\in M}v_{k,\tilde{m},\bar{m}}+c\sum_{a\in A,a'=-a\in A}o_a \\ & +d\sum_{s\in S}\sum_{k\in N}x_{s,k}d(s,k) \\ & +e\sum_{\bar{s}\in S}\sum_{\tilde{s}\in S}\sum_{\bar{k}\in N}\sum_{\tilde{k}\in N}1_{\{x_{\bar{s},\bar{k}}+x_{\tilde{s},\tilde{k}}-1>0\}}violation(\bar{s},\bar{k},\tilde{s},\tilde{k}) \\ & +f\sum_{m\in M}1_{\{\text{line } m \text{ is a loop}\}}\end{aligned} \tag{4.1}$$

where,

- a, b, c, d, e, f are penalties for turns, intersections, overlapping edges, deviations from actual geographic coordinates, violations of relative positions, and loops.
- $a = a'$ indicates edges a and a' share the same terminal nodes, but are in opposite directions.
- $d(s,k)$ represents the geographic distance from node k to substation s.
- $1_{\{x_{\bar{S},\bar{k}}+x_{\tilde{S},\tilde{k}}-1>0\}}$ is an indicator variable indicating whether substations $\bar{S}$ and $\tilde{S}$ are located at nodes $\bar{k}$ and $\tilde{k}$, and $violation(\bar{s},\bar{k},\tilde{s},\tilde{k}) \in \{0,1\}$ indicates whether locating substations $\bar{S}$ and $\tilde{S}$ at nodes $\bar{k}$ and $\tilde{k}$ violates their initial relative position.

Different combinations of penalties are selected according to the rank of the above criteria to achieve different objective preferences.

Note that the *sixth* component of the objective function, $f\sum_{m\in M}1_{\{\text{line } m \text{ is a loop}\}}$, is not directly linked to any decision variable and is thus much more difficult to examine in the solution process. To get around this difficulty, we replace $\sum_{m\in M}1_{\{\text{line } m \text{ is a loop}\}}$ by $\sum_{m\in M}\sum_{a\in A}y_{m,a}\text{length(a)}$ to minimize the total length of all transmission lines for the rest of this paper. Although this approximation does not necessarily give the minimal number of loops, these two are no doubt (strongly) positively correlated. Later from the computational results, we can see that it works well enough to give a practical solution.

We now list all the constraints starting with the logic ones.

$$\sum_{k\in N}x_{s,k}=1 \qquad s\in S \tag{4.2}$$

$$\sum_{s\in S}x_{s,k}\le 1 \qquad k\in N \tag{4.3}$$

$$y_{m,a}+y_{m,a'}\le 1 \qquad a\in A,\ a'=-a,\ m\in M \tag{4.4}$$

$$x_{s,k} + \sum_{a \in I_1(k) \cup I_2(k)} y_{m,a} = \sum_{a \in O_1(k) \cup O_2(k)} y_{m,a} + x_{t,k} \qquad k \in N, m = (s,t) \in M \tag{4.5}$$

$$\sum_{a \in I_1(k) \cup I_2(k)} y_{m,a} \leq 1 \qquad k \in N, m \in M \tag{4.6}$$

$$\sum_{a \in O_1(k) \cup O_2(k)} y_{m,a} \leq 1 \qquad k \in N, m \in M \tag{4.7}$$

$$\sum_{m \in M} y_{m,a} + \sum_{m \in M} y_{m,a'} - 1 \leq 2000 o_a \qquad a \in A, a' = -a \tag{4.8}$$

$$y_{m,e} + y_{m,f} - 1 \leq 2u_{m,k} \qquad k \in N,\ m \in M,\ e \in I_1(k), f \in O_2(k) \text{ or } e \in I_2(k), f \in O_1(k) \tag{4.9}$$

$$y_{\tilde{m},\tilde{e}} + y_{\tilde{m},\tilde{f}} + y_{\bar{m},\bar{e}} + y_{\bar{m},\bar{f}} - 3 \leq 4v_{k,\tilde{m},\bar{m}} \qquad k \in N,\ \tilde{m}, \bar{m} \in M,\ \tilde{e} \in I_1(k), \tilde{f} \in O_1(k),\ \bar{e} \in I_2(k), \bar{f} \in O_2(k) \text{ or } \tilde{e} \in I_2(k), \tilde{f} \in O_2(k), \bar{e} \in I_1(k), \bar{f} \in O_1(k) \tag{4.10}$$

$$x_{s,k},\ y_{m,a},\ u_{m,k},\ v_{k,\tilde{m},\bar{m}},\ o_a\ \in \{0,1\} \tag{4.11}$$

Constraints (4.2) assign each substation to a node. Constraints (4.3) and (4.4) state that we can assign at most one substation to a node and no circles (i.e., a transmission line *first* traverse from node A to B through edge a and *then* traverse back to node A through edge a') are allowed in the network. Constraints (4.5) – (4.7) model the paths (transmission lines) in the network. These paths are modeled by using the following common principles:

a. There is a single edge emanating from the origin of the path.

b. There is a single edge going into the destination of the path.

c. For the other nodes on the path, the number of edges "flowing into" the node must equal to the number of edges "flowing out of" the node.

d. The "flow-in" and "flow-out" must be less than 1.

Finally, constraints (4.8) – (4.10) link the decision variables capturing the objectives. Notice that the *fifth* term of the objective function, $1_{\{x_{\bar{s},\bar{k}} + x_{\tilde{s},\tilde{k}} - 1 > 0\}}$, is piece-wise linear. By a common trick employed in linear optimization, we can easily linearize it by introducing a dummy binary variable and adding constraints associated with it. However, we choose to leave it as (4.1) since commercial optimization software (e.g., CPLEX, gurobi) has no difficulty of handling objective function with piece-wise linear components.

Below is an example of how this model works. In Figure 5, $x_{s,7} = x_{t,19} = 1$ and all the other x's are 0. For the transmission line from node 7 to node 19 (depicted in bold), we also have $y_{m,(7,8)} = y_{m,(8,13)} =$

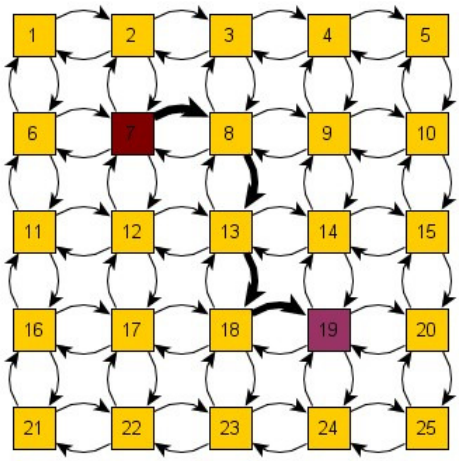

Figure 5: A Path in the Network

$y_{m,(13,18)} = y_{m,(18,19)} = 1$ and all of the remaining y's are 0. The incoming and outgoing flow modeled in (6) at nodes 7, 8, 13, 18, and 19 are 1 while for all of the remaining nodes they are 0.

4.2 Algorithms

Unfortunately, due to the size of the problem, the model developed in Section 4.1 cannot be solved to a satisfactory quality within a reasonable computational time by any existing software. Therefore in this section, a sequential routing algorithm, which does not solve the global optimization problem and hence significantly reduces the running time, is presented first. Next, two clustering-based optimization algorithms (Lagrangian relaxation based and progressive hedging based algorithms) are proposed to improve the quality of the solution due to the serious drawbacks the sequential routing approach processes. These two algorithms will decompose the problem into smaller regions and then iteratively solve the problem in each region by readjusting some selected parameters.

4.2.1 Sequential Routing Algorithm

The oldest and perhaps the most straight-forward approach to route multiple lines in a grid network is to pick an order and then route them sequentially. In this section, we develop a sequential routing algorithm based on a revised version of Dijkstra's shortest path algorithm. We will first show how to relocate each substation to a node on the grid, and then discuss the revised Dijkstra's algorithm and the routing strategy in details.

4.2.2 Locating the Substations

As we can see from (4.1) – (4.11), we create far more edge-related variables (i.e., y's and hence the associated u's, v's and o's) than node-related variables (i.e., x's) in the process of solving the optimization problem. Therefore, it is natural to ask whether the problem is solvable if only node-related variables are considered. Not surprisingly, the answer is *yes*. This implies that we can solve the problem in a hierarchical manner: *first* locate each substation by solving a simpler optimization problem and *then* route the transmission lines given the coordinate of each substation.

Below is the optimization problem we use to locate the substations:

$$\min \quad \sum_{s\in S}\sum_{k\in N} x_{s,k}d(s,k) \tag{4.12}$$

subject to

$$\sum_{k\in N} x_{s,k} = 1 \qquad s \in S \tag{4.13}$$

$$\sum_{s\in S} x_{s,k} \leq 1 \qquad k \in N \tag{4.14}$$

$$\big(x_{\bar{s},\bar{k}} + x_{\tilde{s},\tilde{k}} - 1\big)violation\big(\bar{s},\tilde{s},\bar{k},\tilde{k}\big) \leq 0 \qquad \bar{s},\tilde{s} \in S,\ \bar{k},\tilde{k} \in neighbor(\bar{s}), neighbor(\tilde{s}) \tag{4.15}$$

$$x_{s,k} \in \{0,1\} \tag{4.16}$$

In this fashion, we must also ensure that the substations do not deviate too much from the actual geographic coordinates. And this can be easily done by setting $x_{s,k} = 0$ for all nodes k with distance $d(s,k) \geq L$ where L is a threshold.

Notice that instead of minimizing the total violations of relative geographic relationships as we did in (4.1), a set of constraints (4.15) are introduced so that for each pair of substations $\bar{s}$ and $\tilde{s}$, any possible violations caused by relocating $\bar{s}$ and $\tilde{s}$ within their neighborhoods are forbidden. This will prevent most of the violations because according to the objective function (4.1), substations will most likely be relocated within the nearest neighborhoods. Thus, we make this compromise to avoid 'billions of'associated constraints and hence significantly reduce the running time.

4.2.3 Revised Dijkstra's Shortest Path Algorithm

In section 4.2.2, we have located each substation to a node on the grid. The next move will be routing the transmission lines to capture the rest components of the objective function: minimization of the total

number of turns, intersections, overlapping edges, and the total length of all the transmission lines. To do so, we first introduce the following revised Dijkstra's shortest path algorithm, which performs exactly the same as the general Dijkstra's algorithm, except that each time when we consider all the unvisited neighbors of a visited node and update the tentative distances, we need to trace back to the second last node along the current shortest path to check for turns and intersections. For more details about Dijkstra's algorithm, we refer the readers to [36].

Algorithm 1 The Revised Dijkstra's Shortest Path Algorithm

```
1: Initialize dist[s] ⟵ 0
2: for each v ∈ V − {s} do
3:    dist[s] ⟵ ∞
4: end for
5: S ⟵ ∅
6: Q ⟵ V
7: while Q ≠ ∅ do
8:    u ⟵ minimum distance(Q, dist)
9:    S ⟵ S ∪ {u}
10:   for each v ∈ neighbors[u] do
11:      // Check the occurrence of turns or intersections
12:      if a turn or intersection is incurred then
13:         // Update the tentative distance
14:         if dist[v] > dist[u] + w(u, v) + a(or b) then
15:            dist[v] ⟵ dist[u] + w(u, v) + a(or b)
16:         end if
17:      else
18:         // Update the tentative distance
19:         if dist[v] > dist[u] + w(u, v) then
20:            dist[v] ⟵ dist[u] + w(u, v)
21:         end if
22:      end if
23:   end for
24: end while
25: return dist
```

Since we only add two steps - checking the occurrence of turns or intersections - in each iteration of the general Dijkstra's algorithm, the complexity remains the same.

We should also be aware that this revised Dijkstra's algorithm cannot guarantee an optimal solution. A graphic illustration is shown in Figure 6. Let's assume that $path[C]$ is the current revised shortest path ending at node C. According to the algorithm, when we consider the next possible node D adjacent to C, we should trace back along $path[C]$ (the thicker arrow) to node B and hence find a turn happening at C. A penalty cost associated with this turn will then be imposed on $path[D]$. However, if we can trace back to node C' rather than B, the turn penalty could be avoided and as a consequence a shorter $path[D]$ could be obtained. This looks adorable, but unfortunately, the revised Dijkstra's algorithm we just developed cannot achieve it because node C' is not on the current path.

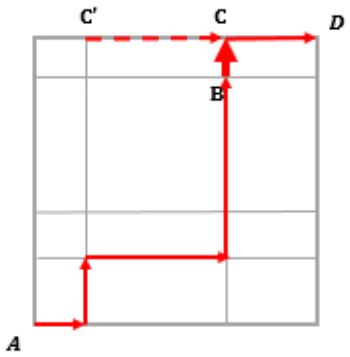

Figure 6: Counter-example of Revised Dijkstra's Algorithm

4.2.4 The Sequential Routing Algorithm

Before applying the revised Dijkstra's algorithm to the relocated substations, we should first set the weights to the edges. For each edge $a \in A$, we assign a weight $w_a := f \times length(a)$ proportional to its length. If the edge has already been used by other lines, w_a will be updated to $w_a := w_a + c$ to capture the penalty cost for overlaps. We formalize the sequential routing algorithm as below.

Algorithm 2 The Sequential Routing Algorithm

```
Initialize the embedded grid network
Locate each substation to a grid node by solving Eqn (3.1) - (3.5)
Sort transmission lines into descending order with respect to the taxicab distance between terminal
substations, let M_s denote the set of sorted lines
for k ∈ M_s do
    Call the revised Dijkstra's algorithm to generate a path P_k
    for each edge e ∈ P_k do
        if e has not been used by other lines than P_k then
            Set w_e := w_e + c
        end if
    end for
end for
```

The primary drawback of this sequential approach is that the quality of the solution highly depends on the order in which the transmission lines are processed, and there is no systematic way of finding a good order. Furthermore, the routing of lines and the relocating of substation coordinates are determined separately with respect to partial objectives, and by doing so, the correlation (or interaction) between these two families of decision variables are neglected. Later we will develop optimization based algorithms which consider locating substations and routing transmission lines simultaneouly.

Despite these drawbacks, we also see positive aspects from this approach. Since we don't have to solve the global optimization problem, the running time drops significantly. Therefore, this approach is recommended when time and computational power are highly limited. Furthermore, this approach also allows the

congestion information (e.g., turns, intersections and overlaps) for previously routed lines to be taken into consideration while routing a new line, and thus provides a descent feasible solution to the problem formulated in (4.1) – (4.11). We start from the longest line in Algorithm 2 because it has the highest probablity to intersect or overlap with subsequent lines and hence exerts the greatest influences to the following routing process.

4.3 Clustering-Based Optimization Algorithms

We start this section by introducing the following clustering algorithm with which the entire network can be decomposed into smaller solvable regions.

4.3.1 The Clustering Algorithm

We start by formally defining the grid discretization. To facilitate the solution process, it is crucial to reduce the size of the grid while at the same time generate enough grid nodes and edges to place substations and route transmission lines. In line with this purpose, the proposed clustering algorithm is designed to find the areas with highest substation densities and then create finer grids (i.e., more latitude/longitude lines) within these areas. After that, a unique distance measure, which captures both geographic distance and connectivity of the substations, is defined so that a classic *separation* algorithm (e.g., *k-means*) can be applied to achieve the following objectives:

1. **Compactness**: geographically compact substations are more likely to be in the same cluster;
2. **Connectivity**: substations with a transmission line connecting between them are more likely to be in the same cluster. Or equivalently, the algorithm should discourage intercluster lines.

The following multi-stage clustering algorithm is then developed accordingly.

1). **Group substations into clusters and generate the intial grid network.**
A simple distance matrix (i.e., using the geographic distance between each pair of substations) and the standard *k-means* algorithm are applied to divide the substations into n_1 clusters. Within each cluster, generate latitude lines according to the latitudes of the north- and south-most substations. And similarly, generate longitude lines according to the longitudes of the east- and west-most substations. This gives us the initial network grid.

2). **Find areas with the highest substation densities and then create finer discretization within these areas.**

Given the initial network grid from step 1), the number of substations in each grid square (i.e., substations falling on the grid edges are excluded) is calculated. Extra latitude and longitude lines will be created for the 10 grid squares with the highest number of substations to divide each of them into 4 equal-sized squares. Repeatedly doing so until no grid square contains more than n_2 substations.

3). **Group grid nodes into clusters.**

In order to incorporate the connectivity of substations into the clustering of grid nodes, we need the following definition of neighborhood.

Definition 4.1 *For any substation $s \in S$, the neighborhood of s is defined by the following three scenarios:*

a. *If substation s falls on the intersection of grid edges, the neighborhood of s is defined as the eight nodes surrounding s plus the node on which s falls.*

b. *If substation s falls on a single grid edge, the neighborhood of s is defined as the six nodes surrounding s.*

c. *If substation s does not fall on any grid edge, the neighborhood of s is defined as the four nodes surrounding s.*

A graphical illustration of this definition is given in Figure 7, in which the bold dot represents the geographic coordinate of a substation. To continue step 3), if two substations s and t are connected by a transmission line, the distance between any neighborhood node of s and any neighborhood node of t is defined as half of the geographic distance between them. For the remaining nodes, the distance is simply the corresponding geographic distance. With the defined distance matrix, a standard *k-means* algorithm is implemented to divide the grid nodes into n_3 clusters.

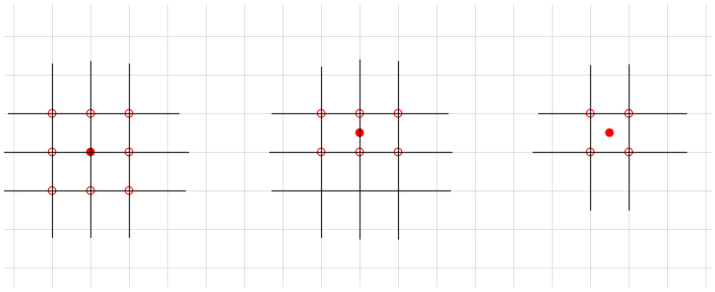

Figure 7: A Graphic Illustration of Neighborhood

4). **Reduce the number of intercluster edges (i.e., edges connecting nodes from different clusters).**

Since later iterative algorithms such as Lagrangain relaxation and progressive hedging based algorithm are to be implemented, in which all constraints at the intercluster edges will be relaxed, the clustering

algorithm should minimize the total number of such edges to improve the quality of the solution. Therefore, a local search algorithm based on tabu-search to reduce the number of these edges is the final step of our clustering algorithm. For details of tabu-search and its application, we refer readers to [37, 38].

In the above 1) - 4), n_1, n_2 and n_3 are selected parameters to control the density of the grid discretization.

4.3.2 Two Clustering-Based Algorithms

4.3.2.1 Lagrangian Relaxation Based Algorithm

Lagrangian relaxation is a common approach of solving difficult problems, such as the large-scale integer programming model formulated in Section 2. The basic principle of Lagrangian relaxation is that the relaxed problem should be solved very easily for fixed values of Lagrange multipliers. Since by applying the clustering technique we just developed, the entire network can be decomposed into smaller regions and the subproblem within each region can be solved in seconds, relaxing constraints at the boundaries (e.g., the edges connecting nodes from different clusters) and solving the problem separately in each region is a natural starting point.

In this section, we first reformulate the problem so that the interior network and the boundaries are modeled separately and hence the boundary-related constraints could be relaxed regardless of the interior constraints. An iterative algorithm will then be developed to solve the corresponding Lagrangian-dual.

4.3.2.1.1 The Model

To formulate the problem in a decomposed network, we introduce the following region specific notations:

- Let S_i be the set of substations located in region i, $i = 1, ..., n$. $S = S_1 \cup \dots S_n$.
- Let A_i be the set of interior edges in region i and $A_{i,j}$ be the set of intercluster edges starting from region i to an adjacent region j. $\bar{A}_i = A_i \cup \bigcup_{j \in adj(i)} A_{i,j} \cup \bigcup_{j \in adj(i)} A_{j,i}$ denotes all the edges related to region i.
- Let N_i be the set of interior nodes in region i and N_i' be the set of boundary nodes in region i. Interior nodes are connected only by interior edges, and boundary nodes are connected by intercluster edges.
- Let M_i be the set of interior transmission lines in region i, whose terminal substations are both located in region i. Let $M_{i,j}$ be the set of intercluster transmission lines starting from region i to an adjacent region j. Similarly, $\bar{M}_i = M_i \cup \bigcup_{j \in adj(i)} M_{i,j} \cup \bigcup_{j \in adj(i)} M_{j,i}$ denotes all the lines related to region i.
- Let $I_1^i(k), O_1^i(k)$ be the set of all incoming, outgoing horizontal edges of node k within region i.

· Let $I_2^i(k), O_2^i(k)$ be the set of all incoming, outgoing vertical edges of node k within region i.

The complete formulation is overwhelmingly long (shown in Appendix A), but fortunately very similar to the original form in Section 4.1. In particular, the decision variables remain the same, and the objective function only needs slight modification to adjust within each smaller region.

$$\begin{aligned}\min \quad & a\sum_i \sum_{m\in\bar{M}_i} \sum_{k\in N_i\cup N_i'} u_{m,k} + b\sum_i \sum_{k\in N_i\cup N_i'} \sum_{\tilde{m}\in\bar{M}_i} \sum_{\bar{m}\in\bar{M}_i} v_{k,\tilde{m},\bar{m}} + c \sum_{a\in A, a'=-a\in A} o_a \\ & + d\sum_i \sum_{s\in S_i} \sum_{k\in N_i\cup N_i'} x_{s,k} d(s,k) \\ & + e\sum_i \sum_{\bar{s}\in S_i} \sum_{\tilde{s}\in S_i} \sum_{\bar{k}\in N_i\cup N_i'} \sum_{\tilde{k}\in N_i\cup N_i'} 1_{\{x_{\bar{s},\bar{k}}+x_{\tilde{s},\tilde{k}}-1>0\}} violation(\bar{s},\bar{k},\tilde{s},\tilde{k}) \\ & + e\sum_i \sum_{\bar{s}\in S_i} \sum_{\tilde{s}\in S\setminus S_i} \sum_{k\in N_i\cup N_i'} x_{\bar{s},\bar{k}} violation(\bar{s},\bar{k},\tilde{s}) + f\sum_{m\in M}\sum_{a\in A} y_{m,a}\text{length}(a)\end{aligned} \tag{4.17}$$

As we can see from (4.17), the *fifth* objective of (4.1) has been replaced by two components to indicate: (1) whether locating substations $\bar{s}$ and $\tilde{s}$ at nodes $\bar{k}$ and $\tilde{k}$ in the same region i violates their initial relative position; and (2) whether locating substation $\bar{s}$ at node $\bar{k}$ violates the relative position between $\bar{s}$ and the other substations outside region i.

The constraints are formulated separately for interior network and boundaries. To model the interior network, we need to adapt (4.2) - (4.4) and (4.6) - (4.8) within each region; and to deal with the boundaries, we need to split (4.5) into the following two types.

1. Interior lines whose terminal substations are located in the same region i are modeled in the same way as (4.5).

$$x_{s,k} + \sum_{a\in I_1^i(k)\cup I_2^i(k)} y_{m,a} = \sum_{a\in O_1^i(k)\cup O_2^i(k)} y_{m,a} + x_{t,k} \qquad k\in N_i\cup N_i',\ m=(s,t)\in M_i \tag{4.18}$$

2. To handle the intercluster lines whose terminal substations are located in two adjacent regions i and j, we should first route the line separately in i and j to a boundary node, and then connect them through the intercluster edge between the boundary nodes.

$$x_{s,k} + \sum_{a\in I_1^i(k)\cup I_2^i(k)} y_{m,a} = \sum_{a\in O_1^i(k)\cup O_2^i(k)} y_{m,a} \qquad k\in N_i,\ m=(s,t)\in \bigcup_{j\in adj(i)} M_{i,j} \tag{4.19}$$

$$x_{t,k} + \sum_{a\in O_1^i(k)\cup O_2^i(k)} y_{m,a} = \sum_{a\in I_1^i(k)\cup I_2^i(k)} y_{m,a} \qquad k\in N_i,\ m=(s,t)\in \bigcup_{j\in adj(i)} M_{j,i} \tag{4.20}$$

$$x_{s,p} + \sum_{e\in I_1^i(p)\cup I_2^i(p)} y_{m,e} = y_{m,a} + \sum_{e\in O_1^i(p)\cup O_2^i(p)} y_{m,e} \qquad m=(s,t)\in \bigcup_{j\in adj(i)} M_{i,j} \tag{4.21}$$

$$x_{t,p} + \sum_{e \in O_1^i(p) \cup O_2^i(p)} y_{m,e} = y_{m,a'} + \sum_{e \in I_1^i(p) \cup I_2^i(p)} y_{m,e} \qquad m = (s,t) \in \bigcup_{j \in adj(i)} M_{j,i} \tag{4.22}$$

$$y_{m,a} + \sum_{e \in O_1^i(p) \cup O_2^i(p)} y_{m,e} \leq 1 \qquad m = (s,t) \in \bigcup_{j \in adj(i)} M_{i,j} \tag{4.23}$$

$$y_{m,a'} + \sum_{e \in I_1^i(p) \cup I_2^i(p)} y_{m,e} \leq 1 \qquad m = (s,t) \in \bigcup_{j \in adj(i)} M_{j,i} \tag{4.24}$$

where $a = (p,q) \in A_{i,j}$ and $a' = (q,p) \in A_{j,i}$ are intercluster edges.

Next, we need to link the variables capturing the objectives. To model turns and intersections which do not involve intercluster edges, the constraints remain the same as (4.9) and (4.10). On the other hand, to model turns and intersections constructed by intercluster edges, we need to introduce the following constraints. More specifically, if $a = (p,q)$ is an intercluster edge starting from region i, we have the following:

$$y_{m,a} + y_{m,e} - 1 \leq 2u_{m,p} \qquad m \in \bigcup_{j \in adj(i)} M_{i,j},\ e \in I_1^i(p) \text{ or } I_2^i(p) \tag{4.25}$$

$$\begin{aligned} y_{\tilde{m},a} + y_{\tilde{m},\tilde{e}} + y_{\bar{m},\bar{e}} + y_{\bar{m},\bar{f}} - 3 \leq 4v_{p,\tilde{m},\bar{m}} \qquad & \tilde{m} \in \bigcup_{j \in adj(i)} M_{i,j},\ \bar{m} \in \bar{M}_i, \\ & \tilde{e} \in I_1^i(p),\ \bar{e} \in I_2^i(p),\ \bar{f} \in O_2^i(p) \text{ or} \\ & \tilde{e} \in I_2^i(p),\ \bar{e} \in I_1^i(p),\ \bar{f} \in O_1^i(p) \end{aligned} \tag{4.26}$$

Similarly, if $a' = (q,p)$ is an intercluster edge going into region i, we have the following:

$$y_{m,a'} + y_{m,e} - 1 \leq 2u_{m,p} \qquad m \in \bigcup_{j \in adj(i)} M_{j,i},\ e \in O_1^i(p) \text{ or } O_2^i(p) \tag{4.27}$$

$$\begin{aligned} y_{\tilde{m},a'} + y_{\tilde{m},\tilde{e}} + y_{\bar{m},\bar{e}} + y_{\bar{m},\bar{f}} - 3 \leq 4v_{p,\tilde{m},\bar{m}} \qquad & \tilde{m} \in \bigcup_{j \in adj(i)} M_{j,i},\ \bar{m} \in \bar{M}_i, \\ & \tilde{e} \in O_1^i(p),\ \bar{e} \in I_2^i(p),\ \bar{f} \in O_2^i(p) \text{ or} \\ & \tilde{e} \in O_2^i(p),\ \bar{e} \in I_1^i(p),\ \bar{f} \in O_1^i(p) \end{aligned} \tag{4.28}$$

Finally, we should be aware that this reformulated model cannot capture those transmission lines going across more than two regions, and hence is not equivalent to the original model. We define these lines as *jump lines* to indicate that they can *jump* over an (or several) entire region(s). Fortunately, the jump lines only account for less than 5% of all the transmission lines, so they can be well taken care of by some simple heuristic (e.g., sequential routing) after the majority others are processed.

To obtain the Lagrangian relaxation, all the constraints related to the intercluster edges are relaxed. For each intercluster edge a, λ_a is the Lagrange multiplier for constraint (4.8) and $\lambda_{m,a}^1,\ \lambda_{m,a}^2,\ \lambda_{m,a}^3,\ \lambda_{m,a}^4$ are

for constraints (4.21) – (4.24). Moreover, multipliers $\lambda^5_{m,a}$, $\lambda^6_{m,a}$, $\lambda^7_{m,a}$, $\lambda^8_{m,a}$, $\lambda^9_{m,a}$, $\lambda^{10}_{m,a}$ $\lambda^{11}_{m,a}$, $\lambda^{12}_{m,a}$ are for constraints (4.25) – (4.28) since each of them consists of two different scenarios.[1] The complete form of the Lagrangian relaxation problem can be found in the Appendix.

4.3.2.1.2 The Algorithm

~

In this section, an iterative algorithm is proposed to solve the formulated Lagrangian-dual, in which we improve the handling of intercluster lines through the notion of penalties that encourage these lines to be more compatible at boundaries in each iteration. A brief graphical explanation is provided below in Figure 8. As we can see along the first arrow, after a number of iterations, the intercluster line (s, t) (i.e. **BLACK** line) is more compatible at the boundary. And after more iterations, (s, t) is fully connected at the boundary.

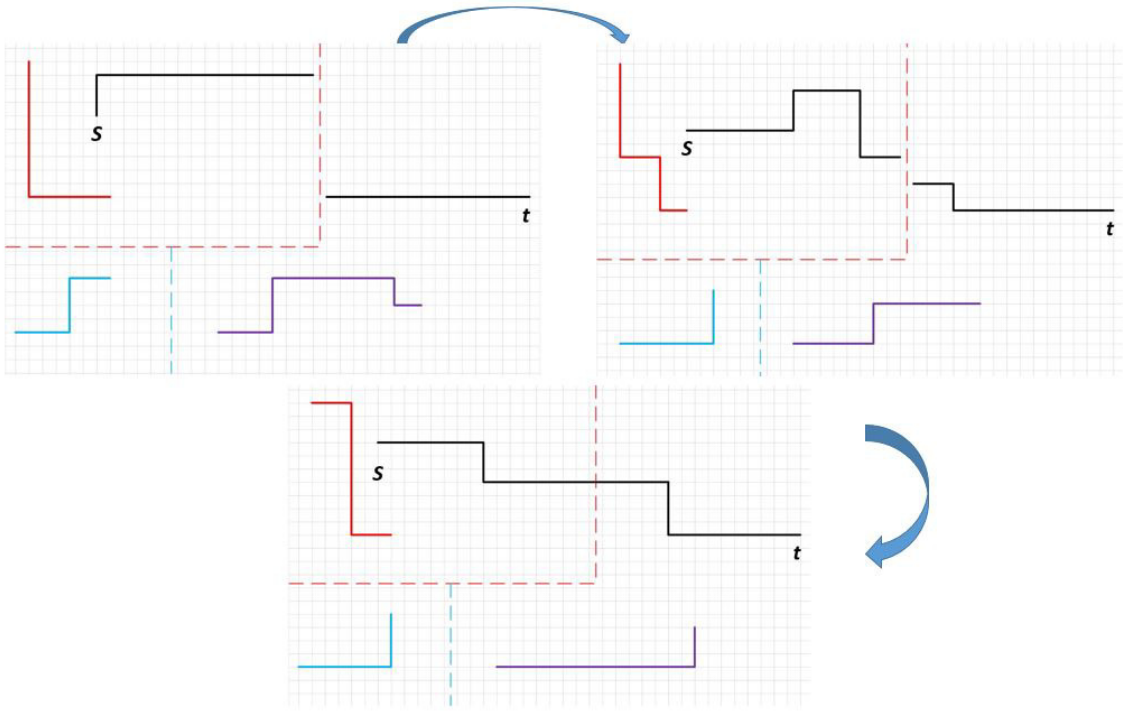

Figure 8: Graphic Illustration of the Iterative Algorithm

With the grid nodes being clustered into n regions, the following gradient optimization procedure is implemented to solve the Lagrangian relaxation problem.

1) **Group substations into n regions.**

Note that the clustering algorithm is performed on the grid network (i.e., nodes) rather than on the

[1] If edge a falls on the borderline of the entire grid network, each of the constraints (4.25) – (4.28) consists of only one scenario.

substations. Therefore, in order to assign each substation into a region, we have to construct a link between substations and nodes. A natural way of building such a link is to borrow (4.12) – (4.16) from Section 4.2.2 to initially locate each substation s to a node k. Then s can be assigned to the region which k belongs to.

2) **Solve the relaxed problem.**

Since all the constraints related to the intercluster edges are relaxed, the problem decomposes into n smaller subproblems, which can be readily solved independent of each other. Furthermore, for fixed values of Lagrange multipliers, the problem at the boundaries (i.e., solution for $y_{m,a}$) can be determined by the following very simple rule: if $\lambda_a + \sum_{i=3}^{12} \lambda_{m,a}^i - \sum_{i=1}^{2} \lambda_{m,a}^i + f \text{ length}(a) > 0$, $y_{m,a} = 0$; otherwise, $y_{m,a} = 1$. We could then compute the gradients within each region. For example, in region i, the gradients of constraint (4.25) is computed as $y_{m,a} + y_{m,e} - 1 - 2u_{m,p}$ right after the subproblem is solved.

3) **Find a primal feasible solution related to the Lagrangian solution.**

The values that result from solving the subproblems are not likely to be feasible for the original problem. However, we can readily find a feasible solution from these values by the following simple heuristic.

a. For any $m = (s, t)$, if both s and t are in the same region, we will locate the substations and route the lines according to the solutions from solving the subproblems.

b. For any $m = (s, t)$, if s and t are not in the same region, we will first locate the substations according to the solutions from solving the subproblems and then find a shortest path between s and t using the revised Dijkstra's algorithm. The edge weights are set in the same way as Section 4.3 and furthermore, to avoid routing the lines across the boundaries, we set the weights of intercluster edges (i, j) as $w_{i,j} = 100\times$(geographic distance between i and j).

The order of processing is determined by the value of $\sum_a(\sum_{i=3}^{12} \lambda_{m,a}^i - \sum_{i=1}^{2} \lambda_{m,a}^i)$, where a is any intercluster edge, which indicates the *level of difficulty* to pass through the boundaries for each transmission line m. In particular, if $\sum_a(\sum_{i=3}^{12} \lambda_{m_1,a}^i - \sum_{i=1}^{2} \lambda_{m_1,a}^i) > \sum_a(\sum_{i=3}^{12} \lambda_{m_2,a}^i - \sum_{i=1}^{2} \lambda_{m_2,a}^i)$, m_1 will be routed before m_2. Notice that this order does not necessarily guarantee the best solution, and there is nothing wrong to pick an alternative such as routing the lines in terms of their length.

4) **Update the Lagrange multipliers.**

First, we need to compute a stepsize $t^{(n)}$. An increasing $t^{(n)} = a_0 \times a_1^n$ at the n^{th} iteration of the Lagrangian procedure is chosen for this problem, where a_0 and a_1 are random variables between (0, 2). The Lagrange multipliers are then updated using the gradient method: $\lambda^{(n+1)} = \lambda^{(n)} + t^{(n)}$(gradient).

5) **Termination.**

Since it is practically impossible to run the iterative algorithm to convergence and the objective value is

observed to improve (decrease) dramatically in the first several iterations of the Lagrangian algorithm, it is reasonable to run the program a prescribed number of iterations.

We formalize the Lagrangian relxation based algorithm as below.

Algorithm 3 The Lagrangian Relxation Based Algorithm

1: Decompose the network grid into n regions
2: Group substations into n regions
3: Temporarily remove all the jump lines from the network
4: Initialize Lagrange multipliers, and parameters $a_0,\ a_1$
5: Set $k := 1$
6: **for** each $i \in 1, ..., n$ **do**
7: Solve the Lagrangian relaxation subproblem in region i
8: Compute the gradients related to the subproblem in region i
9: **end for**
10: Set $lowerbound := current\ solution\ from\ solving\ the\ subproblems$
11: Construct a feasible solution based on the current solution and set $upperbound := feasible\ solution$
12: Update step size: $t^{(k)} = a_0 \times a_1^k$
13: Update Lagrange multipliers: $\lambda^{(k+1)} = \lambda^{(k)} + t^{(k)}$(gradient)
14: Set $k := k + 1$
15: **if** $k \geq num$ or $\|upperbound - lowerbound\| \longleftarrow 0$ **then**
16: Stop
17: **else**
18: Go to step 6
19: **end if**
20: Call algorithm 1 to route jump lines sequentially

4.3.2.2 The Progressive Hedging Based Algorithm

When confronted with a very large or difficult mixed-integer programming problem for which there exist effective algorithms to solve individual scenarios, the Progressive Hedging (PH) method proposed by Rockafellar and Wets [35] could be leveraged. According to [39, 40, 41], in the presence of discrete variables, progressive hedging can be effectively used as a heuristic. Therefore, in this section we develop a PH based algorithm by taking the subproblem in each region as a scenario. Unlike the Lagrangian relaxation approach in which intercluster edges do not belong to any region, the PH approach decomposes the network in such a way that each region includes intercluster edges either originating from the region or going into it.

4.3.2.2.1 The Model

The notations and decision variables are defined in the same way as the Lagrangian approach, except that within each region the interior nodes and boundary nodes are no longer differentiated. Thus, N_i denotes all the nodes in region i. In addition, since each intercluster edge belongs to two adjacent regions (i.e., two scenarios), we have two scenario-dependent solutions, denoted as $y^i_{m,a}$ and $y^j_{m,a}$, for each pair of adjacent

regions (i, j). In order to consolidate the scenario-dependent solutions to an implementable solution, we must force them to be equal.

The objective function is different from (3.6) since we have to take scenarios into considerations as below.

$$\min \sum_i Q_1^i + 0.5 \sum_i Q_2^i \tag{4.29}$$

where Q_1^i's do not depend on the scenario explicitly but Q_2^i's do. Suitable choices for Q_1^i and Q_2^i are:

$$\begin{aligned} Q_1^i = {} & a \sum_{m \in \bar{M}_i} \sum_{k \in N_i} u_{m,k} + b \sum_{k \in N_i} \sum_{\tilde{m} \in \bar{M}_i} \sum_{\bar{m} \in \bar{M}_i} v_{k,\tilde{m},\bar{m}} + c \sum_{a \in A_i, a' = -a \in A_i} o_a \\ & + d \sum_{s \in S_i} \sum_{k \in N_i} x_{s,k} d(s,k) \\ & + e \sum_{\bar{s} \in S_i} \sum_{\tilde{s} \in S_i} \sum_{\bar{k} \in N_i \cup N_i'} \sum_{\tilde{k} \in N_i \cup N_i'} 1_{\{x_{\bar{s},\bar{k}} + x_{\tilde{s},\tilde{k}} - 1 > 0\}} violation(\bar{s}, \bar{k}, \tilde{s}, \tilde{k}) \\ & + e \sum_{\bar{s} \in S_i} \sum_{\tilde{s} \in S \setminus S_i} \sum_{k \in N_i \cup N_i'} x_{\bar{s},\bar{k}} violation(\bar{s}, \bar{k}, \tilde{s}) + f \sum_{m \in \bar{M}_i} \sum_{a \in A_i} y_{m,a} \text{length(a)} \end{aligned}$$

$$Q_2^i = c \sum_{a \in \bar{A}_i \setminus A_i, a' = -a} o_a + f \sum_{m \in \bar{M}_i \setminus M_i} \sum_{a \in \bar{A}_i \setminus A_i} y_{m,a} \text{length(a)}$$

We assume that for each intercluster edge, the two regions to which it is connected are equally weighted.

Since the constraints are very similar to the Lagrangian approach, to save the paper from overwhelming equations, the replicate constraints will be referred back to those formulated in previous sections. To be more specific, constraints (4.2) – (4.4) and (4.6) – (4.10) are adapted for each region i, and constraints (4.18) remain the same for modeling the interior lines. The other constraints are unique to the PH approach, and thus are listed as below.

$$x_{s,k} + \sum_{a \in I_1^i(k) \cup I_2^i(k)} y_{m,a} = \sum_{a \in O_1(k) \cup O_2(k)} y_{m,a} \qquad k \in N_i,\ m = (s,t) \in \bigcup_{j \in adj(i)} M_{i,j} \tag{4.30}$$

$$x_{t,k} + \sum_{a \in O_1^i(k) \cup O_2^i(k)} y_{m,a} = \sum_{a \in I_1(k) \cup I_2(k)} y_{m,a} \qquad k \in N_i,\ m = (s,t) \in \bigcup_{j \in adj(i)} M_{j,i} \tag{4.31}$$

For each region i, we need to impose the following conditions to make the scenario-dependent solutions implementable. As we can see that if the following constraints hold, the new objective function (3.18) is equivalent to the original one.

$$(y_{m,a})^i = (y_{m,a})^j \qquad j \in adj(i),\ a \in A_{i,j},\ m \in \bigcup_j M_{i,j} \tag{4.32}$$

Similar to the formulation of Lagrangian approach in Section 3.2.2.1.1, this reformulated model cannot take

jump lines into considerations either.

4.3.2.2.2 The Algorithm

Like the Lagrangian algorithm, we should first decompose the network into n regions and assign each substation into a region by solving (4.12) – (4.16). Next, due to the model's intrinsic inability of handling jump lines, these lines should be temporarily removed before the start of the iterative algorithm and then processed after the majority others have been routed.

With these pre-processing steps accomplished, we now formalize the PH based algorithm as below, taking ρ (penalty factor), ϵ (termination factor) and num (a prescribed number of iterative execution) as inputs.

Algorithm 4 The Progressive Hedging Based Algorithm

1: Set $k := 0$
2: **for** each $i,\ i = 1, 2, ..., n$ **do**
3: Solve the subproblem and obtain $(x^i,\ y^i,\ o^i,\ u^i\ , v^i)^{(k)} := \arg min\ (Q_1^i + Q_2^i)$
4: **end for**
5: **for** two adjacent regions i and j **do**
6: **for** each intercluster edge a and intercluster line m between i and j **do**
7: $\bar{y}_{m,a}^{(k)} = 0.5(y_{m,a}^i)^{(k)} + 0.5(y_{m,a}^j)^{(k)}$,
$(w_{m,a}^i)^{(k)} = \rho[(y_{m,a}^i)^{(k)} - \bar{y}_{m,a}^{(k)}]$
8: **end for**
9: **end for**
10: Set $k := k + 1$
11: **for** each $i,\ i = 1, 2, ..., n$ **do**
12: Solve the subproblem and obtain $(x^i, y^i, o^i, u^i, v^i)^{(k)} := \arg min\ \Big(Q_1^i +$
$\sum_{m\in\bar{M}_i\setminus M_i}\sum_{a\in\bar{A}_i\setminus A_i}(w_{m,a}^i)^{(k-1)}y_{m,a}^i + \frac{\rho}{2}\sum_{m\in\bar{M}_i\setminus M_i}\sum_{a\in\bar{A}_i\setminus A_i}\|y_{m,a}^i - \bar{y}_{m,a}^{(k-1)}\|^2 + Q_2^i\Big)$ $(*)$
13: **end for**
14: Repeat 5 - 9
15: **for** each $i,\ i = 1, 2, ..., n$ **do**
16: Set $g_i^{(k)} := \sum_{m\in\bar{M}_i\setminus M_i}\sum_{a\in\bar{A}_i\setminus A_i}\|(y_{m,a}^i)^{(k)} - \bar{y}_{m,a}^{(k)}\|$
17: **end for**
18: **if** $\sum_i g_i^{(k)} < \epsilon$ or $k \geq num$ **then**
19: Stop
20: **else**
21: Go to step 10
22: **end if**
23: Construct a feasible solution based on the current solution if necessary
24: Call algorithm 1 to route jump lines sequentially

Notice that in the above algorithm ρ is a pre-selected constant and has nothing to do with decision variables or cost functions. Intensive numerical experiments have to be conducted in order to choose a suitable ρ value which leads to a high quality solution. However, examination of the weighted objective (*) suggests that relatively large ρ values are required to achieve faster improvement in a reasonable time. In

particular, an effective ρ value should be close in magnitude to the unit cost of $y_{m,a}$, $f \times length(a)$; otherwise, $w^i_{m,a}$ will yield a small fraction of (*) and the per-iteration change in the penalty terms $(w^i_{m,a})^{(k)} y^i_{m,a}$ will be small. Small changes in the penalty terms will yield little improvements in $y_{m,a}$ which in turn triggers slower PH convergence.

Therefore, based on these observations, we choose $\rho_{m,a}$ in proportion to $f \times length(a)$ as $\rho_{m,a} := \rho_0 \times (f \times length(a))$ to obtain a faster (i.e., greater improvements in each iteration) and thus better solution. ρ_0 is a constant.

4.4 Computational Results

4.4.1 Implementation

All computational experiments in this section are performed on a machine with Dual Core AMD Opteron Processor 2220 SE @ 2.8GHz, and 8GB RAM. The subproblems are solved by Gurobi optimization software. The data we used to test the algorithms is derived from the New York ISO State Electrical System Map, which represents the network of existing and proposed substations and transmission lines connecting them. In total, there are 692 substations and 809 transmission lines connecting between them. Most substations are transmission stations; while the others are generating stations. Transmission lines are located either overhead or underground, ranging from 115 to 765 kilovolts. To simplify the problem, different types of substations and transmission lines are not differentiated in our decluttering algorithms.

Through intensive computational experiments, we decided $n_1 = 35$, $n_2 = 10$ and $n_3 = 180$ to create a 72×72 grid network and then decomposed it into 180 regions. With such discretization, the major computational difficulty will be caused by the huge number of intersection-related variables. In Section 2, a binary variable $v_{k,\tilde{m},\bar{m}}$ is defined to tell whether two transmission lines $\tilde{m}$ and $\bar{m}$ intersect at a particular node k. Due to these variables, even the much smaller size subproblems become too big to be handled in a reasonable time to find a feasible solution. For example, even if we further decompose the network into, say 300 regions, so that the average number of nodes in each region is less than 20, we still cannot get a feasible solution for some of the subproblems within 20 minutes. This implies that running an iterative algorithm for only 5 iterations will be as long as 12 hours (i.e., $20 \times 300 \times 5 = 30000$ minutes $= 8.33$ hours, but we also need extra time to construct a feasible solution in each iteration, perform the clustering algorithm and assign the substations). Such a horrible time consumption will make the iterative algorithm(s) less attractive and even worse - impractical. Thus, a hierarchical approach is employed to *first* minimize the turns and *then* intersections so that each subproblem can be approximately solved in seconds. To be more specific, only the number of turns is minimized when the problem is solved in each region, and intersections will be taken care of during later step to construct a feasible solution.

Furthermore, to make the Lagrangian algorithm executable on a usual laptop with less than 4GB RAM, we did not follow the traditional '*one constraint - one multiplier*' rule but initialized a common multiplier for a set of similar constraints. Referring back to Section 3.2.2.1, $\lambda^1_{m,a}$ and $\lambda^2_{m,a}$ would be replaced by $\eta^1_{m,a}$; and $\lambda^3_{m,a}$, $\lambda^4_{m,a}$ by $\eta^2_{m,a}$. Similarly, we substituted $\lambda^5_{m,a}$, $\lambda^6_{m,a}$, $\lambda^7_{m,a}$ and $\lambda^8_{m,a}$ by $\eta^3_{m,a}$. The new gradient can be computed by taking average over each component's gradient.

Finally, due to the size and complexity of the problem, it might take *forever* for the iterative algorithm(s) to converge to the theoretical results. Fortunately, the ultimate goal of this paper is to achieve an implementable solution within a reasonable running time rather than to solve the problem to optimality, and the objective value was observed to improve (decrease) dramatically in the first 5 iterations from both algorithms. Thus, it is reasonable to run the program a prescribed number of iterations (i.e., $num = 10$) till the objective value stabilizes. And instead of seeking for an optimal solution, we only need to solve each subproblem to a relatively *good* quality (e.g., optimality gap less than 30%) in a *good* amount of time (e.g., less than 120 seconds).

4.4.2 Results

Given the above parameter estimates and implementation assumptions, Figure 9 depicts the output display from the Lagrangian algorithm (on the left, with penalties $a = b = c = d = e = 1$, $f = 1000$), and compares it with the original display (on the right). As we can see, the reduction of clutter is apparent, and the transmission lines become more traceable by naked eye. The applicability of the proposed decluttering algorithm(s) is hence demonstrated.

We then performed computational experiments with various combinations of penalty terms (i.e., *a, b, c, d, e* and *f*) to evaluate and compare the performance of each algorithm. From the results given in Table 1, we can easily see that the sequential routing algorithm grants a significant reduction in running time compared with the iterative algorithms. Furthermore, it also requires lower memory by avoiding numerous numbers of variables created in the process of solving the integer program. Therefore, the sequential routing algorithm is recommended when time and computational power are highly limited.

However, the major drawback of this sequential approach is that the quality of the solution highly depends on the order (i.e., the sequence) in which the transmission lines are routed, and unfortunately, it is hard to find a good ordering. Also, as we can see from Table 1, this solution possesses a significant number of loops (i.e. up to 25% of all the lines), which could bring in unnecessary turns and congestions and thus make the lines more difficult to trace on the display interface. In reality, such solution might be considered as *non-implementable* and subsequent post-processing algorithms to eliminate those loops should be developed.

Table 1 also suggests that as the penalty for loops (i.e., f value) gradually increases, the iterative al-

Figure 9: Comparison of Decluttering and Original Display

gorithms start to outperform the sequential routing algorithm.[2] As shown in Table 1, when $f \leq 100$, the sequential routing algorithm produces a smaller objective value and is thus superior to the iterative ones. However, when $f \geq 200$, the iterative algorithms will take over. The case when $f = 140$ is the trickiest since the PH algorithm beats the sequential routing approach while the Lagrangian algorithm loses the battle. But a thorough observation tells that the objective values output by the three algorithms are close, and thus $f = 140$ can be treated as a cutoff point of choosing the iterative algorithms over the sequential routing algorithm. In other words, if a practically *implementable* solution is to be achieved (i.e., by putting a large penalty to the loops), the iterative algorithms should be chosen.

Table 1: Comparison of the Three Decluttering Algorithms

	Performance Measure								
	Sequential Routing			**Lagrangian Relaxation**			**Progressive Hedging**		
f	**running time**	**loops**	**objectives**	**running time**	**loops**	**objectives**	**running time**	**loops**	**objectives**
1	0.45	201	8,650	5.27	8	20,319	4.16	8	17,410
10	0.44	200	10,467	5.24	3	23,794	4.20	6	21,103
100	0.41	200	28,527	6.73	1	37,820	4.90	6	33,177
140	0.41	200	36,520	7.15	0	37,158	5.21	10	35,963
200	0.41	200	48,508	7.40	0	37,436	5.16	9	36,381
1,000	0.40	199	208,518	8.17	0	37,609	5.92	2	41,522

Next, we compared the two iterative algorithms based on the performance measure given in Table 2 and

[2]As we can see, the number of loops output by the PH algorithm is not monotonically decreasing as the penalty term increases. This is because we approximated it by the total length of transmission lines to facilitate our solution process, and certainly these two are not equivalent. Fortunately, such inequivalency does not affect our conclusion in this section; and furthermore, the total length of the lines is indeed monotonically decreasing.

3. In each row of these two tables, we assigned a large penalty (i.e., set penalty 1000) to one particular objective component, and left the other objectives less penalized (i.e., set penalty to 1). The columns give the results in terms of each objective: (1) the number of turns, (2) the number of intersections, (3) the number of repeatedly used grid edges, (4) total deviations of substations from their original geographic coordinates, (5) the number of violations of pair-wise geographic relationship, (6) total length of all the rerouted transmission lines, and (7) the number of loops. Notice from Section 2 that, (6) is not a *real* objective, but an approximation of (7) to simplify the solution process. Finally, the total objective value and running time are given.[3]

Table 2: Performance Analysis of Lagrangian Algorithm

	Performance Measure								
penalties	**turns**	**intersections**	**overlaps**	**$\sum$ deviations**	**violations**	**$\sum$ length**	**loops**	**objectives**	**running time**
$a = 1000$	244	132	764	4,985	12,394	14,064	0	262,275	6.27
$b = 1000$	821	5	891	5,516	16,036	15,866	12	28,276	5.49
$c = 1000$	1,040	453	315	4,930	12,690	16,351	20	334,133	6.91
$e = 1000$	774	130	794	5,215	12,212	15,133	9	12,218,922	5.16
$f = 1000$	529	178	834	7,434	28,634	13,663	0	37,609	8.17

Table 3: Performance Analysis of PH Algorithm

	Performance Measure								
penalties	**turns**	**intersections**	**overlaps**	**$\sum$ deviations**	**violations**	**$\sum$ length**	**loops**	**objectives**	**running time**
$a = 1000$	216	134	708	4,994	12,420	14,941	2	234,258	5.19
$b = 1000$	759	8	806	4,804	11,110	14,477	10	25,489	4.19
$c = 1000$	874	419	330	4,780	11,566	15,470	18	347,657	7.32
$e = 1000$	683	151	780	5,214	10,220	15,006	10	10,226,838	4.09
$f = 1000$	471	167	854	7,804	30,226	13,653	2	41,522	5.92

As expected, assigning a larger penalty to a particular objective component gives a solution with smaller value in that regard. The only exception happens for the number of loops because clearly there is a tie between $a = 1000$ and $f = 1000$. This implies that the approximation we used in our model - the total length of all the transmission lines - is not equivalent to the number of loops. Fortunately, despite the tie, $f = 1000$ still gives a solution with the least number of loops, and hence we can say that the inequivalency does not harm the applicability of our approximation.

From Table 2 and 3, for the same combination of penalties, Lagrangian and PH algorithms output very similar results. It is not easy to distinguish them by a clear cutoff value as what we did between sequential routing and iterative algorithms. However, we can still list out a few guidelines regarding how to select an appropriate algoriothm based on the numerical results at hand. As observed from the first, second and fourth

[3]The unit of total deviations ($\sum$ deviations) and total length of all the transmission lines ($\sum$ length) is *mile*, and the unit of total running time is *hour*.

rows of each table, when a large penalty is assigned to *turns*, *intersections* or *violations*, the PH algorithm delivers a better solution (with smaller objective value) within a shorter time, and thus outperforms the Lagrangian algorithm. By a similar argument, when a large penalty is assigned to *overlaps*, we conclude that the Lagrangian algorithm performs better. Finally, when loops are penalized with $f = 1000$, a trade-off between the quality of the solution and running time is involved. We did not consider the case when $d = 1000$, because the total deviations had already been minimized when we assigned each substation into a cluster region no matter what combination of penalties is selected to solve the subproblems. Thus, the total deviations in the final solution is not (solely) determined by the ranking of the penalties, and should not be compared in the same way as the other objective components.

As shown in Figure 10, majority of the running time is spent on solving the 180 subproblems. Therefore, parallel computing has a great potential to reduce the running time by solving 2^n subproblems at the same time. Moreover, as we can see that PH algorithm spends a larger proportion of time on subproblems, it will benefit more from parallel computing.

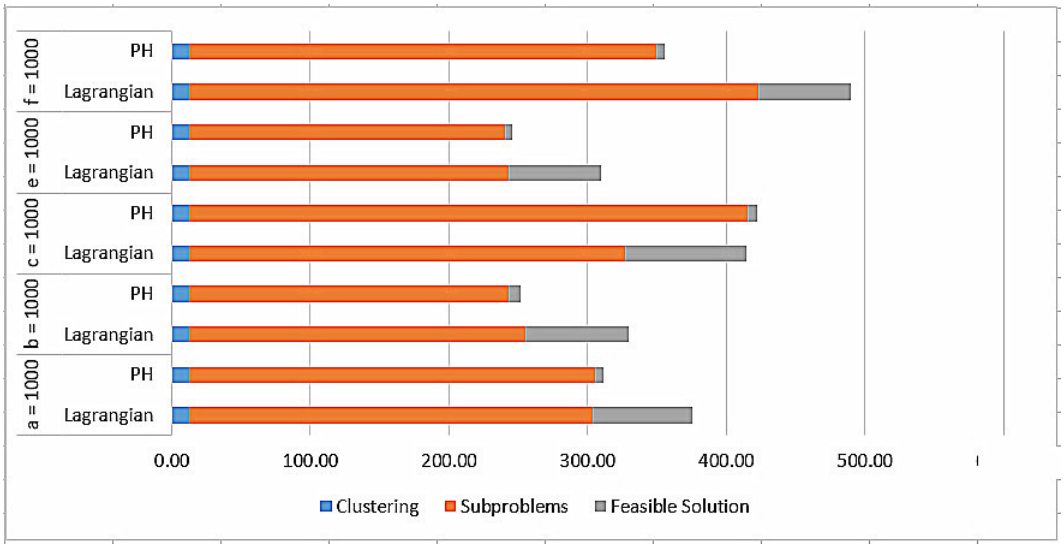

Figure 10: Running Time of Major Components in the Solution Process

4.4.3 Discussions

As we can see from Table 2 and 3, assigning a large penalty to one of the six objective components could improve (i.e., decreases) the solution in terms of that particular objective. However, it also implies that no matter how large the penalties are, we still possess quite a number of overlapping edges, deviations and violations of relative geographic locations due to the sparse grid discretization. Thus, it is worth asking what will happen to these *imperfections* if we have a finer grid discretization and enough computational power to solve the problem on this finer grid? Furthmore, what if the discretization is infinitely fine?

First of all, it is straight-forward to argue that an infinitely fine grid could effectively eliminate deviations and (or) violations of relative geographic relationship from the objective function because we can locate each substation to the node corresponding to its original position. Even if we might allow some (or all) of the substations to be slighly moved, we can still find very small, mutually exclusive neighborhoods centered at their original positions to locate them so that all relative geographic relationships are preserved. The proof is trivial and thus omitted in this paper.

Next we derive some theoretical results in terms of the number of overlaps when an infinitely fine grid is at hand. Clearly, the overlapping edges cannot be eliminated if there exists any substation connecting by more than eight transmission lines. But as we will see in the following lemma, these overlapping edges are negligible when the discretization approaches infinitely fine.

Lemma 1 *Given a finite set of substations located at the nodes of a 2D square grid. Some of these substations are connected through edges on the grid (i.e., we call them transmission lines). The minimum overlaps among all transmission lines are infinitely small; or equivalently, the total length of the overlapping edges approaches zero if the grid discretization approaches infinitely fine.*

The proof of the lemma is not trivial and can be found in the Appendix C.

4.5 Redrawn Maps

The problem turned out to be more difficult that we anticipated and its size, even for just one state (NY) area, required breaking it down to smaller pieces (a grid) manageable by the computer. A cluster-based modeling approach was used to decompose the problem into smaller regions in the grid and an iterative algorithm was implemented to solve the problem in each region by readjusting some selected parameters.

A total of 8 different solutions were created. The parameters varied to create these solutions included penalization for turns (T), penalization for line crossings (C), penalization for overlapping line segments (O), and penalization for stations deviating from its geographical coordinates (D). Below are the parameter values for each solution (Table 4) and the corresponding transmission maps (Figures 11–19).

An optimization algorithm requires solving a mathematical program, which usually yields a more accurate solution than a heuristic. This research used a mixed integer problem, which is hard and computationally very intensive to solve. Therefore, a very large (fine) grid would create too many integer variables, which in turn would require prohibitively long time to solve (20+ hours). All computational results for this research were derived on a server with Dual Core AMD Opteron Processor 2220 SE, running at 2.8GHz, and with 8 GB RAM. All the optimization problems were solved by Gurobi optimization software.

A heuristic algorithm does not solve the global mathematical program, and thus yields a much faster solution. Since the complexity drops dramatically in a heuristic approach, a finer (larger) grid may be created to improve the quality of the solution. Thus, there exists a trade-off between creating a larger (finer) grid or using a more accurate algorithm. Both will improve the quality of the solution. However, due to the computation power currently available, both of them cannot be achieved simultaneously.

Within this research, solutions 1–5 use a more accurate algorithm (with solutions 2–5 penalizing different objectives) while solutions 6 and 7 create a larger (finer) grid and use a heuristic . While the accuracy of the algorithm and the grid size trade off against each other, the first 7 solutions deliver as good solution as possible in a reasonable time. Solution 8, it uses a less accurate algorithm (i.e., a heuristic) and a smaller grid. Thus, it is just a benchmark. A full account of the algorithm development and the solutions created within this project is given in sections 4.1–4.4 above.

Table 4:
The Objectives (Parameters: Line Turns = T, Line Crossings = C, Overlapping Line Segments = O, and Deviation from True Geographic Coordinates = D) and Their Values (Penalties) for Producing Alternative Decluttering Solutions

	Parameter			
Solution	T	C	O	D
1	1	1	1	1
2	100	1	1	1
3	1	100	1	1
4	1	1	100	1
5	1	1	1	100
6	1	1	1	100
7	1	1	1	0.01
8	1	1	1	100

Note: Solution 6 was produced with a finer grid than the other solutions, as well as using a heuristic algorithm.

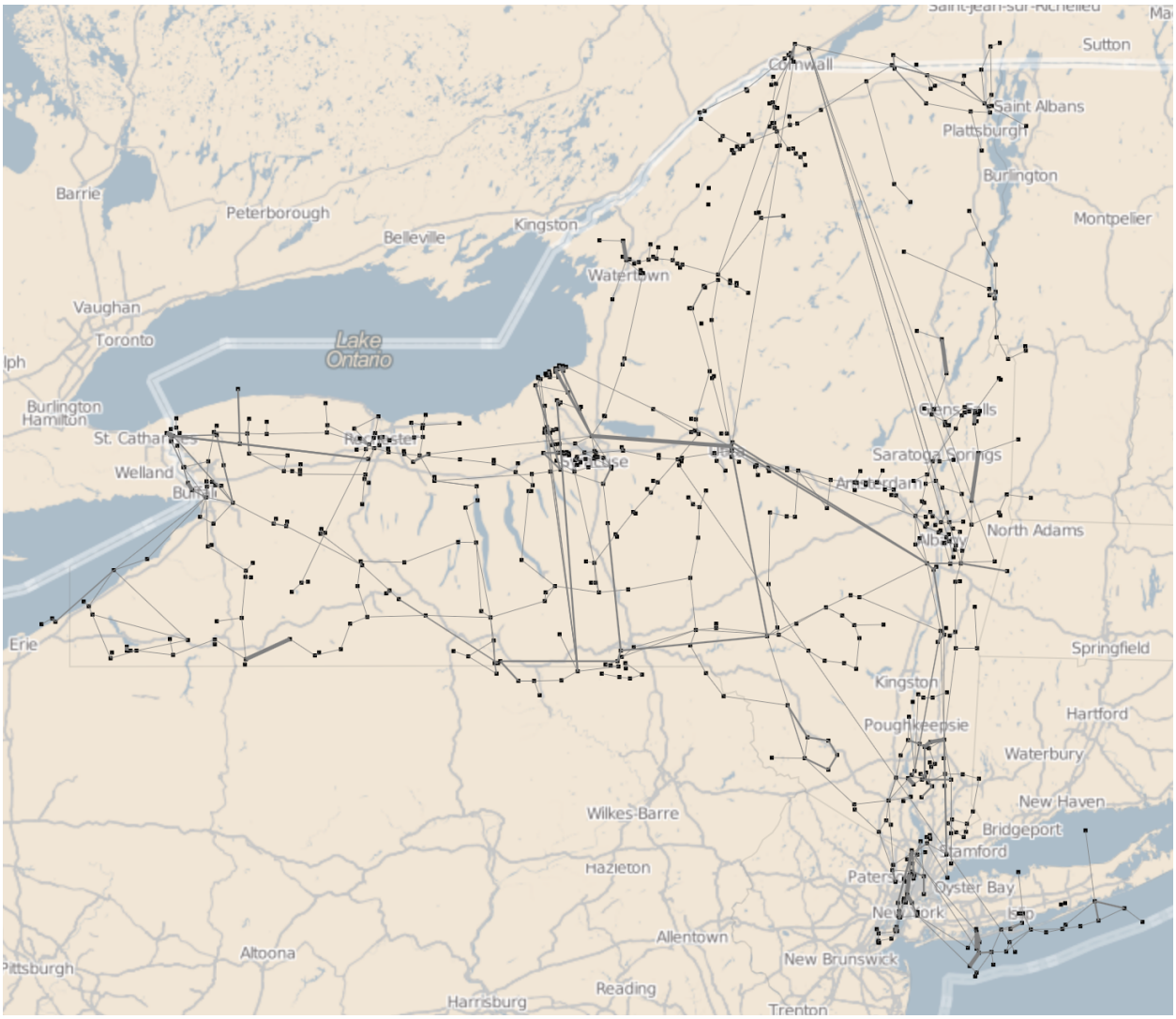

Figure 11: The baseline map was created by simply connecting the true geographic locations of the substations with straight lines representing transmission lines between substations. That the substations on Long Island are "off" is due to the fact that the substation coordinates were translated from coordinates on a PDF map to lat/long values, and that two points in the upstate region of New York were used to get a conversion factor; the Earth's curvature introduced the error seen in the southern part of the state when the grid is overlaid on a geographic map

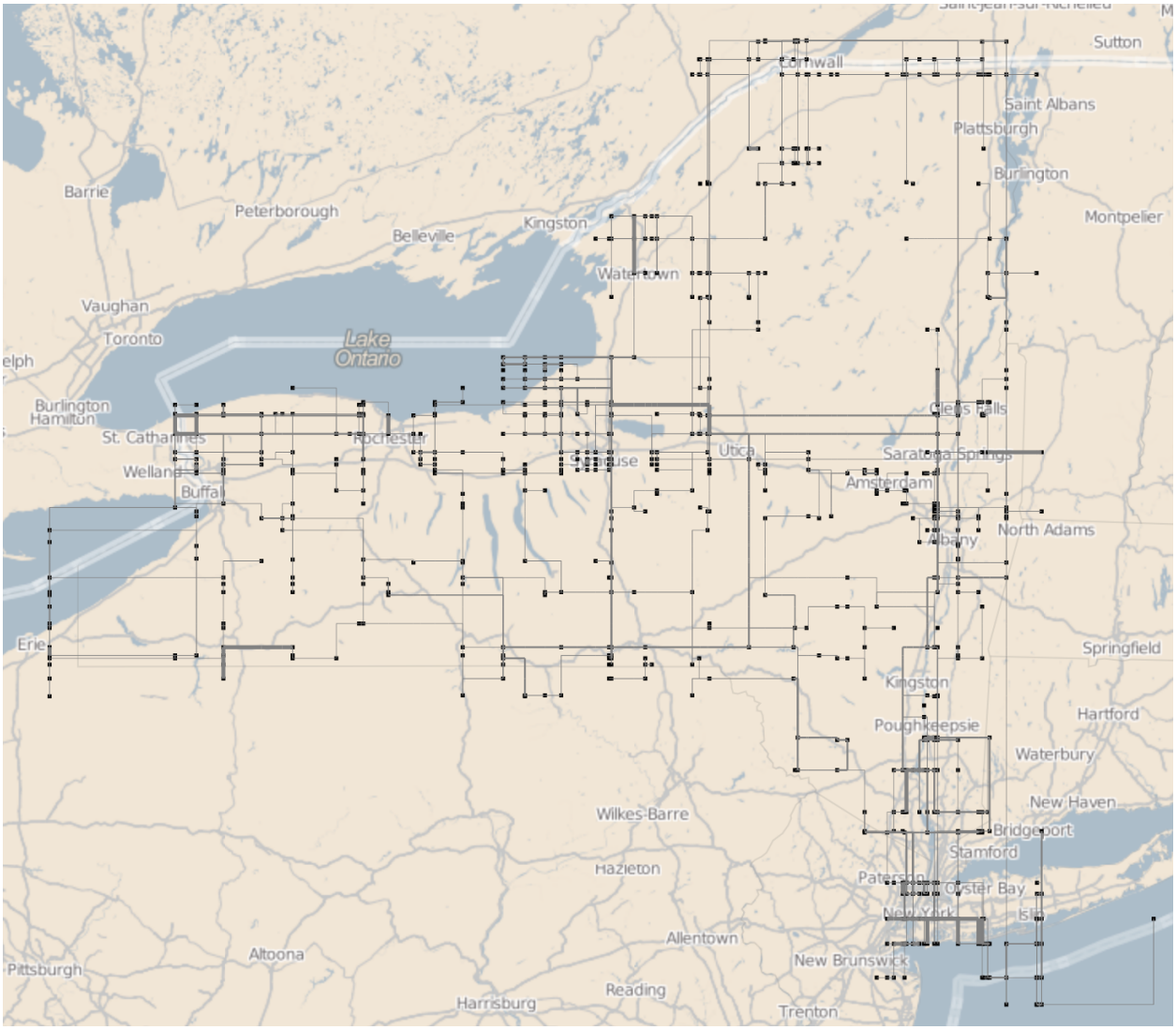

Figure 12: Solution 1, created using an accurate algorithm and a sparse grid. All objectives, line turns (T), line crossings (C), line segment overlaps (O), and deviations (D) from true geographic coordinates are equally penalized: T = C = O = D = 1

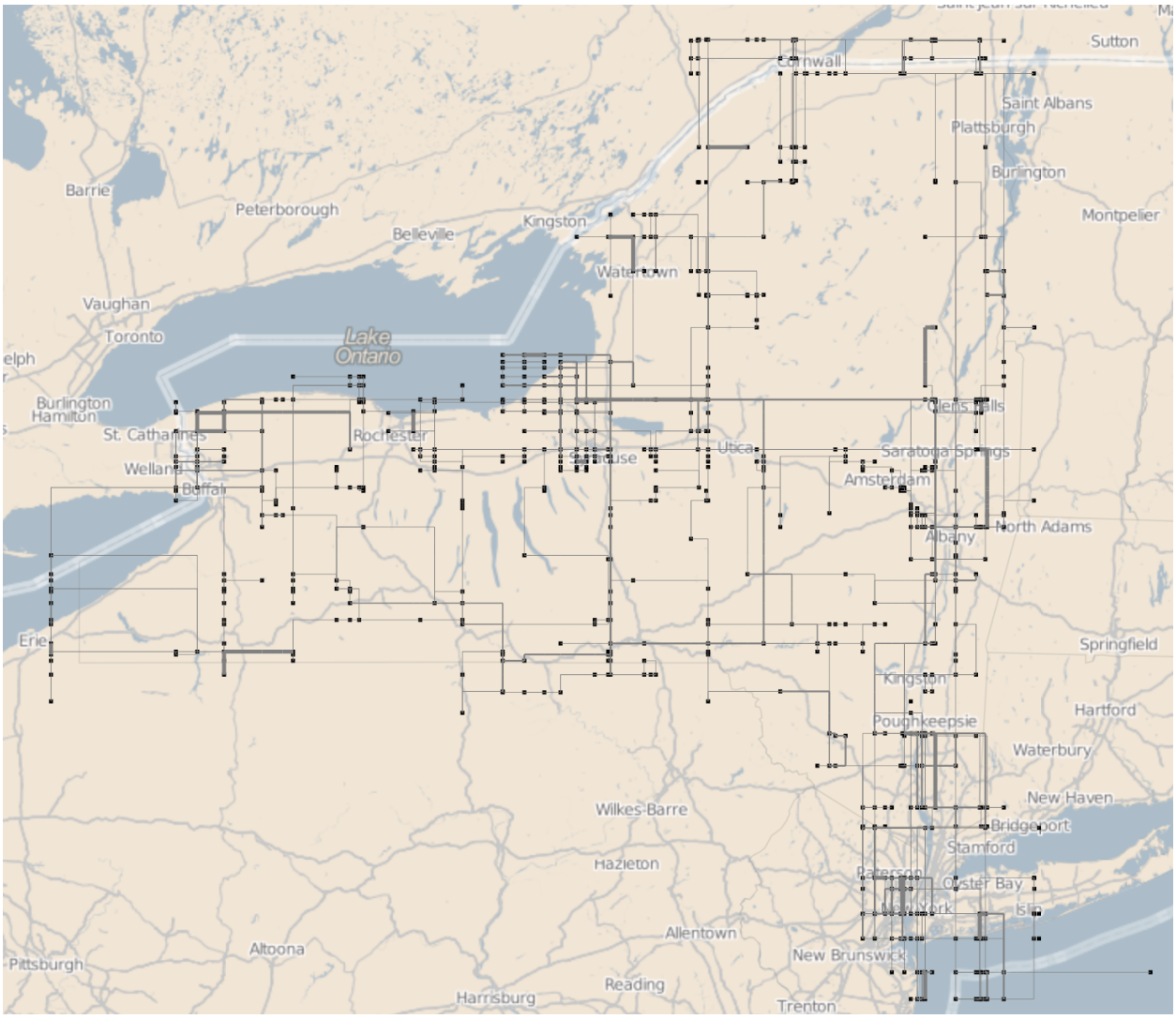

Figure 13: Solution 2, created using an accurate algorithm and a sparse grid. Line turns (T), are penalized with respect to the other objectives, line crossings (C), line segment overlaps (O), and deviations (D) from true geographic coordinates: T = 100, C = O = D = 1

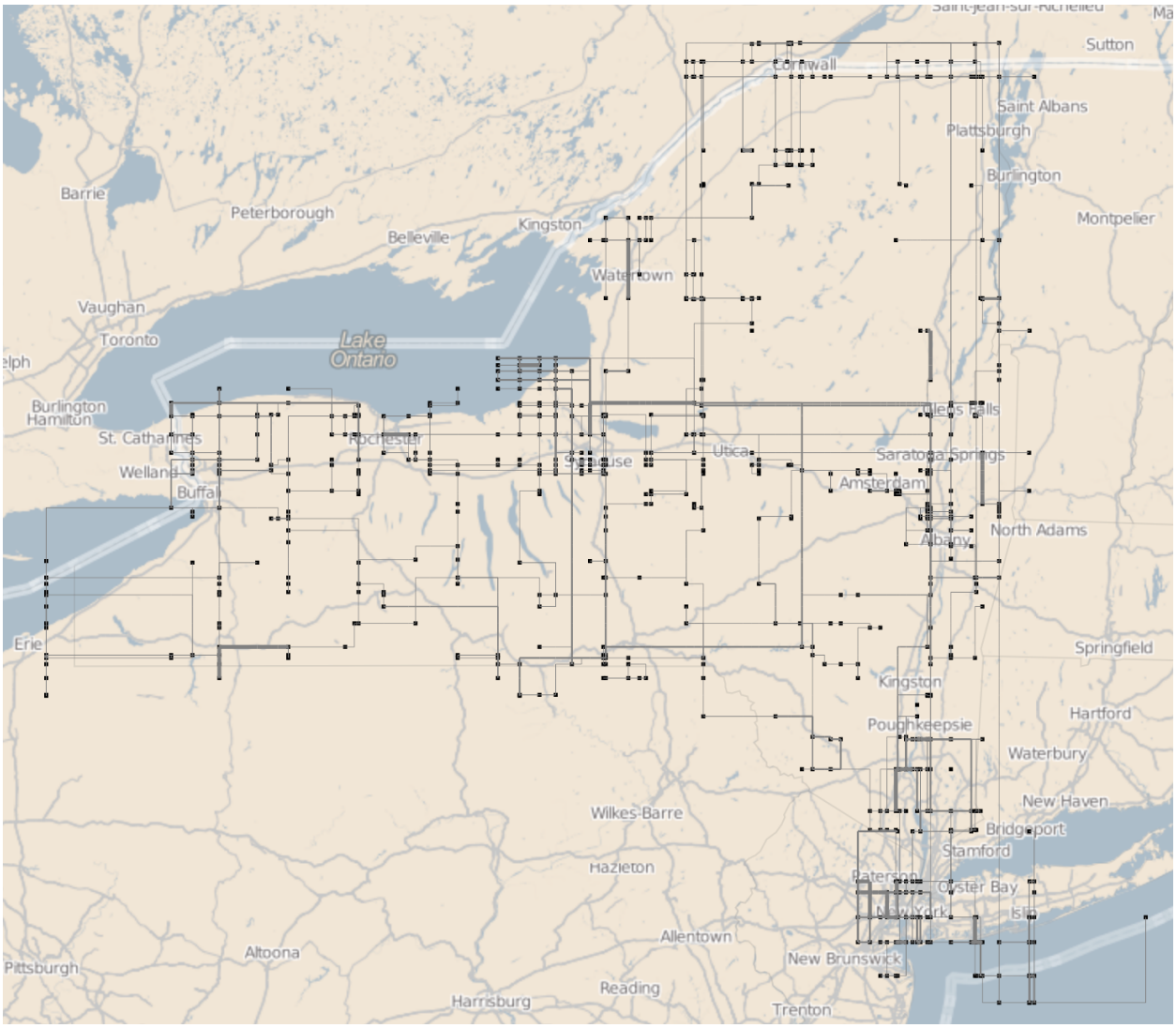

Figure 14: Solution 3, created using an accurate algorithm and a sparse grid. Line crossings (C), are penalized with respect to the other objectives, line turns (T), line segment overlaps (O), and deviations (D) from true geographic coordinates: C = 100, T = O = D = 1

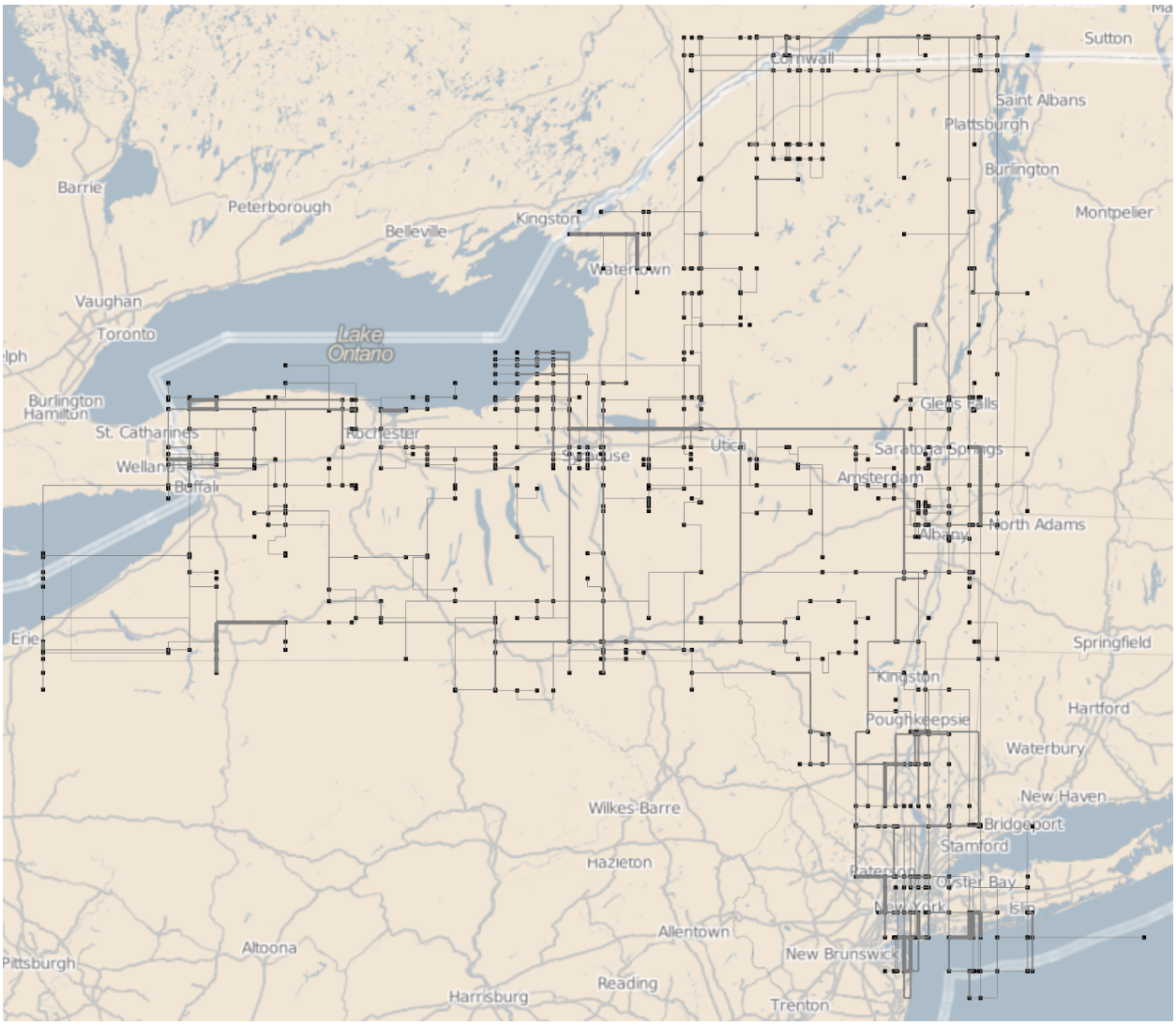

Figure 15: Solution 4, created using an accurate algorithm and a sparse grid. Line segment overlaps (O) are penalized with respect to the other objectives, line turns (T), line crossings (C), , and deviations (D) from true geographic coordinates: O = 100, T = C = D = 1

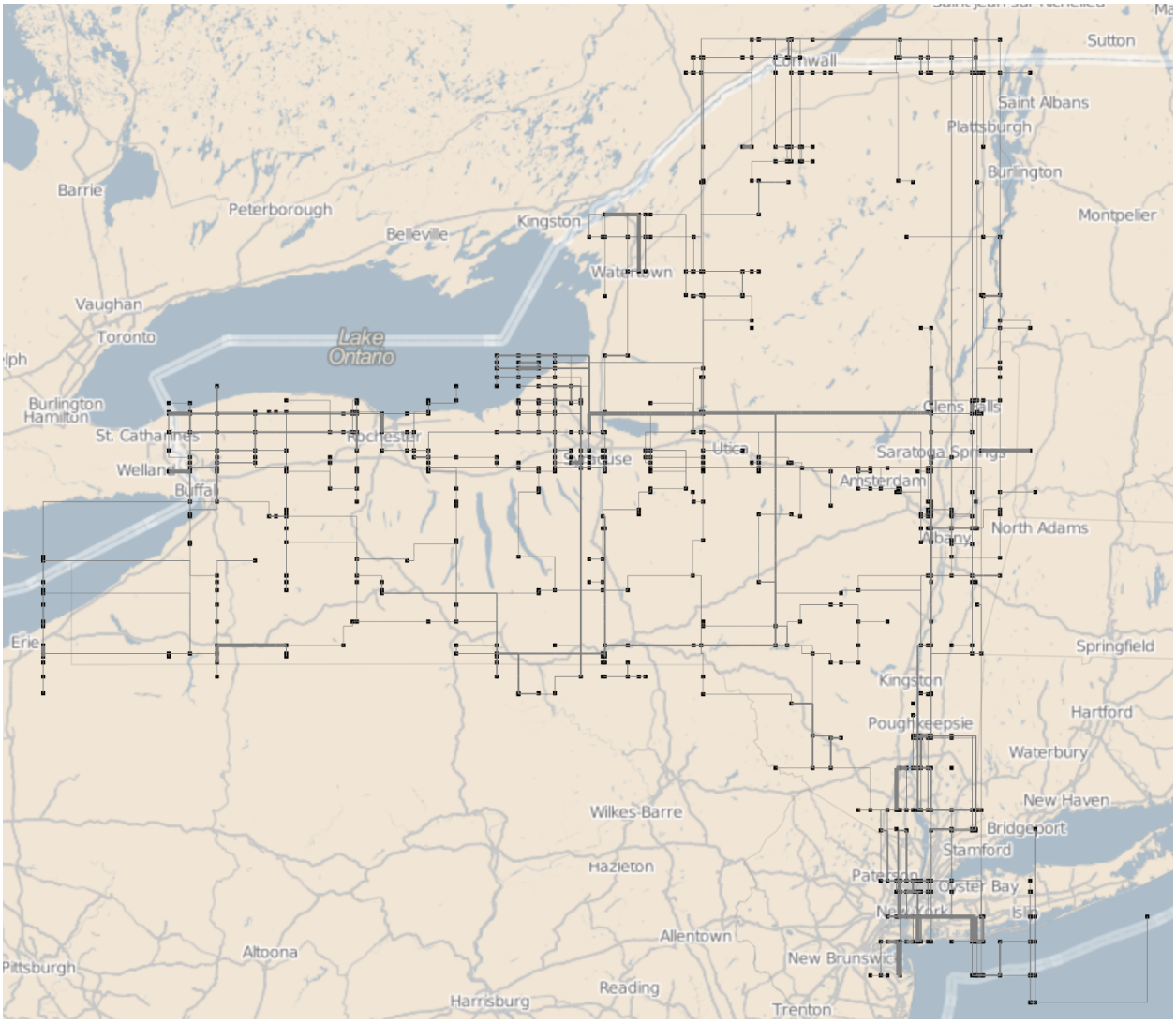

Figure 16: Solution 5, created using an accurate algorithm and a sparse grid. Deviations (D) from true geographic coordinates are penalized with respect to the other objectives, line turns (T), line crossings (C), and line segment overlaps (O): D = 100, T = C = O = 1

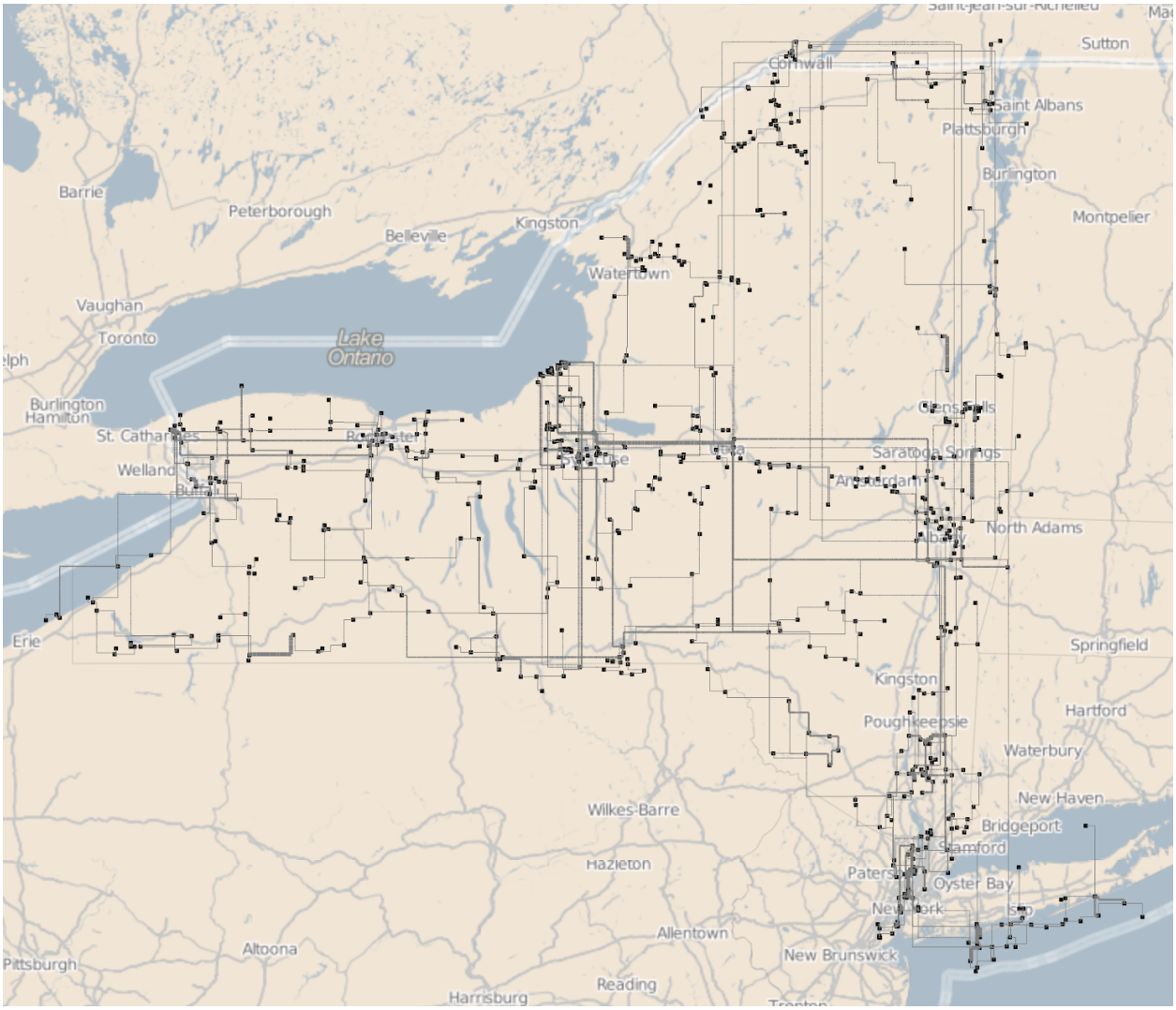

Figure 17: Solution 6, created using a less accurate algorithm and a finer grid than solutions 1–5. Deviations (D) from true geographic coordinates are strongly penalized with respect to the other objectives, line turns (T), line crossings (C), and line segment overlaps (O): D = 1000, T = C = O = 1. These parameter values are identical to those in solution 5 (Figure **??** but this solution used a finer grid and a heuristic algorithm rather than a sparse grid and an optimization algorithm used in the other solutions

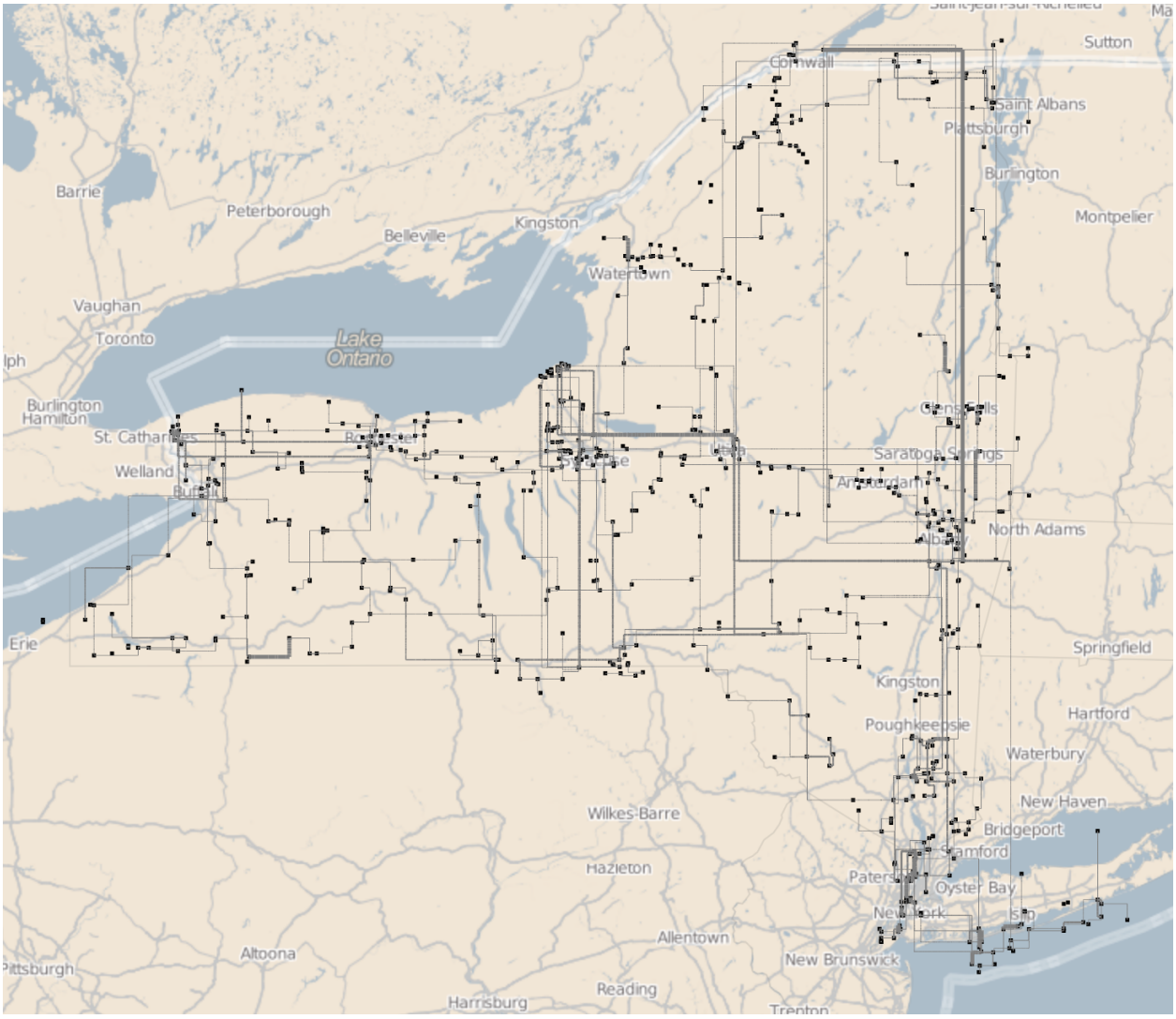

Figure 18: Solution 7, created using a less accurate algorithm and a finer grid than solutions 1–5. Deviations (D) from true geographic coordinates are weakly penalized with respect to the other objectives, line turns (T), line crossings (C), and line segment overlaps (O): D = 0.01, T = C = O = 1

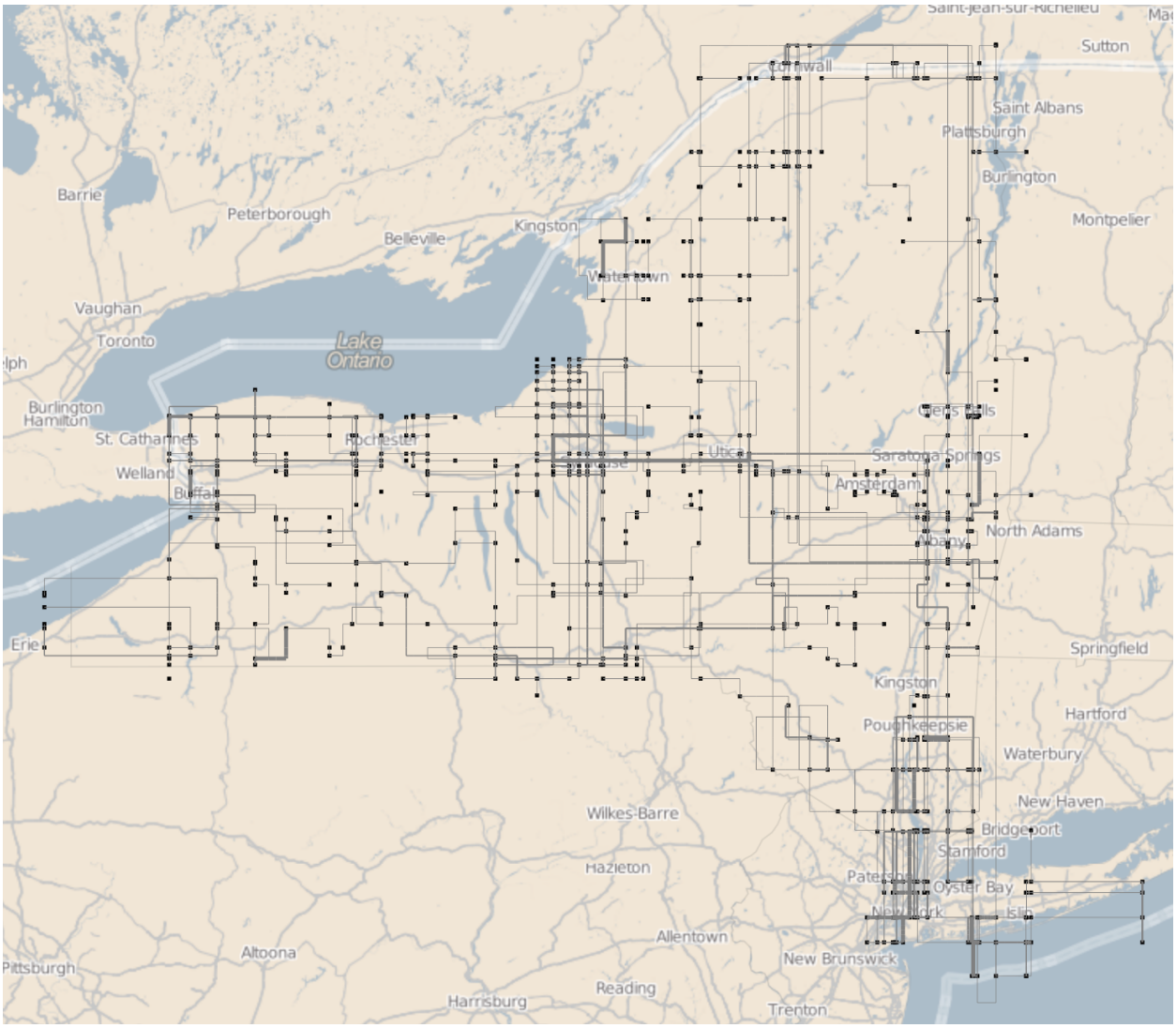

Figure 19: Solution 8, created with a less accurate algorithm (i.e., a heuristic) and a small (sparse) grid as a benchmark. Deviations (D) from true geographic coordinates are penalized with respect to the other objectives, line turns (T), line crossings (C), and line segment overlaps (O): D = 100, T = C = O = 1

5 Empirical Testing of the Solutions

5.1 Method

5.1.1 Participants

A total of 30 participants, 22 male and 8 female, with a mean age of 23.65 (SD = 5.58) years, were recruited from the student population at RIT; one of the participants was a staff member who volunteered to do the experiment. The first 7 participated in a pilot study to test the experimental task and procedure. Subsequently, the task was changed to the final one described below. Additionally, three participants failed to follow the instructions and indicate what they were doing during experimental trials and their data were excluded from analyses. Eventually, we analyzed data from 20 participants, 15 male and 5 female, with a mean age of 24.5 (SD = 6.23) years.

5.1.2 Apparatus

We used a SensoMotoric Instruments (SMI) RED250 remote eye tracking system coupled with a Dell 2210 TFT LCD 22-inch diagonal monitor. The viewable area of the monitor measures 474 × 296 mm, and has a resolution of 1680 × 1050 pixels (a pixel pitch of 0.282 mm/pixel). The display was driven at full resolution at 60 Hz. Observers were seated at a viewing distance of approximately 70 cm in a chair with fixed position to minimize body movement. Mean angular subtense of the full monitor at mean viewing distance was 37.4 × 23.9 degrees of visual angle, yielding an angular resolution of approximately 45 pixels/degree. The system recorded gaze at 250 Hz with a spatial accuracy of approximately 1 deg. Participants could make natural head movements within a 20 × 20 × 10 cm head volume, and the system quickly re-acquires gaze if the participant moves out of the volume or looks away from the stimulus display.

Prior to the experiment, an automated 9-point calibration using SMI's iViewX software was run for each participant and validated with four locations independent of the calibration sequence locations. Any validations that did not fall within 1.0 degrees of goal in either the horizontal or vertical direction were repeated before commencing the study.

5.1.3 Experimental Materials

Out of the 8 solutions created, we chose 3 for the experiment: solutions 1, 3, and 4, as well as the baseline map with straight lines connecting substations. Our rationale for choosing the experimental maps is as follows: First, 4 maps total, with two replicates each, was a maximum that could be run in about 30

minutes, which in turn is about the maximum time students would volunteer for and perform the task without becoming fatigued. Solution 1 was another "baseline" solution with equal penalizing of turns, crossings, overlapping segments, and deviations. We skipped solution 2 as it appeared very confusing, and in our judgment line crossings were more detrimental than turns (Figure 13. Solutions 3 and 4 penalized line crossings and overlaps, respectively, and were therefore included in the experiment. Solutions 5–8 were not chosen because the task was abstracted, deviations were not relevant to the naïve participants, and any differences in deviations would result in the idiosyncrasies of the actual New York map so solution would not be generalizable.

The experimental maps were created by a Python program that read the substation and line coordinates as translated by the decluttering algorithm and the different penalties assigned to the parameters. The experimental maps contained a central section the New York state, roughly from Rochester in the northwest to Poughkeepsie in the southeast and had 1680 $\times$ 1050 pixel resolution for the eye tracker display. We did not expect the participants to recognize the geography from these maps, and geography was irrelevant to the experimental task in any case.

5.1.4 Experimental Task

Because our participants were naïve to electrical power systems operation, the experimental task had to be sufficiently abstract so that it could be performed with minimal training but that would nevertheless reveal any performance differences (hypothetically) brought about the differences in the maps. Such a task was to visually trace a line between two points.

The participants were presented an experimental map with a green circle and a blue square, as well as one line segment highlighted in red. They were instructed to visually trace a path from the green circle to the blue square *without* going through the red line segment and noting where two line segments were connected (at substations marked by black dots) and where they were not (no dots at line crossings). Figures 20, 21, 22, and 23 show the experimental maps based on the baseline and solutions 1, 3, and 4.

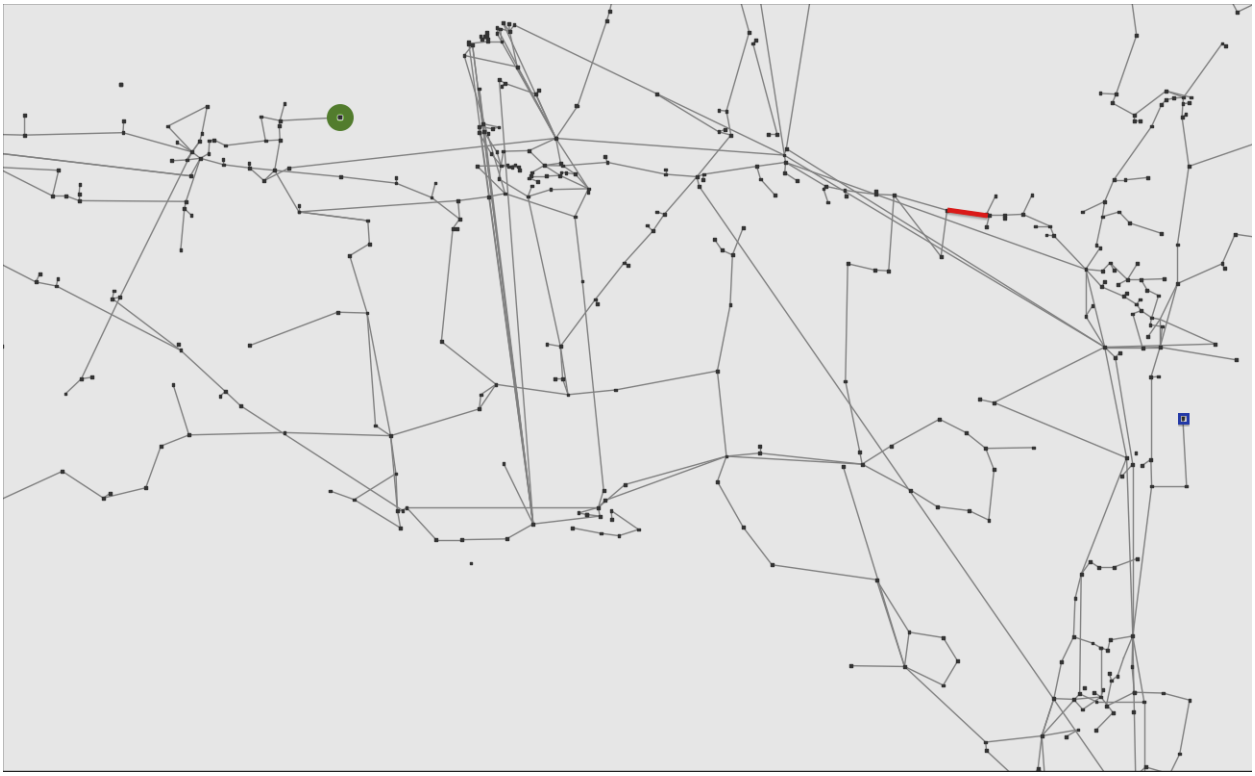

Figure 20: The nodes (substations and generators) were marked with black dots and connected with straight lines to create a baseline experimental map. The participants' task was to visually trace a path through connected line segments while avoiding the line segments highlighted in red

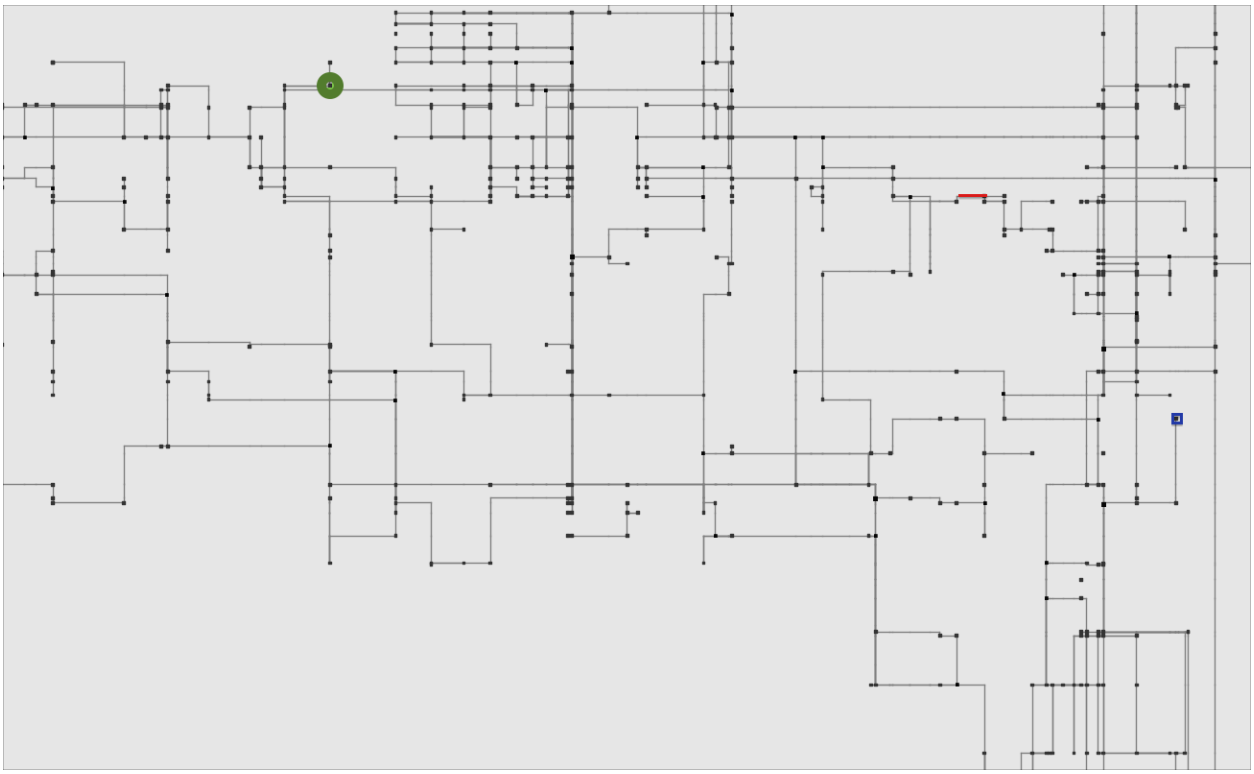

Figure 21: An experimental map based on solution 1, where turns, line crossings, line overlaps, and substation (marked with black dots) deviations from their true geographic locations were equally penalized. The participants' task was to visually trace a path through connected line segments while avoiding the line segments highlighted in red

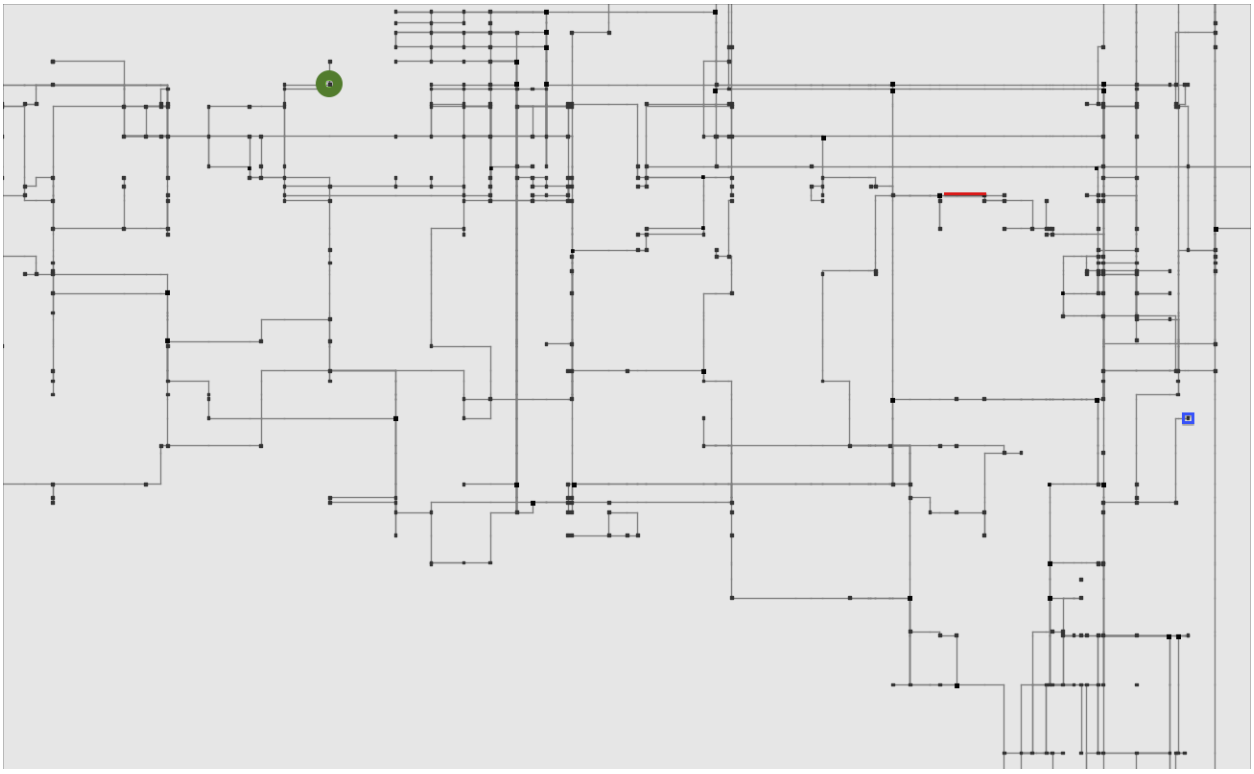

Figure 22: An experimental map based on solution 3, where line crossings were heavily penalized over turns, overlaps, and substation (marked with black dots) deviations from their true geographic locations. The participants' task was to visually trace a path through connected line segments while avoiding the line segments highlighted in red

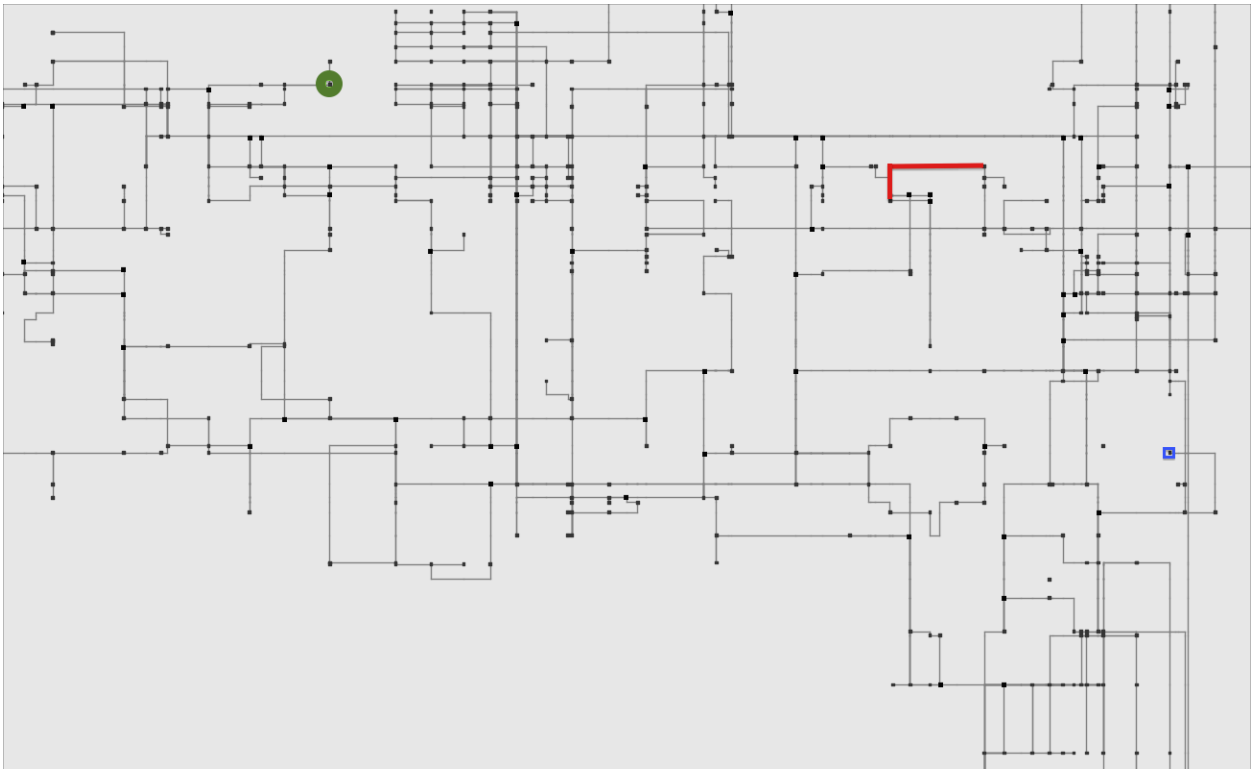

Figure 23: An experimental map based on solution 4, where line overlaps were heavily penalized over line turns, crossings, and substation (marked with black dots) deviations from their true geographic locations. The participants' task was to visually trace a path through connected line segments while avoiding the line segments highlighted in red

5.1.5 Independent Variables

Independent variable was the weight of penalties for turns, crossings, and overlaps of transmission lines on the experimental maps, compared to the baseline map with straight lines between substations.

5.1.6 Dependent Variables

We measured several dependent variables for analyses. We are not aware of any research on electric power systems that has collected eye movement data. Instead, past research has relied on task time, system performance indices, and subjective measures [42, 43] . Because of the simple, abstract task and naiv̈e participants, task performance was not applicable as a dependent measure, except at a very gross level of time to complete the task. Eye movements have been used to examine otherwise covert cognitive processes in many other domains and particularly in reading tasks [44]. In reading, it has been shown that increased difficulty of the text results in shorter saccades and longer fixations [45]. The dependent variables recorded

and analyzed were:

1. The time to complete the task (i.e., visually tracing the path between the two highlighted points without going through the line segment highlighted in red). The shorter the time, the easier the map is to read.

2. The time participants to orient themselves on the map before starting the experimental task. Here, too, shorter times suggest an easier map to read.

3. From eye movement data, amplitude (length) of saccades, the movements of the eye between fixations. Longer saccades indicate an easier map to read [45].

4. From eye movement data, peak velocities of saccades. Higher saccade peak velocities indicate an easier map to read.[46]

5. From eye movement data, durations of fixations (or dwell times). Shorter dwell times indicate an easier map to read [45].

6. From eye movement data, pupil diameter. Pupil dilation is an indicator of mental workload, and thus smaller pupils indicate an easier map to read.

7. Subjective ratings of the difficulty of the task using each map.

5.1.7 Experimental Design

This was a within-subjects design, each participant performing the experimental task on each of the four maps, plus a similar task (different only by the start and end points and the line segment marked "out") on a replicate for each map. Analyses of the resulting data compared the four maps along several dependent measures.

5.1.8 Procedure

As the participants arrived to the eye tracker lab for the experiment, they were greeted asked for their name that was entered in a list and given a running number with which all data would be associated. They were also asked to read and sign an informed consent form. After that, the participants were explained how the eye tracker worked and what they were to do. They were shown a demonstration map and explained the meaning of the nodes and line segments, how lines were connected, and how to find a valid path between the two highlighted nodes. They were also asked to press the control key on a keyboard when they had oriented themselves on the map (i.e., visually found the start and end points on the map as well as the "open" line

segment in red) and were ready to begin the tracing task. They were asked to press the control key again when they were satisfied that they had found and successfully traced a valid path between the highlighted nodes.

The participants were given 3 practice trials with a map that was different from the experimental maps (solution 5). After both the participant and the experimenter were satisfied that the participant understood the instructions and was able to perform the task, experimental maps were presented in a counterbalanced order. Each map was replicated once, with a different task (different highlighted nodes and the "open" line segment. Before the experimental maps and between every two trials a calibration screen was showed to the participants to make sure the eye tracker remained properly calibrated throughout the experiment. After each trial and blank screen was displayed offering the participants a rest break before continuing. At the end of the experiment, a short questionnaire was administered to the participants and their responses recorded.

5.2 Results

5.2.1 Data Reduction and Cleanup

Only data between the two key presses (where the participants indicated that they were starting the task and that they had successfully traced the path between the two nodes) were analyzed. We also excluded saccades that were longer than 23 degrees of visual angle (VA) vertically and 34 degrees of VA horizontally, for they indicated saccades larger that the display and thus outside the task.

Fixation durations shorter than 80 ms were excluded from data analyses. Research literature suggests that dwell times (fixations) shorter than 80 ms reflect false saccade planning rather than meaningful information processing [47, 48]. The 80 ms "rule" may be found in several research articles, for example in [49] and [50]. Three participants' data were excluded from the analyses as they did not follow the instructions to indicate their task performance with key presses.

5.2.2 Data Analyses

All analyses of all of the dependent variables followed the same procedure. We first visually inspected the data (histograms) to check assumptions for ANOVAs and determine the need for data transformations. We then created plots of the data and calculate descriptive statistics, means, medians, and standard deviations across participants by map and replicate. Finally, we performed inferential statistical tests for differences between the maps, including pairwise comparisons.

We performed linear mixed effects (LME) analyses on all dependent variables [51]. This approach was

chosen as a more robust method than a standard repeated measures ANOVA, assumptions of which were violated by the nature of our data (positively skewed, unequal number of observations for each participant) and large individual differences between participants. All graphics were created and analyses performed with R, a free software environment for statistical computing and graphics [52]. The R package *lme4* provided functions for fitting and analyzing mixed models [53]. Tukey contrasts were used for multiple comparisons of means. [54].

5.2.3 Orientation and Task Times

The data on time the participants needed to orient themselves on the experimental maps as well as the time they took to perform the visual tracing task were very positively skewed. This is very common with timing data. Therefore, we included medians in Table 5. For the same reason, we used a natural logarithm (ln) transformation on the data to restore normality of the distributions before performing analyses on these data.

Arranged by the median orientation time no map appears to be superior to others in terms of the time needed to find the highlighted nodes and the "open" line segment on the map and to begin the experimental task. The task performance times show show some differences. In Table 5 map 1 appears to have the shortest task performance time and map 0 the longest (with R2 showing very large standard deviation and therefore a less reliable result than R1). See also Figure 24. The LME analysis confirms this. The effect of map was statistically significant, $\chi^2(6) = 22.46, p < 0.001$, and pairwise comparisons indicated that Map 1 had significantly lower task performance time than Map 0 ($p < 0.001$) and Map 3 ($p < 0.001$).

We also examined whether longer orientation time contributed to shorter time on task, that is, whether some participants might have use the time they took to create a preliminary plan for the ultimate path between the designated nodes. This did not seem to be the case. There was essentially zero correlation (Pearson) between orientation and task times, $r = 0.0031$, $t(138) = 0.0365$, $p = 0.9709$.

Table 5: Descriptive Statistics of the Task Performance Times (in milliseconds)

Map	Replicate	Mean	Median	SD
Map1	R2	11180	10899	3811
Map0	R2	19238	14422	13025
Map1	R1	15908	14462	7466
Map4	R2	15364	15689	6363
Map3	R1	20449	15767	14311
Map3	R2	17428	16425	6716
Map4	R1	17097	18640	6840
Map0	R1	21546	20300	7576

Note: The results in this table are ordered by the median from smallest to largest, or from best to worst performance in terms of time spent tracing the path.

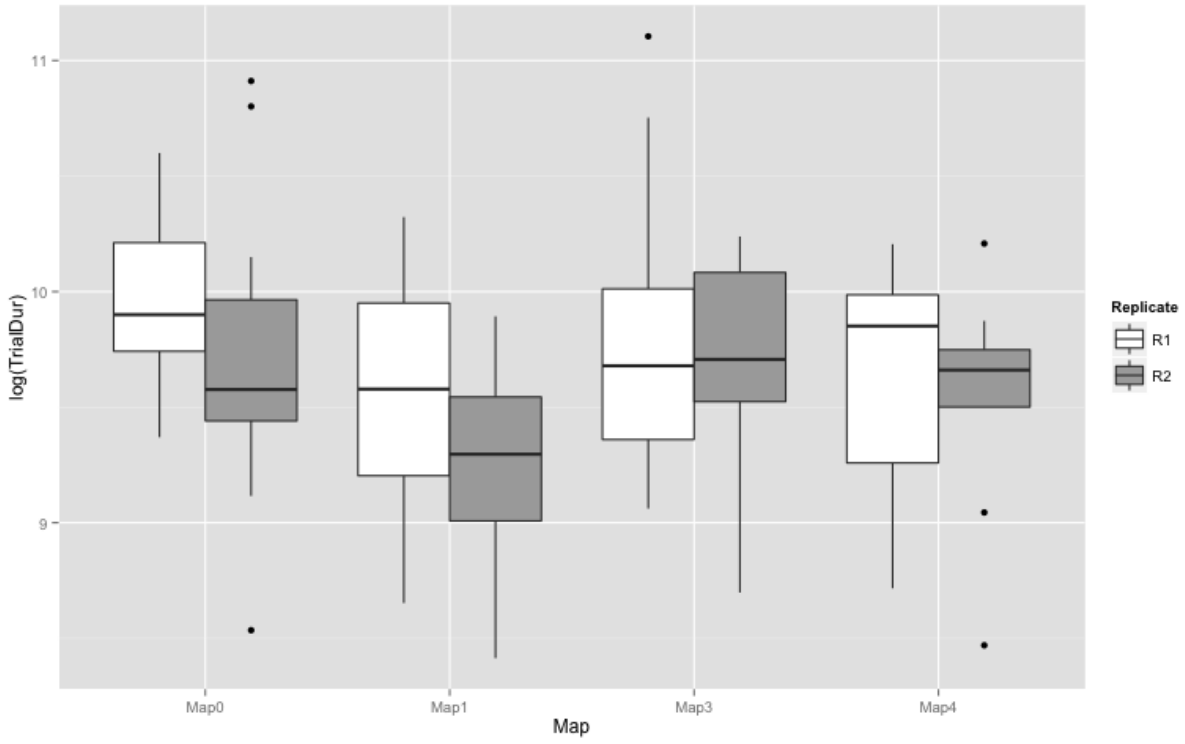

Figure 24: Plot of trial durations, or the times to perform the experimental task, tracing a path between two highlighted nodes on the maps. The times on Map 1 were significantly lower than on Map 0 and Map 3

5.2.4 Saccade Amplitude

Saccade amplitude, or the length of the movement of the eyes between successive fixations when information is actually gleaned from the image the eyes focused on, has been used as an indicator of task difficulty or mental workload incurred by performing a task. Longer saccades indicate an easier map to read [45]. The results appear mixed. By Table 6 there were much variability between replicates, which prevents us from drawing firm conclusions. Figure 25 does not clarify the results. Although Map turned out to have had a statistically significant effect, $\chi^2(6) = 27.78, p < 0.001$, the only significant difference was between Map 0 and Map 3, and this difference was very small.

Table 6: Descriptive Statistics of Saccade Amplitudes

Map	Replicate	Mean	Median	SD
Map0	R1	2.87	1.8	3.14
Map4	R2	2.66	1.8	2.59
Map3	R1	2.39	1.7	2.45
Map1	R1	2.33	1.7	2.14
Map1	R2	2.23	1.7	1.93
Map0	R2	2.17	1.7	1.92
Map4	R1	2.43	1.6	2.64
Map3	R2	2.02	1.5	1.80

Note: The results in this table are ordered by the median from largest to smallest, or from lowest to highest workload in terms of length of saccades between fixations.

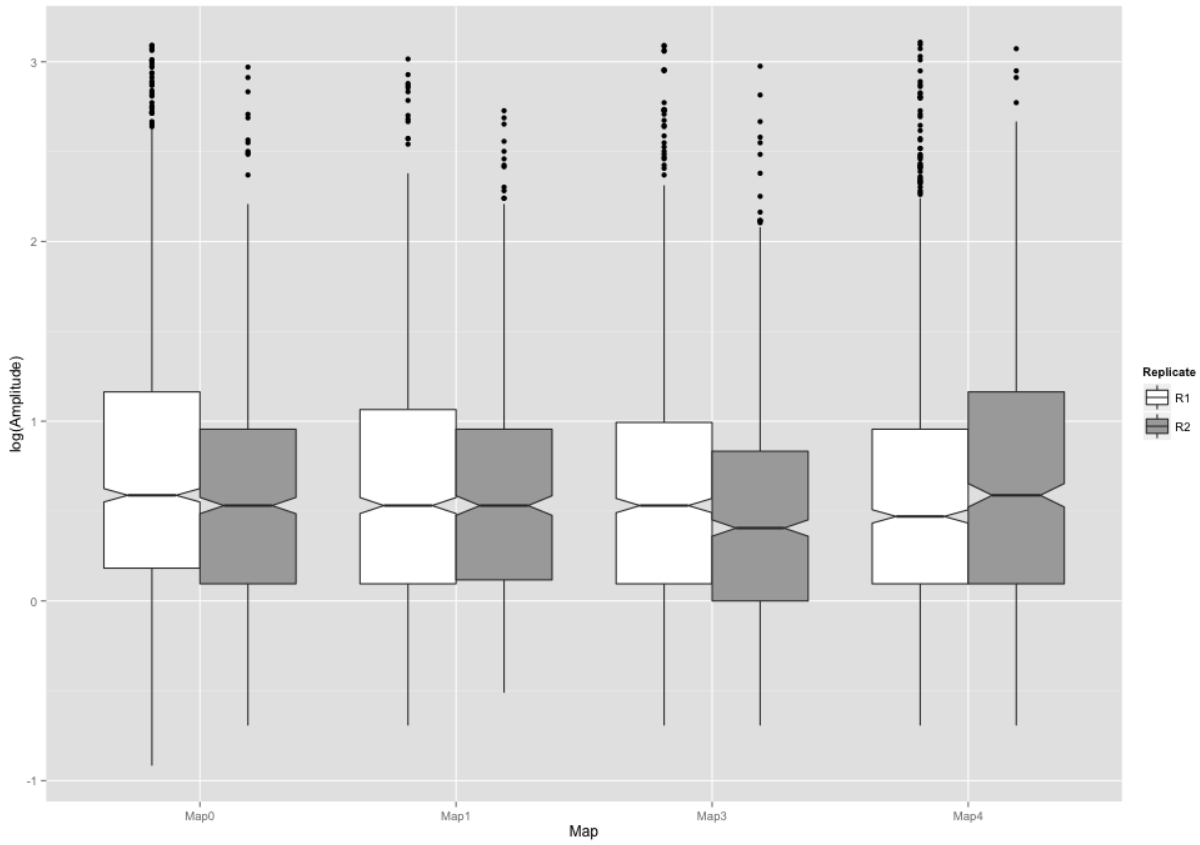

Figure 25: Plot of ln transformed saccade amplitudes. Only the difference between Map 3 and Map 0 (Tukey) was statistically significant, but as the difference was very small, we should not draw final conclusions

5.2.5 Saccade Peak Velocity

The peak velocities of saccades is another indicator of task difficulty. In this case, higher saccade peak velocities would indicate an easier map to read[46]. By the descriptive statistics in Table 7 it appears that Map 1 would be the best. However, such advantage is not evident in Figure 26 and not differences between the maps were statistically significant in our LME analyses.

Table 7: Descriptive Statistics of Saccade Peak Velocities

Map	Replicate	Mean	Median	SD
Map0	R1	145.62	103.9	129.30
Map1	R2	121.30	100.5	74.94
Map1	R1	129.19	100.0	95.19
Map4	R2	137.83	99.1	124.75
Map0	R2	121.24	97.1	83.39
Map3	R1	130.44	96.3	106.36
Map4	R1	123.77	91.2	97.14
Map3	R2	113.72	89.9	78.27

Note: The results in this table are ordered by the median from largest to smallest, as higher saccade peak velocities would indicate an easier map to read.

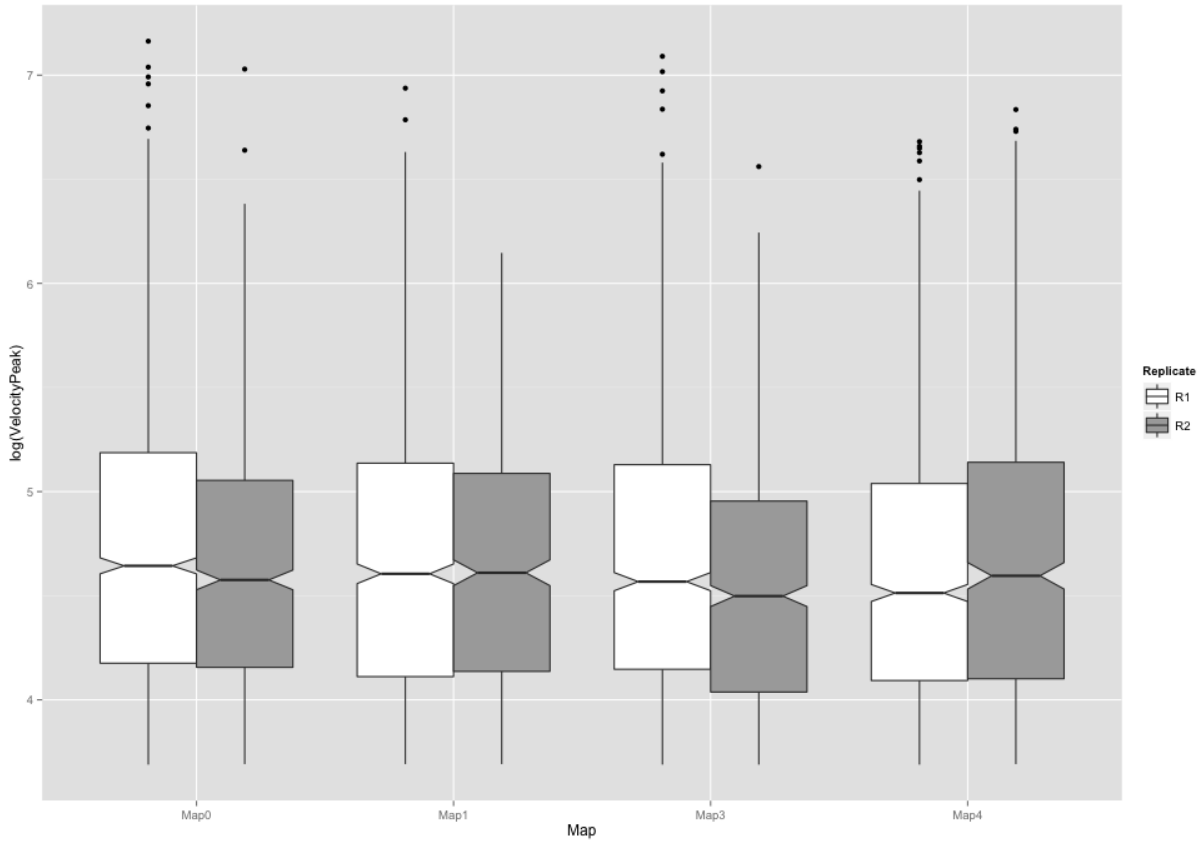

Figure 26: Plot of ln transformed saccade peak velocities. No statistically significant differences were found between maps

5.2.6 Fixation Durations

Fixation duration, or dwell time, refers to the time the eye remains fixed on some detail on the scene. It is during fixations that information is gleaned from whatever a person may be looking at. Hence, in our case, shorter fixation durations would indicate an easier map to read [45]. Examining the descriptive statistics in Table 8 the advantage seems to go to Map 4, which had consistently (also smallest SD) smaller fixation durations than other maps.

Table 8: Descriptive Statistics of Fixation Durations

Map	Replicate	Mean	Median	SD
Map4	R2	259.42	184	244.63
Map0	R1	318.06	188	1217.06
Map4	R1	299.10	200	315.74
Map1	R1	345.94	222	875.58
Map3	R1	399.18	240	1175.21
Map1	R2	370.27	264	357.35
Map3	R2	412.82	268	452.07
Map0	R2	416.72	282	430.69

Note: The results in this table are ordered by the median from smallest to largest, as shorter fixation durations would indicate an easier map to read.

However, although the effect of map was significant in the LME analysis, $\chi^2(6) = 35.102, p < 0.0001$, only Map 3 was significantly different from Map 0 ($p = 0.04$) and Map 1 ($p = 0.037$). These effects are quite weak, too.

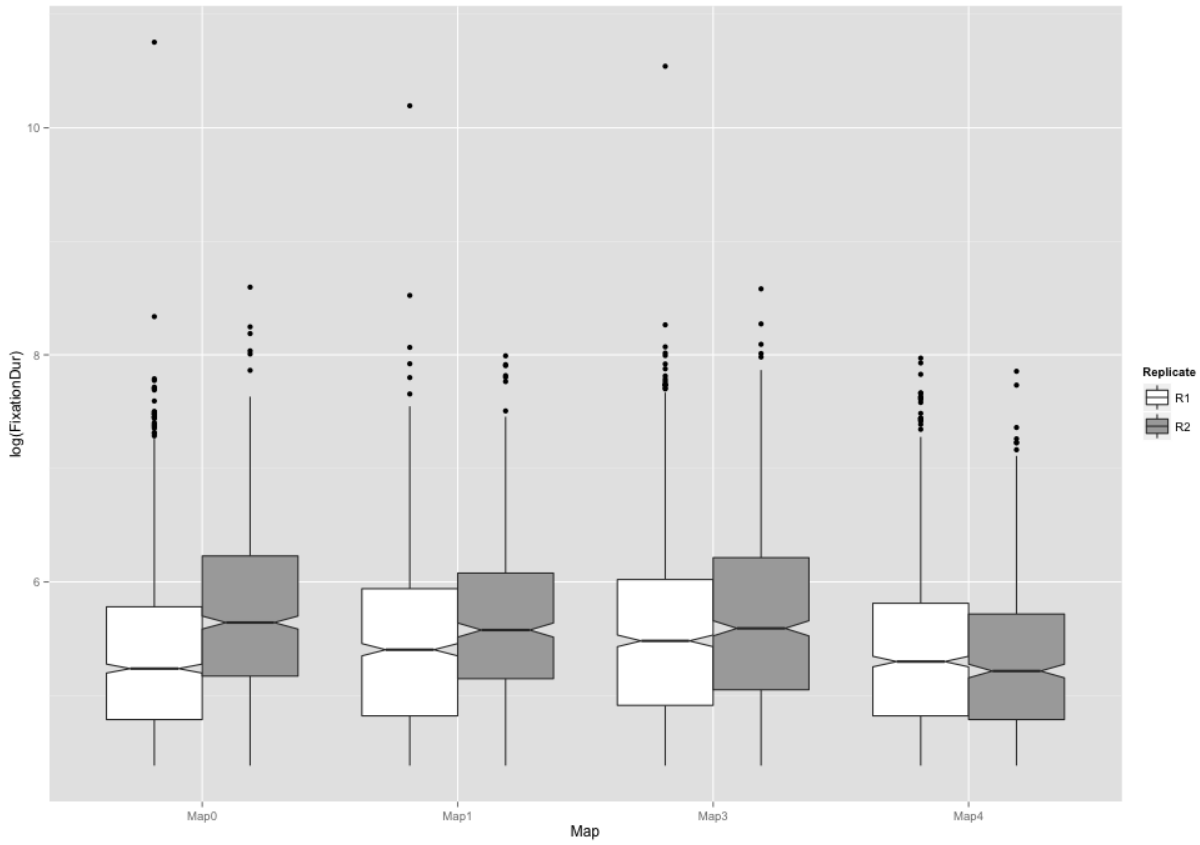

Figure 27: Plot of ln transformed fixation durations. No statistically significant differences were found between maps

5.2.7 Pupil Diameter

Finally, we analyzed pupil size data. pupil diameter. Pupil dilation is an indicator of mental workload, and thus smaller pupils indicate lower workload an easier map to read. The results did not show any differences in pupil diameter between the experimental map conditions. In Table 9 the mean an median values of pupil diameter are nearly the same across the experimental conditions. Similarly, in Figure 28 the medians in the box plots nearly line up across the maps. Our LME analyses did not show any statistically significant differences, either, as expected.

Table 9: Descriptive Statistics of Pupil Diameter

Map	Replicate	Mean	Median	SD
Map4	R2	12.60	12.58	1.85
Map0	R2	12.72	12.73	1.50
Map1	R1	12.81	12.80	1.88
Map3	R2	12.82	12.80	2.03
Map1	R2	12.82	12.93	1.74
Map0	R1	12.82	12.96	1.88
Map3	R1	13.22	13.06	1.87
Map4	R1	12.91	13.07	2.10

Note: The results in this table are ordered by the median from smallest to largest, as smaller pupil diameters would indicate an easier map to read.

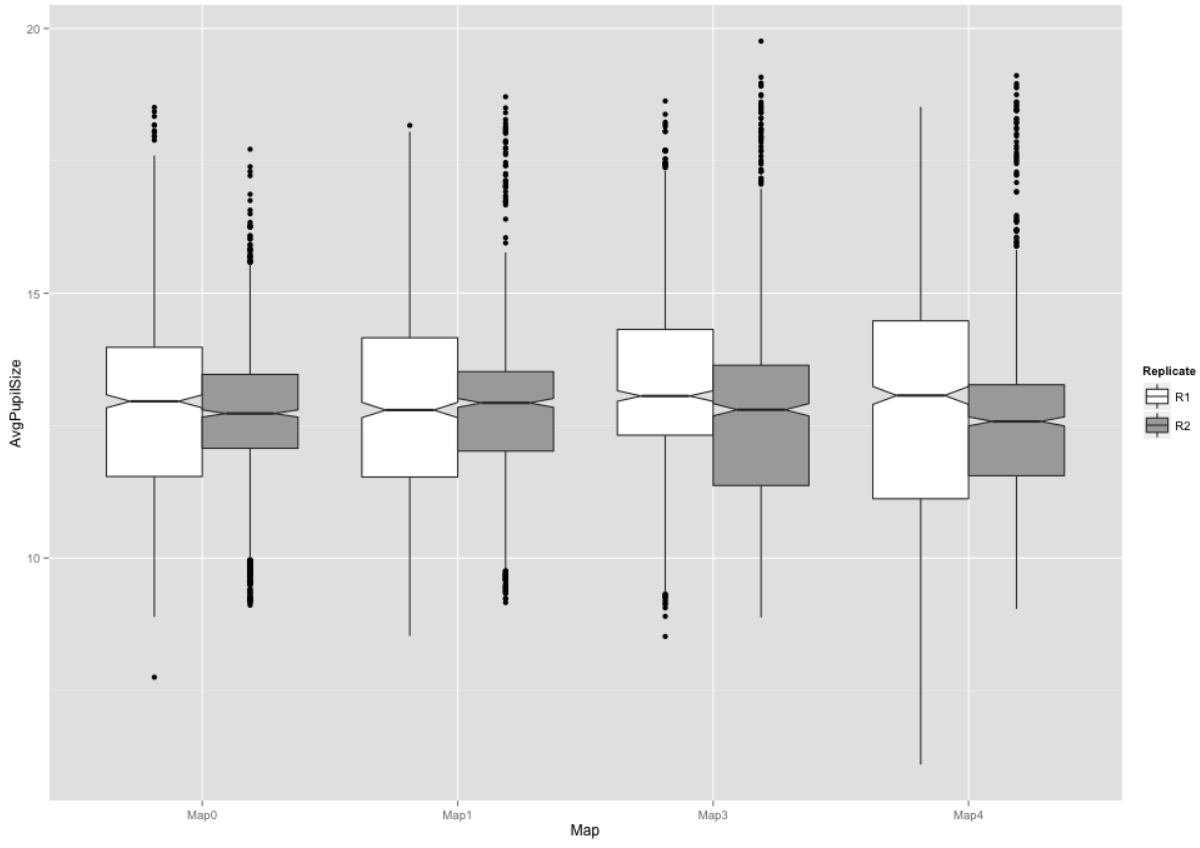

Figure 28: Plot of pupil diameters. No statistically significant differences were found between maps

5.2.8 Subjective Responses

We administered a post-experimental survey to all participants, with 6 questions:

1. How difficult did you find this task (on a scale from 1–easy, to 7–hard)
2. Why did you find the task easy/hard? What was hard/easy about it?
3. Did you use any strategies?
4. How was it following the node/line crossing rule? Did you find that hard/easy? Were you usually able to follow it?
5. Did you recognize any differences between the maps? Did any stick out as particularly easy or hard?
6. Any other comments

Task difficulty was rated on average 3.8 (SD = 1.4, range = 1–6). The participants found following the rule about connected line segments at nodes difficult and demanding their attention; forgetting about the rule necessitated retracing the path. Avoiding the red "open" line segment also demanded attention.

The baseline map, with straight lines connecting the nodes, was judged to be the most difficult by the majority of participants (14; only 4 thought the experimental maps to have been more difficult). Specifically, participants reported getting lost among the non-rectilinear lines forcing them to retrace the path. In general, participants commented that the experimental maps appeared more "structural" and that this helped in tracing the paths. Fewer line crossings made the maps easier to read, while closeness of lines and nodes added to the map difficulty.

The participants did not appear to have used any particular strategies to do the task. A few reported to have started by forming a "big picture" of a potential path circumventing the open line segment or identifying a straightest path between the nodes and using that as a reference. Such strategies were especially helpful with the experimental, rectilinear maps.

Most participants reported having worked from the green start-node to the blue end-node as instructed, but if they were not able to find a path, some attempted to trace the path in reverse direction, or from both nodes to a reference point in the middle. Participants also reported using their peripheral vision to guide them in their path-tracing task.

5.3 Subsequent Operator Interviews

Two experienced RG&E operators visited RIT in May 2014 to review the redrawn maps produced within this project and to discuss their work in some further detail. These operators' familiarity with the electric power infrastructure in the Rochester area was amply evident: For example, due to an error in transferring the substation and line segment coordinates from a PDF copy of the NYISO system map to a spreadsheet, from where the data were used to produce the redrawn maps (see below), a power line was missing southwest of Rochester; the operators immediately noticed and commented on it.

The operators did not like the redrawn maps where the lines were only vertical or horizontal. They commented that the true geographic orientation of a particular line (e.g., running from northwest to southeast) greatly helped them identify particular lines and orient themselves on the map. This reaction is not unusual, however. Experienced operators always prefer displays and tools they are familiar with to new designs. To test the improvement of new designs over existing ones operator performance on common tasks using new displays and tools should be measured in simulations and the learning time to match their performance using current tools noted. If the new design is advantageous, subsequent experimental trials should show improvement in performance beyond the (baseline) performance with current tools.

5.4 Discussion

The experimental results are largely inconclusive. This is most likely due to at least three factors: (1) Our participants were mostly students at RIT who had little or no experience in reading wiring diagrams and no knowledge of power systems. (2) Therefore, the experimental task had to be abstract and simple, so that naïve participants could perform it without much training (the limiting factor was the time commitment a participant would have to make; based on much past experience, more than an hour would severely limit the number of participants volunteering for an experiment). (3) Finally, although the task was simple, it was still too complex for the capabilities of the eye tracker we used. In other words, even in a simple line-tracing task the participants' eyes moved in very complex patterns across the display of the experimental maps and the resulting variability in the data likely masked subtle differences in their performance in the task on the different maps.

Table 10 summarizes the experimental results. It is difficult to draw any firm conclusions from the eye movement data, for all the reasons mentioned above, but qualitatively some maps appear to have been more advantageous than others in our experimental task. In particular, Map 1, where line turns, line crossings, overlapping line segments, and deviations from true geographic coordinates, were equally penalized seemed to have had perhaps the most robust advantage in terms of time to complete the task, which in turn was probably the best measure of performance. In a short task, an average of 4 s time advantage also is a

reasonably large effect.

All the experimental (decluttered) maps seem to have had the same advantage over the baseline maps in terms of task time. This result was corroborated by the participants' responses to the post-experiment survey, where the majority preferred the more rectilinear structure of the experimental maps to the baseline map with straight lines connecting the nodes, which they thought to be visually confusing and requiring retracing paths between the designated nodes.

Map 4, which penalized overlap of map elements (nodes and lines) appeared to have had small advantage over the other maps in terms of fixation duration and pupil diameter. This seems reasonable as Map 4 appears the "clearest" of all maps generated with most space between the map elements (cf. Figures 15 and 23).

Table 10: Summary Table of Experimental Results

Variable	Advantage	Effect Size	Sig.
Task Performance Time	Map 1	4 s [1]	Yes
Saccade Amplitude	None	¡ 0.1 deg [2]	No
Saccade Peak Velocity	Map 0, 1	7 deg/s [3]	No
Fixation Duration	Map 4	24 ms [4]	No
Pupil Diameter	Map4	0.01 mm [5]	No

Note: [1]The difference between the median task time for Map 1 and the second fastest task time (Map 3). [2]The maximum difference in median degrees of visual angle between any two maps. [3]The difference between saccade peak velocities for Maps 0 and 1 (0.55 deg/s apart) and the next closest map (3). [4]The difference in median fixation duration between Map 4 and the next smallest median duration with Map 0. [5]The difference with the map with smallest pupil diameter and the map with next smallest pupil diameter (Map 0).

That the experienced RG&E operators did not agree with the naïve participants in the experiment was most likely due to their decades-long familiarity with the existing transmission system maps and tools they use daily in their jobs, and the very limited time they spent reviewing and evaluating the decluttering solutions created through this research (only about 2 hours). We will discuss the implications of experience in development of visualizations for operational use in more detail in the next section.

6 General Discussion

The goal of this project was to provide an optimized layout for geographic data view (GDV) displays and electric system visualizations. The optimization algorithm we developed indeed achieved this goal, despite the fact that the task turned out to be much more difficult (and as such, also much more interesting) than

we anticipated, requiring substantial computational resources. Moreover, the difficulties emerged from a relatively "small" problem of an electrical system within only one state (NY)—in contrast to, say, the entire Eastern interconnect—and with only high voltage ($>$ 115 kV lines). The size of the problem, modeled as a multicommodity flow problem with side constraints and a complex objective function over an embedded display grid, thus leaves room for heuristics to simplify the process.

The solutions we generated are optimal only with respect to a set of constrains and objectives, which themselves were based on research in other than operational electric power control contexts. Truly optimal solutions for electric control centers should reflect expert operators' inputs and be validated in series of realistic scenarios. Operators could potentially be source of heuristics, which while making the problem computationally feasible would also provide for optimal solutions in terms of human factors. Such an effort would necessarily be iterative in nature, with electric power system maps revised and redesigned according to feedback from operators and objective performance measures from simulations.

6.1 GDV Displays in Control Centers

Our observations at RG&E ECC revealed a mixture of GDV displays and maps the operators had to consult simultaneously as they worked the problems at hand. The SCADA system used black-background power systems map deals with color coding that does not match the line color coding in other maps at the ECC. The SmartMap application had myriad different colors used to code different lines and the overall visual presentation was markedly different from the other GDV applications at the ECC. Finally, the operators were ofter forced to retrieve hand-drawn system maps from microfiche to access detail necessary for switching operations. Although experienced operators are familiar with their tools and can compensate for inconsistent color coding and other map features, such poor human factors nevertheless increase the probability of human error, especially in emergency situations where the operators are under severe time stress (see, e.g., [55]). Fortunately, at the time of this writing the visualization system at RG&E ECC has been upgraded.

Upgrades to the geographic (or pseudo-geographic) maps in control centers at both NYISO and RG&E happened during our project. The new visualization systems for NYISO were supplied by a Primate Technologies. We were not able to make contact with anyone in the company, however, to review the new NYISO system, and NYISO would not allow any tours to their new control center when it was finished in the fall 2013. A view of the new displays could be had from an observation area above the control room floor, but without direct access to the floor (or the operators), this was not a worthwhile option for us. Figure 1 is the best we could have in terms of evaluating the new displays at NYISO. The RG&E ECC was upgraded to Siemens Spectrum system some time last year. We attempted to contact Siemens about the new system with the help of our liaison at RG&E, but no contact was ever established. We were thus not privy to the new Siemens Spectrum specifications and visualization solutions at RG&E ECC.

6.2 Participatory Ergonomics in Systems Development

This research highlighted the need for participatory ergonomics in development of solutions for operational use [56] [57]. Although we are grateful to RG&E personnel for access to the ECC and to the operators there for sharing their "job smarts" and challenges with us and showing us their displays and other tools, we could not conduct in-depth interviews that would have been necessary for a thorough CWA while the operators were working at their designated desks. The two RG&E operators who reviewed the decluttering solutions provided us with valuable additional information but there were no further opportunities for revision and re-evaluation of the alternative maps.

The new maps we produced (Figures 12–19) were very minimalistic and lacked much information operators would expect on an electric power system map (such as different symbols for different generating stations and substations, color-coded transmission line ratings). The minimalistic maps were appropriate for use in an experiment with naïve participants, but it is also understandable why they would appear strange to experienced operators. In this project we did not have the resources to produce maps with the usual visual elements found in electric power system map or novel visualizations of variables the operators might have found helpful. Such effort would require much closer collaboration between researchers and experienced operators that what we could have in this project.

6.3 Recommendations for Future Research

Based on our experiences in this project, we make several recommendations for future research on the same and similar topics:

1. Decluttering large-scale (i.e., covering geographic areas of several U. S. states) wide-area GDV displays remains a problem. There are innumerable possible decluttering solutions to be generated using various OR techniques (such as Lagrangian relaxation techniques, path variables, and branch-and-price algorithms as used here) and different weighting of the model parameters. The eight solutions presented here represent therefore just the tip of the iceberg. Input from experienced operators at all stages of decluttering solutions development is essential to narrow down the model parameters and their weights and to produce a small set of solutions among which an optimal one may be found.

2. As was mentioned above, display and visualizations development is necessarily an iterative process. It is therefore critical to ensure close collaboration between researchers and experienced operators serving as subject matter experts (SMEs) in all phases of the work. This would necessarily require a firm commitment from a companies like NYISO or RG&E in terms of operators' time to fully participate in the research and development work. Presumably, such agreements would need to be negotiated at a

level above individual operators and their immediate supervisors and the researchers at an university.

3. Experienced operator participation in development of realistic experimental problems and their presentation in simulations, and then participation in experiments using these materials is also essential for the external validity of the experimental results. Simulation capability may be developed at university settings, albeit with substantial cost in computer programming. I would be better to have access to existing simulator facilities and implement novel visualization solutions and experimental problems there. Again, an agreement to run experimental simulations at existing facilities would have to be negotiated at a higher, corporate, level.

4. The iterative algorithms we used could not explicitly handle transmission lines which are routed over more than two regions, as would be the case in control center applications covering areas of multiple U.S. states. A more general algorithm that is able to resolve this difficulty should be considered. Also, a revised Dijkstra's algorithm to take the minimization of turns and line intersections into consideration should be explored in future research.

5. Besides the direct application of the efficient solution methodologies we developed in power system control centers or more generally in display technology, we can also find potential application areas in transportation and logistics fields. For example, to make the drone delivery possible in the future, logistics companies have to design routes to avoid intersections and overlaps to mitigate risk of collision and avoid loops to save time and energy costs. They also need to decide the candidate locations to build the control centers and 'parking' facilities. More applications are being looked forward in future research.

6. There are also many related topics worth of future effort. First, our iterative algorithms could not handle lines which are routed over more than two cluster regions (i.e., we call them jump lines in Section 4.2). Thus, a more general algorithm which is able to resolve this difficulty should be a great improvement upon this paper. Second, we propose a revised Dijkstra's algorithm to take the minimization of turns and line intersections into consideration, and argue that it does not guarantee an optimal solution. Although a virtual layer method could be applied to handle the minimization of turns in lattice graphs, to our best knowledge, an optimal algorithm to take care of both does not exist and is thus left for future research.

7 Conclusion

We have developed efficient solution methodologies to solve a difficult optimization problem which considers relocating substations and rerouting transmission lines simultaneously to declutter wide-area GDV displays

of electric power systems. To our knowledge, computational solutions to the decluttering problem have not been attempted before.

Our research relied on related to the topics that have received considerable attention from both computer science and operations research communities. We developed two clustering-based iterative algorithms—a Lagrangian relaxation-based algorithm and a progressive hedging (PH)-based algorithm—to decompose the global network into smaller regions and then iteratively solve the subproblem in each region by readjusting some values. Intuitively, the nature of such solution methodologies is quite coherent with the traditional hierarchical routing methods, but in this research we incorporated several novel aspects.

We generated a total of eight alternative NY state electric power system maps. Three of these solutions were selected for experimental evaluation. The experimental results were largely inconclusive, primarily due to the naïve participants (i.e., they had little or no experience in reading maps or wiring diagrams), the simple task, and the limitations of the eye tracker. Nevertheless, two of the decluttered maps appeared to have distinct advantage over the baseline map, where substations were simply connected by straight lines, in terms of performance time and workload.

Future research on this topic should be able to produce a truly optimal GDV display layout for electric power systems control applications. However, a successful outcome will require close collaboration between researchers and experiences operators serving as subject matter experts (SMEs). A more sophisticated simulation capability that what was available to us will also be required to thoroughly test the GDV layouts and other visualization solutions in realistic settings and with realistic problems.

References

[1] R Klump, D Schooley, and T Overbye. An advanced visualization platform for real-time power system operations. In *Proc. of the 14th Power Systems Computation Conference*, volume 2, 2002.

[2] R Klump, G Dooley, and W Wu. Displaying aggregate data, interrelated quantities, and data trends in electric power systems. In *System Sciences, 2003. Proceedings of the 36th Annual Hawaii International Conference on*, pages 10–pp. IEEE, 2003.

[3] EPRI. Visualizing power system data. Technical Report TR-102984, Electric Power Research Institute, Palo Alto, CA, 1994.

[4] TJ Overbye and DA Wiegmann. Reducing the risk of major blackouts through improved power system visualization. In *15th Power System Computation Conference, Liege*, 2005.

[5] TJ Overbye. Visualization enhancements for power system situational assessment. In *Power and Energy Society General Meeting-Conversion and Delivery of Electrical Energy in the 21st Century, 2008 IEEE*, pages 1–4. IEEE, 2008.

[6] TJ Overbye, AP Meliopoulos, DA Wiegmann, and GJ Cokkinides. Visualization of power systems and components. Technical Report PSERC Publication 05-65, PSERC, 2005.

[7] TJ Overbye and JD Weber. Visualizing the electric grid. *IEEE Spectrum*, 38(2):52–58, 2001.

[8] JD Weber and TJ Overbye. Voltage contours for power system visualization. *Power Systems, IEEE Transactions on*, 15(1):404–409, 2000.

[9] EM Rantanen, JA Winkle, and TJ Overbye. Cognitive task analysis of electric power system control center operations. In *Proceedings of the Human Factors and Ergonomics Society Annual Meeting*, volume 52, pages 1934–1938. Sage Publications, 2008.

[10] TJ Overbye, EM Rantanen, and S Judd. Electric power control center visualization using geographic data views. In *Bulk Power System Dynamics and Control-VII. Revitalizing Operational Reliability, 2007 iREP Symposium*, pages 1–8. IEEE, 2007.

[11] MISO Energy. https://www.misoenergy.org, September 2014.

[12] G Lintern. The foundations and pragmatics of cognitive work analysis: A systematic approach to design of large-scale information systems. http://www. cognitivesystemsdesign.net/home.html, 2009.

[13] KJ Vicente. Ecological interface design: Progress and challenges. *Human Factors*, 44(1):62–78, 2002.

[14] KB Bennett and JM Flach. *Display and interface design: Subtle science, exact art.* CRC Press, 2011.

[15] CM Burns and J Hajdukiewicz. *Ecological interface design.* CRC Press, 2013.

[16] J Rasmussen, AM Pejtersen, and LP Goodstein. *Cognitive systems engineering*. Wiley, 1994.

[17] RH Miller and JH Malinowski. *Power Systems Operation*. McGraw-Hill, New York, 3rd edition, 1994.

[18] DA Crowe, BB Averbeck, MV Chafee, JH Anderson, and AP Georgopoulos. Mental maze solving. *Journal of Cognitive Neuroscience*, 12(5):813–827, 2000.

[19] MV Chafee, BB Averbeck, DA Crowe, and AP Georgopoulos. Impact of path parameters on maze solution time. *Archives Italiennes de Biologie*, 140(3):247–251, 2002.

[20] D Crundall, GG Cole, and G Underwood. Attentional and automatic processes in line tracing: Is tracing obligatory? *Perception & psychophysics*, 70(3):422–430, 2008.

[21] Charles Chiang, Majid Sarrafzadeh, and Chak-Kuen Wong. Global routing based on steiner min-max trees. *IEEE Transactions on Computer-Aided Design of Integrated Circuits and Systems*, 9(12):1318–1325, 1990.

[22] Charles Chiang, Chak-Kuen Wong, and Majid Sarrafzadeh. A weighted steiner tree-based global router with simultaneous length and density minimization. *IEEE Transactions on Computer-Aided Design of Integrated Circuits and Systems*, 13(12):1461–1469, 1994.

[23] E Shragowitz and S Keel. A global router based on a multicommodity flow model. *INTEGRATION, the VLSI journal*, 5(1):3–16, 1987.

[24] Prabhakar Raghavan and Clark D Thompson. Multiterminal global routing: a deterministic approximation scheme. *Algorithmica*, 6(1-6):73–82, 1991.

[25] RC Carden, Jianmin Li, and Chung-Kuan Cheng. A global router with a theoretical bound on the optimal solution. *IEEE Transactions on Computer-Aided Design of Integrated Circuits and Systems*, 15(2):208–216, 1996.

[26] Christoph Albrecht. Provably good global routing by a new approximation algorithm for multicommodity flow. In *Proceedings of the 2000 international symposium on Physical design*, pages 19–25. ACM, 2000.

[27] Masayuki Hayashi and Shuji Tsukiyama. A hybrid hierarchical approach for multi-layer global routing. In *Proceedings of the 1995 European conference on Design and Test*, page 492. IEEE Computer Society, 1995.

[28] Jörg Heisterman and Thomas Lengauer. The efficient solution of integer programs for hierarchical global routing. *IEEE Transactions on Computer-Aided Design of Integrated Circuits and Systems*, 10(6):748–753, 1991.

[29] TC Hu and Man-Tak Shing. *A decomposition algorithm for circuit routing*. Springer, 1985.

[30] Wing K Luk, Paolo Sipala, Markku Tamminen, Donald Tang, Lin S Woo, and Chak-Kuen Wong. A hierarchical global wiring algorithm for custom chip design. *IEEE Transactions on Computer-Aided Design of Integrated Circuits and Systems*, 6(4):518–533, 1987.

[31] Arvind M Patel, Norman L Soong, and Robert K Korn. Hierarchical VLSI routing–an approximate routing procedure. *IEEE Transactions on Computer-Aided Design of Integrated Circuits and Systems*, 4(2):121–126, 1985.

[32] Ulrich Ph Lauther. Top down hierarchical global routing for channelless gate arrays based on linear assignment. In *Proceedings of the IFIP International Conference on VLSI*, pages 141–151, 1987.

[33] K Winter and Dieter A Mlynski. Hierarchical loose routing for gate arrays. *IEEE Transactions on Computer-Aided Design of Integrated Circuits and Systems*, 6(5):810–819, 1987.

[34] Hai Zhou and DF Wong. Global routing with crosstalk constraints. *IEEE Transactions on Computer-Aided Design of Integrated Circuits and Systems*, 18(11):1683–1688, 1999.

[35] R Tyrrell Rockafellar and Roger J-B Wets. Scenarios and policy aggregation in optimization under uncertainty. *Mathematics of operations research*, 16(1):119–147, 1991.

[36] Edsger W Dijkstra. A note on two problems in connexion with graphs. *Numerische mathematik*, 1(1):269–271, 1959.

[37] Fred Glover. Tabu search-part I. *ORSA Journal on computing*, 1(3):190–206, 1989.

[38] Fred Glover. Tabu search—part II. *ORSA Journal on computing*, 2(1):4–32, 1990.

[39] Yueyue Fan and Changzheng Liu. Solving stochastic transportation network protection problems using the progressive hedging-based method. *Networks and Spatial Economics*, 10(2):193–208, 2010.

[40] Ovidiu Listes and Rommert Dekker. A scenario aggregation–based approach for determining a robust airline fleet composition for dynamic capacity allocation. *Transportation Science*, 39(3):367–382, 2005.

[41] Arne Løkketangen and David L Woodruff. Progressive hedging and tabu search applied to mixed integer (0, 1) multistage stochastic programming. *Journal of Heuristics*, 2(2):111–128, 1996.

[42] TJ Overbye, DA Wiegmann, AM Rich, and Y Sun. Human factors aspects of power system voltage contour visualizations. *Power Systems, IEEE Transactions on*, 18(1):76–82, 2003.

[43] DA Wiegmann, TJ Overbye, SM Hoppe, GR Essenberg, and Y Sun. Human factors aspects of three-dimensional visualization of power system information, 2006.

[44] CD Wickens, JG Hollands, B Banbury, and R Parasuraman. *Engineering Psychology and Human Performance*. Pearson, 4 edition, 2013.

[45] Keith Rayner. Eye movements and attention in reading, scene perception, and visual search. *The quarterly journal of experimental psychology*, 62(8):1457–1506, 2009.

[46] LL Di Stasi, R Renner, P Staehr, JR Helmert, BM Velichkovsky, JJ Cañas, A Catena, and S Pannasch. Saccadic peak velocity sensitivity to variations in mental workload. *Aviation, Space, and Environmental Medicine*, 81(4):413–417, 2010.

[47] K Rayner and A Pollatsek. *The Psychology of Reading*. Prentice Hall College Division, 1989.

[48] M Bindemann, C Scheepers, and AM Burton. Viewpoint and center of gravity affect eye movements to human faces. *Journal of Vision*, 9(2):7, 2009.

[49] M Nyström and K Holmqvist. An adaptive algorithm for fixation, saccade, and glissade detection in eyetracking data. *Behavior Research Methods*, 42(1):188–204, 2010.

[50] K Rayner, TJ Slattery, D Drieghe, and SP Liversedge. Eye movements and word skipping during reading: effects of word length and predictability. *Journal of Experimental Psychology: Human Perception and Performance*, 37(2):514–528, 2011.

[51] B. Winter. Linear models and linear mixed effects models in R with linguistic applications (arXiv:1308.5499). http://arxiv.org/pdf/1308.5499.pdf, 2013.

[52] R Core Team. *R: A Language and Environment for Statistical Computing*. R Foundation for Statistical Computing, Vienna, Austria, 2013.

[53] D Bates, M Maechler, B Bolker, and S Walker. lme4: Linear mixed-effects models using Eigen and S4. R package version 1.1-7. http://CRAN.R-project.org/package=lme4, 2014.

[54] T Hothorn, F Bretz, and P Westfall. Simultaneous inference in general parametric models. *Biometrical Journal*, 50(3):346–363, 2008.

[55] AD Swain and HE Guttman. Handbook of human reliability analysis with emphasis on nuclear power plant applications. Technical Report NUREG/CR-1278, NuclearRegulatory Commission, Washington, DC, 1980.

[56] W Karwowski. The discipline of human factors and ergonomics. In G Salvendy, editor, *Handbook of human factors and ergonomics*, chapter 1, pages 3–37. John Wiley & Sons, 2012.

[57] IJAL Dos Santos, MS Farias, BG Monteiro, MA Falcão, and FD Marcelino. Using participatory ergonomics to improve nuclear equipment design. *Journal of Loss Prevention in the Process Industries*, 24(5):594–600, 2011.

[58] Jiang Hu and Sachin S Sapatnekar. A survey on multi-net global routing for integrated circuits. *INTEGRATION, the VLSI Journal*, 31(1):1–49, 2001.

[59] Marshall L Fisher. The lagrangian relaxation method for solving integer programming problems. *Management science*, 27(1):1–18, 1981.

[60] Jean-Paul Watson and David L Woodruff. Progressive hedging innovations for a class of stochastic mixed-integer resource allocation problems. *Computational Management Science*, 8(4):355–370, 2011.

[61] Tamás Terlaky, Anthony Vannelli, and Hu Zhang. On routing in VLSI design and communication networks. In *Algorithms and Computation*, pages 1051–1060. Springer, 2005.

[62] Antoine Deza, Chris Dickson, Tamas Terlaky, Anthony Vannelli, and Hu Zhang. Global routing in VLSI design algorithms, theory, and computational practice. *JCMCC-Journal of Combinatorial Mathematicsand Combinatorial Computing*, 80:71, 2012.

Appendices

A Complete Model for Lagrangian Relaxation Algorithm

Given the notations and decision variables defined in Section 2 and Section 3.2.2.1, the complete formulation of the decluttering problem on a decomposed network for Lagrangian relaxation algorithm is as below.

$$\begin{aligned}\min \quad & a\sum_i \sum_{m\in\bar{M}_i} \sum_{k\in N_i\cup N_i'} u_{m,k} + b\sum_i \sum_{k\in N_i\cup N_i'} \sum_{\tilde{m}\in\bar{M}_i} \sum_{\bar{m}\in\bar{M}_i} v_{k,\tilde{m},\bar{m}} + c \sum_{a\in A, a'=-a\in A} o_a \\ & + d\sum_i \sum_{s\in S_i} \sum_{k\in N_i\cup N_i'} x_{s,k} d(s,k) \\ & + e\sum_i \sum_{\bar{s}\in S_i} \sum_{\tilde{s}\in S_i} \sum_{\bar{k}\in N_i\cup N_i'} \sum_{\tilde{k}\in N_i\cup N_i'} 1_{\{x_{\bar{s},\bar{k}}+x_{\tilde{s},\tilde{k}}-1>0\}} violation(\bar{s},\bar{k},\tilde{s},\tilde{k}) \\ & + e\sum_i \sum_{\bar{s}\in S_i} \sum_{\tilde{s}\in S\setminus S_i} \sum_{k\in N_i\cup N_i'} x_{\bar{s},\bar{k}} violation(\bar{s},\bar{k},\tilde{s}) \\ & + f\sum_{m\in M}\sum_{a\in A} y_{m,a}\text{length}(a)\end{aligned} \tag{A.1}$$

s.t. Region-wise constraints:

$$\sum_{k\in N_i\cup N_i'} x_{s,k} = 1 \qquad s\in S_i \tag{A.2}$$

$$\sum_{s\in S_i} x_{s,k} \le 1 \qquad k\in N_i\cup N_i' \tag{A.3}$$

$$y_{m,a} + y_{m,a'} \le 1 \qquad a\in A_i,\ a'=-a,\ m\in\bar{M}_i \tag{A.4}$$

$$x_{s,k} + \sum_{a\in I_1^i(k)\cup I_2^i(k)} y_{m,a} = \sum_{a\in O_1^i(k)\cup O_2^i(k)} y_{m,a} + x_{t,k} \qquad k\in N_i\cup N_i',\ m=(s,t)\in M_i \tag{A.5}$$

$$\sum_{a\in I_1^i(k)\cup I_2^i(k)} y_{m,a} \le 1 \qquad k\in N_i\cup N_i', m\in\ M_i \tag{A.6}$$

$$\sum_{a\in O_1^i(k)\cup O_2^i(k)} y_{m,a} \le 1 \qquad k\in N_i\cup N_i', m\in\ M_i \tag{A.7}$$

$$x_{s,k} + \sum_{a\in I_1^i(k)\cup I_2^i(k)} y_{m,a} = \sum_{a\in O_1^i(k)\cup O_2^i(k)} y_{m,a} \qquad k\in N_i,\ m=(s,t)\in \bigcup_{j\in adj(i)} M_{i,j} \tag{A.8}$$

$$x_{t,k} + \sum_{a\in O_1^i(k)\cup O_2^i(k)} y_{m,a} = \sum_{a\in I_1^i(k)\cup I_2^i(k)} y_{m,a} \qquad k\in N_i,\ m=(s,t)\in \bigcup_{j\in adj(i)} M_{j,i} \tag{A.9}$$

$$\sum_{m\in\bar{M}_i} y_{m,a} + \sum_{m\in\bar{M}_i} y_{m,a'} - 1 \le 2000 o_a \qquad a\in A_i,\ a'=-a \tag{A.10}$$

$$y_{m,e} + y_{m,f} - 1 \leq 2u_{m,k} \qquad k \in N_i \cup N_i',\ m \in \bar{M}_i,\ e \in I_1^i(k), f \in O_2^i(k) \text{ or } e \in I_2^i(k), f \in O_1^i(k) \tag{A.11}$$

$$y_{\tilde{m},\tilde{e}} + y_{\tilde{m},\tilde{f}} + y_{\bar{m},\bar{e}} + y_{\bar{m},\bar{f}} - 3 \leq 4v_{k,\tilde{m},\bar{m}} \qquad k \in N_i,\ \tilde{m}, \bar{m} \in \bar{M}_i,\ \tilde{e} \in I_1^i(k), \tilde{f} \in O_1^i(k), \bar{e} \in I_2^i(k), \bar{f} \in O_2^i(k) \text{ or } \tilde{e} \in I_2^i(k), \tilde{f} \in O_2^i(k), \bar{e} \in I_1^i(k), \bar{f} \in O_1^i(k) \tag{A.12}$$

1) if $a = (p, q)$ is an intercluster edge starting from region i:

$$x_{s,p} + \sum_{e \in I_1^i(p) \cup I_2^i(p)} y_{m,e} = y_{m,a} + \sum_{e \in O_1^i(p) \cup O_2^i(p)} y_{m,e} \qquad m = (s,t) \in \bigcup_{j \in adj(i)} M_{i,j} \tag{A.13}$$

$$y_{m,a} + \sum_{e \in O_1^i(p) \cup O_2^i(p)} y_{m,e} \leq 1 \qquad m = (s,t) \in \bigcup_{j \in adj(i)} M_{i,j} \tag{A.14}$$

$$y_{m,a} + y_{m,e} - 1 \leq 2u_{m,p} \qquad m \in \bigcup_{j \in adj(i)} M_{i,j},\ e \in I_1^i(p) \text{ or } I_2^i(p) \tag{A.15}$$

$$y_{\tilde{m},a} + y_{\tilde{m},\tilde{e}} + y_{\bar{m},\bar{e}} + y_{\bar{m},\bar{f}} - 3 \leq 4v_{p,\tilde{m},\bar{m}} \qquad \tilde{m} \in \bigcup_{j \in adj(i)} M_{i,j},\ \bar{m} \in \bar{M}_i,\ \tilde{e} \in I_1^i(p),\ \bar{e} \in I_2^i(p),\ \bar{f} \in O_2^i(p) \text{ or } \tilde{e} \in I_2^i(p),\ \bar{e} \in I_1^i(p),\ \bar{f} \in O_1^i(p) \tag{A.16}$$

2) if $a' = (q, p)$ is an intercluster edge going into region i:

$$x_{t,p} + \sum_{e \in O_1^i(p) \cup O_2^i(p)} y_{m,e} = y_{m,a'} + \sum_{e \in I_1^i(p) \cup I_2^i(p)} y_{m,e} \qquad m = (s,t) \in \bigcup_{j \in adj(i)} M_{j,i} \tag{A.17}$$

$$y_{m,a'} + \sum_{e \in I_1^i(p) \cup I_2^i(p)} y_{m,e} \leq 1 \qquad m = (s,t) \in \bigcup_{j \in adj(i)} M_{j,i} \tag{A.18}$$

$$y_{m,a'} + y_{m,e} - 1 \leq 2u_{m,p} \qquad m \in \bigcup_{j \in adj(i)} M_{j,i},\ e \in O_1^i(p) \text{ or } O_2^i(p) \tag{A.19}$$

$$y_{\tilde{m},a'} + y_{\tilde{m},\tilde{e}} + y_{\bar{m},\bar{e}} + y_{\bar{m},\bar{f}} - 3 \leq 4v_{p,\tilde{m},\bar{m}} \qquad \tilde{m} \in \bigcup_{j \in adj(i)} M_{j,i},\ \bar{m} \in \bar{M}_i,\ \tilde{e} \in O_1^i(p),\ \bar{e} \in I_2^i(p),\ \bar{f} \in O_2^i(p) \text{ or } \tilde{e} \in O_2^i(p),\ \bar{e} \in I_1^i(p),\ \bar{f} \in O_1^i(p) \tag{A.20}$$

Global constraints:

$$\sum_{m \in M} y_{m,a} + \sum_{m \in M} y_{m,a'} - 1 \leq 2000o_a \qquad a \in A \backslash \bigcup_i A_i,\ a' = -a \tag{A.21}$$

$$x_{s,k},\ y_{m,a},\ u_{m,k},\ v_{k,\tilde{m},\bar{m}},\ o_a\ \in \{0,1\} \tag{A.22}$$

In the following Lagrangian relaxation, all the constraints related to the intercluster edges are relaxed.

$$
\begin{aligned}
\max\min\quad & a\sum_i \sum_{m\in\bar{M}_i} \sum_{k\in N_i\cup N_i'} u_{m,k} + b\sum_i \sum_{k\in N_i\cup N_i'} \sum_{\tilde{m}\in\bar{M}_i} \sum_{\bar{m}\in\bar{M}_i} v_{k,\tilde{m},\bar{m}} + c \sum_{a\in A, a'=-a\in A} o_a \\
& + d\sum_i \sum_{s\in S_i} \sum_{k\in N_i\cup N_i'} x_{s,k} d(s,k) + e\sum_i \sum_{\bar{s}\in S_i} \sum_{\tilde{s}\in S_i} \sum_{\bar{k}\in N_i\cup N_i'} \sum_{\tilde{k}\in N_i\cup N_i'} 1_{\{x_{\bar{s},\bar{k}}+x_{\tilde{s},\tilde{k}}-1>0\}} violation(\bar{s},\bar{k},\tilde{s},\tilde{k}) \\
& + e\sum_i \sum_{\bar{s}\in S_i} \sum_{\tilde{s}\in S\setminus S_i} \sum_{k\in N_i\cup N_i'} x_{\bar{s},\bar{k}} violation(\bar{s},\bar{k},\tilde{s}) + f\sum_{m\in M}\sum_{a\in A} y_{m,a}\text{length}(a) \\
& + \sum_{\substack{a\in A\setminus \bigcup_i A_i, \\ a'=-a}} \lambda_a\Big(\sum_{m\in M} y_{m,a} + \sum_{m\in M} y_{m,a'} - 1 - 2000 o_a\Big) \\
& + \sum_i \sum_{m\in \bigcup_{j\in adj(i)} M_{i,j}} \sum_{a\in \bigcup_{j\in adj(i)} A_{i,j}} \lambda^1_{m,a}\Big(x_{s,p} + \sum_{e\in I_1^i(p)\cup I_2^i(p)} y_{m,e} - y_{m,a} - \sum_{e\in O_1^i(p)\cup O_2^i(p)} y_{m,e}\Big) \\
& + \sum_i \sum_{m\in \bigcup_{j\in adj(i)} M_{j,i}} \sum_{a\in \bigcup_{j\in adj(i)} A_{j,i}} \lambda^2_{m,a}\Big(x_{t,p} + \sum_{e\in O_1^i(p)\cup O_2^i(p)} y_{m,e} - y_{m,a'} - \sum_{e\in I_1^i(p)\cup I_2^i(p)} y_{m,e}\Big) \\
& + \sum_i \sum_{m\in \bigcup_{j\in adj(i)} M_{i,j}} \sum_{a\in \bigcup_{j\in adj(i)} A_{i,j}} \lambda^3_{m,a}\Big(y_{m,a} + \sum_{e\in O_1^i(p)\cup O_2^i(p)} y_{m,e} - 1\Big) \\
& + \sum_i \sum_{m\in \bigcup_{j\in adj(i)} M_{j,i}} \sum_{a\in \bigcup_{j\in adj(i)} A_{j,i}} \lambda^4_{m,a}\Big(y_{m,a'} + \sum_{e\in I_1^i(p)\cup I_2^i(p)} y_{m,e} - 1\Big) \\
& + \sum_i \sum_{m\in \bigcup_{j\in adj(i)} M_{i,j}} \sum_{a\in \bigcup_{j\in adj(i)} A_{i,j}} \sum_{e\in I_1^i(p)} \lambda^5_{m,a}(y_{m,a} + y_{m,e} - 1 - 2u_{m,p}) \\
& + \sum_i \sum_{m\in \bigcup_{j\in adj(i)} M_{i,j}} \sum_{a\in \bigcup_{j\in adj(i)} A_{i,j}} \sum_{e\in I_2^i(p)} \lambda^6_{m,a}(y_{m,a} + y_{m,e} - 1 - 2u_{m,p}) \\
& + \sum_i \sum_{m\in \bigcup_{j\in adj(i)} M_{j,i}} \sum_{a\in \bigcup_{j\in adj(i)} A_{j,i}} \sum_{e\in O_1^i(p)} \lambda^7_{m,a}(y_{m,a'} + y_{m,e} - 1 - 2u_{m,p}) \\
& + \sum_i \sum_{m\in \bigcup_{j\in adj(i)} M_{j,i}} \sum_{a\in \bigcup_{j\in adj(i)} A_{j,i}} \sum_{e\in O_2^i(p)} \lambda^8_{m,a}(y_{m,a'} + y_{m,e} - 1 - 2u_{m,p}) \\
& + \sum_i \sum_{\tilde{m}\in \bigcup_{j\in adj(i)} M_{i,j}} \sum_{\bar{m}\in\bar{M}_i} \sum_{a\in \bigcup_{j\in adj(i)} A_{i,j}} \sum_{\substack{\tilde{e}\in I_1^i(p), \\ \bar{e}\in I_2^i(p),\ \bar{f}\in O_2^i(p)}} \lambda^9_{m,a}(y_{\tilde{m},a} + y_{\tilde{m},\tilde{e}} + y_{\bar{m},\bar{e}} + y_{\bar{m},\bar{f}} - 3 - 4v_{p,\tilde{m},\bar{m}}) \\
& + \sum_i \sum_{\tilde{m}\in \bigcup_{j\in adj(i)} M_{i,j}} \sum_{\bar{m}\in\bar{M}_i} \sum_{a\in \bigcup_{j\in adj(i)} A_{i,j}} \sum_{\substack{\tilde{e}\in I_2^i(p), \\ \bar{e}\in I_1^i(p),\ \bar{f}\in O_1^i(p)}} \lambda^{10}_{m,a}(y_{\tilde{m},a} + y_{\tilde{m},\tilde{e}} + y_{\bar{m},\bar{e}} + y_{\bar{m},\bar{f}} - 3 - 4v_{p,\tilde{m},\bar{m}}) \\
& + \sum_i \sum_{\tilde{m}\in \bigcup_{j\in adj(i)} M_{j,i}} \sum_{\bar{m}\in\bar{M}_i} \sum_{a\in \bigcup_{j\in adj(i)} A_{j,i}} \sum_{\substack{\tilde{e}\in O_1^i(p), \\ \bar{e}\in I_2^i(p),\ \bar{f}\in O_2^i(p)}} \lambda^{11}_{m,a}(y_{\tilde{m},a'} + y_{\tilde{m},\tilde{e}} + y_{\bar{m},\bar{e}} + y_{\bar{m},\bar{f}} - 3 - 4v_{p,\tilde{m},\bar{m}}) \\
& + \sum_i \sum_{\tilde{m}\in \bigcup_{j\in adj(i)} M_{j,i}} \sum_{\bar{m}\in\bar{M}_i} \sum_{a\in \bigcup_{j\in adj(i)} A_{j,i}} \sum_{\substack{\tilde{e}\in O_2^i(p), \\ \bar{e}\in I_1^i(p),\ \bar{f}\in O_1^i(p)}} \lambda^{12}_{m,a}(y_{\tilde{m},a'} + y_{\tilde{m},\tilde{e}} + y_{\bar{m},\bar{e}} + y_{\bar{m},\bar{f}} - 3 - 4v_{p,\tilde{m},\bar{m}})
\end{aligned}
\tag{A.23}
$$

subject to

Constraints $(A.2) - (A.12)$ and $(A.22)$

B Complete Model for Progressive Hedging Algorithm

Similar to Section A, given the notations and decision variables defined in Section 2 and Section 3.2.2.2, the complete formulation of the decluttering problem for progressive hedging (PH) algorithm is listed below. Unlike the Lagrangian relaxation approach in which intercluster edges do not belong to any region, the PH approach decomposes the network in such a way that each region includes intercluster edges either originating from the region or going into it.

$$\min \sum_i Q_1^i + 0.5 \sum_i Q_2^i \tag{B.1}$$

where Q_1^i's do not depend on the scenario explicitly but Q_2^i's do. Suitable choices for Q_1^i and Q_2^i are:

$$\begin{aligned} Q_1^i = {} & a \sum_{m \in \bar{M}_i} \sum_{k \in N_i} u_{m,k} + b \sum_{k \in N_i} \sum_{\tilde{m} \in \bar{M}_i} \sum_{\bar{m} \in \bar{M}_i} v_{k,\tilde{m},\bar{m}} + c \sum_{a \in A_i, a' = -a \in A_i} o_a \\ & + d \sum_{s \in S_i} \sum_{k \in N_i} x_{s,k} d(s,k) \\ & + e \sum_{\bar{s} \in S_i} \sum_{\tilde{s} \in S_i} \sum_{\bar{k} \in N_i \cup N_i'} \sum_{\tilde{k} \in N_i \cup N_i'} 1_{\{x_{\bar{s},\bar{k}} + x_{\tilde{s},\tilde{k}} - 1 > 0\}} violation(\bar{s}, \bar{k}, \tilde{s}, \tilde{k}) \\ & + e \sum_{\bar{s} \in S_i} \sum_{\tilde{s} \in S \setminus S_i} \sum_{k \in N_i \cup N_i'} x_{\bar{s},\bar{k}} violation(\bar{s}, \bar{k}, \tilde{s}) \\ & + f \sum_{m \in \bar{M}_i} \sum_{a \in A_i} y_{m,a} \text{length(a)} \end{aligned}$$

$$Q_2^i = c \sum_{a \in \bar{A}_i \setminus A_i, a' = -a} o_a + f \sum_{m \in \bar{M}_i \setminus M_i} \sum_{a \in \bar{A}_i \setminus A_i} y_{m,a} \text{length(a)}$$

s.t. Region-wise constraints:

$$\sum_{k \in N_i} x_{s,k} = 1 \qquad s \in S_i \tag{B.2}$$

$$\sum_{s \in S_i} x_{s,k} \leq 1 \qquad k \in N_i \tag{B.3}$$

$$y_{m,a} + y_{m,a'} \leq 1 \qquad a \in A_i,\ a' = -a,\ m \in \bar{M}_i \tag{B.4}$$

$$x_{s,k} + \sum_{a \in I_1^i(k) \cup I_2^i(k)} y_{m,a} = \sum_{a \in O_1^i(k) \cup O_2^i(k)} y_{m,a} + x_{t,k} \qquad k \in N_i,\ m = (s,t) \in M_i \tag{B.5}$$

$$x_{s,k} + \sum_{a \in I_1^i(k) \cup I_2^i(k)} y_{m,a} = \sum_{a \in O_1(k) \cup O_2(k)} y_{m,a} \qquad k \in N_i,\ m = (s,t) \in \bigcup_{j \in adj(i)} M_{i,j} \tag{B.6}$$

$$x_{t,k} + \sum_{a \in O_1^i(k) \cup O_2^i(k)} y_{m,a} = \sum_{a \in I_1(k) \cup I_2(k)} y_{m,a} \qquad k \in N_i,\ m = (s,t) \in \bigcup_{j \in adj(i)} M_{j,i} \tag{B.7}$$

$$\sum_{a \in O_1(k) \cup O_2(k)} y_{m,a} \leq 1 \qquad k \in N_i,\ m \in \bar{M}_i \tag{B.8}$$

$$\sum_{a \in I_1(k) \cup I_2(k)} y_{m,a} \leq 1 \qquad k \in N_i,\ m \in \bar{M}_i \tag{B.9}$$

$$\sum_{m \in \bar{M}_i} y_{m,a} + \sum_{m \in \bar{M}_i} y_{m,a'} - 1 \leq 2000 o_a \qquad a \in \bar{A}_i,\ a' = -a \tag{B.10}$$

$$y_{m,e} + y_{m,f} - 1 \leq 2u_{m,k} \qquad \begin{array}{r} k \in N_i,\ m \in \bar{M}_i,\ e \in I_1(k), f \in O_2(k) \\ or\ e \in I_2(k), f \in O_1(k) \end{array} \tag{B.11}$$

$$y_{\tilde{m},\tilde{e}} + y_{\tilde{m},\tilde{f}} + y_{\bar{m},\bar{e}} + y_{\bar{m},\bar{f}} - 3 \leq 4v_{k,\tilde{m},\bar{m}} \qquad \begin{array}{l} k \in N_i,\ \tilde{m}, \bar{m} \in \bar{M}_i,\ \tilde{e} \in I_1(k), \tilde{f} \in O_1(k) \\ \bar{e} \in I_2(k), \bar{f} \in O_2(k) \text{ or} \\ \tilde{e} \in I_2(k), \tilde{f} \in O_2(k), \bar{e} \in I_1(k), \bar{f} \in O_1(k) \end{array} \tag{B.12}$$

Global constraints: for each region i, we need to impose the following conditions to make the scenario-dependent solutions implementable

$$(y_{m,a})^i = (y_{m,a})^j \qquad j \in adj(i),\ a \in A_{i,j},\ m \in \bigcup_j M_{i,j} \tag{B.13}$$

$$x_{s,k},\ y_{m,a},\ u_{m,k},\ v_{k,\tilde{m},\bar{m}},\ o_a\ \in \{0,1\} \tag{B.14}$$

C Proof of Lemma 1

Lemma 2 *Given a finite set of substations located at the nodes of a 2D square grid. Some of these substations are connected through edges on the grid (i.e., we call them transmission lines). The minimum overlaps among all transmission lines are infinitely small; or equivalently, the total length of the overlapping edges approaches*

zero if the grid discretization approaches infinitely fine.

Proof. To prove Lemma 1, it suffices to prove the following equivalent claim:

Claim C.1 *Given a pair of substations (s, t) to be connected and all the other already-connected transmission lines on a 2D square grid, construct p from s to t to minimize the number of overlapping edges between p and the other connected lines. As the grid discretization approaches infinitely fine, the total length of overlapping edges becomes infinitely small.*

With this claim proved, start with any pair of to-be-connected substations $(s_0,\ t_0)$ and connect them arbitrarily through edges on the grid. Then, iteratively pick a pair of unconnected substations $(s_n,\ t_n)$ and connect them by P_n so that the total number of overlapping edges between P_0 and the other existing transmission lines is minimized. We know that if the grid discretization approaches infinitely fine, the total length of overlapping edges is infinitely small in each iteration. The lemma hence follows from the fact that we have finite number of iterations, and finite sum of $x \to 0^+$ also approaches zero. Before we give the proof of this claim, we define the *radius of a node* as below:

Definition C.1 *Given $G = (V, E)$ as a 2D square grid, the radius of node v, $v \in V$, is defined as the set of edges incident to v.*

With this definition, to prove Claim C1, it suffices to prove that for any pair of to-be-connected substations $(s,\ t)$, we can always construct a line p from s to t in such a way that it does not overlap with the other existing lines outside the radius of s and t. Figure 1 gives a graphical illustration of how to construct p.

Suppose the coordinates for substations s and t are $(x_0,\ y_0)$ and $(m,\ n)$, where $m > x_0$ and $n > y_0$. That means, t lies north east of s. The other relative positions between s and t can be proved in exactly the same way, and is thus omitted.

1. Start from $s = (x_0,\ y_0)$. Consider all the horizontal edges intersecting with $x = x_0$ and being used by other existing tranmission lines. Since we are dealing with finite number of transmission lines with finite lengths, the number of such edges is also finite. Pick the one with the smallest y-coordinate, y_1. As the grid discretization is infinitely fine, we can always find a horizontal edge intersecting with $x = x_0$ at $(x_0,\ y_1^*)$, where $y_1^* < y_1$. Therefore, the first edge (① in Figure 8) on line p will be $((x_0,\ y_0),\ (x_0,\ y_1^*))$.
2. Now we are at node $(x_0,\ y_1^*)$. Consider all the vertical edges intersecting with $y = y_1^*$ and being used by other existing tranmission lines. By a similar argument, we can say that the number of such edges is also finite. Pick the one with the smallest x-coordinate, x_1. Since the grid discretization is infinitely

fine, we can always find a vertical edge intersecting with $y = y_1^*$ at $(x_1^*,\ y_1^*)$, where $x_1^* < x_1$. Thus, the second edge (② in Figure 8)on line p will be $((x_0,\ y_1^*),\ (x_1^*,\ y_1^*))$.

3. Continue to to find unoverlapping edges towards north east using the methodology described in step 1 - 2 until $m < x_M,\ n < y_M$ after M iterations. Line p is then directed into t and complete the process.

It is obvious that p only overlaps with the other existing transmission lines on the radius of s and t if either s or t is connected with more than 4 (or 8 for directed grid) other substations. Since the total number of substations and transmission lines are finite, and the length of edges approaches zero once the grid discretization is infinitely fine, the total overlaps occurring on these radius edges will also approach zero. Thus, we proved the Claim C1. ■

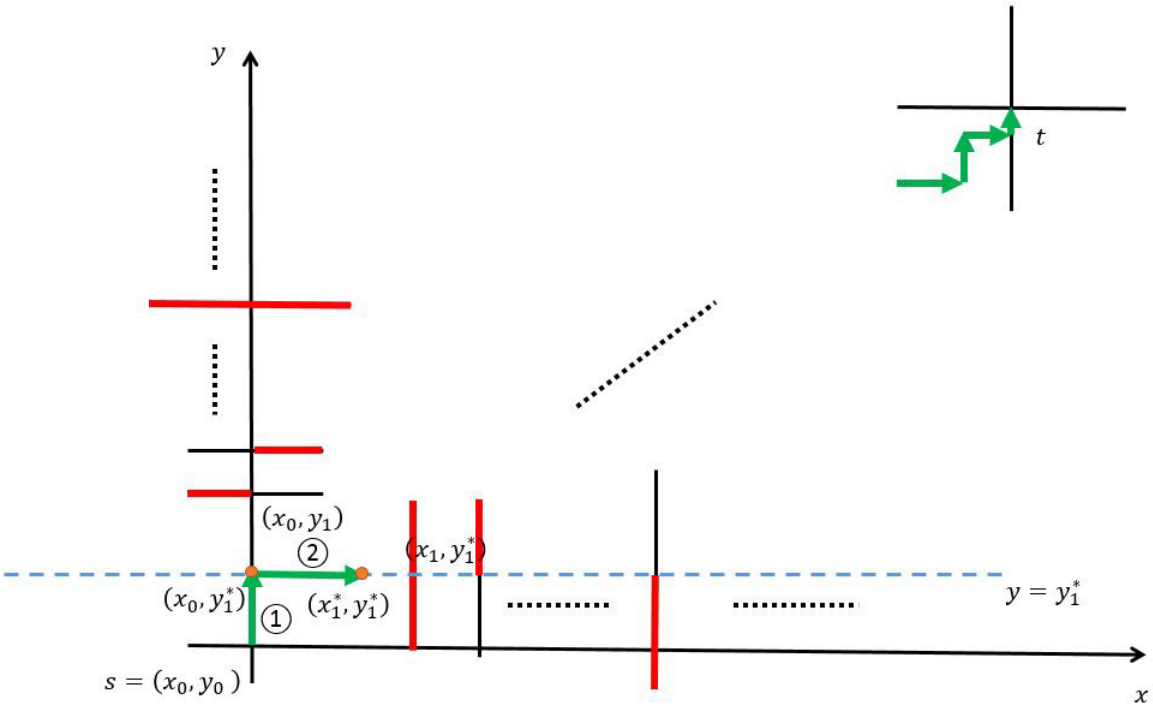

Figure 29: A Graphical Illustration of How to Construct p